The NMDA Receptor Transmembrane Region in Receptor Function and Inhibition

by

Madeleine Ruth Wilcox

B.S. Biochemistry, University of California Los Angeles, 2013

Submitted to the Graduate Faculty of

the Dietrich School of Arts and Sciences in partial fulfillment

of the requirements for the degree of

Doctor of Philosophy

University of Pittsburgh

2019

UNIVERSITY OF PITTSBURGH

DIETRICH SCHOOL OF ARTS AND SCIENCES

This dissertation was presented

by

Madeleine Ruth Wilcox

It was defended on

May 15, 2019

and approved by

Tija C. Jacob, PhD, Department of Pharmacology and Chemical Biology

Elias Aizenman, PhD, Department of Neurobiology

Thanos Tzounopoulos, PhD, Department of Otolaryngology

Stephen Meriney, PhD, Departments of Neuroscience and Psychiatry

Committee Chair: Jon W. Johnson, PhD, Departments of Neuroscience and Psychiatry

The NMDA Receptor Transmembrane Region in Receptor Function and Inhibition

Madeleine Ruth Wilcox, PhD

University of Pittsburgh, 2019

NMDA Receptors (NMDARs) are glutamate- and glycine- gated ion channels present at most excitatory synapses in the mammalian brain. NMDARs are typically composed of four subunits, two GluN1 and two GluN2, which each contain a transmembrane domain (TMD). The TMDs of all four subunits assemble to form the NMDAR ion channel, which opens in response to agonist binding in the extracellular region. The TMD is critical to ion permeation and channel block of NMDARs and small alterations in the TMD can have powerful effects on receptor function. This dissertation discusses work by myself and my coauthors centered around the NMDAR TMD. My coauthors and I first examined the functional effects of mutating a tryptophan residue present at homologous sites in the GluN1 and GluN2 subunit TMDs. We discovered that the conserved tryptophan modulates NMDAR function in a subunit-dependent manner. We next explored the kinetics of NMDAR recovery from inhibition by the therapeutically relevant NMDAR open channel blockers memantine and ketamine. Examination of the kinetics of NMDAR unblock by memantine and ketamine led us to conclude that memantine, but not ketamine, inhibits NMDARs through an additional mechanism that is distinct from traditional open channel block. Building on data from the Johnson lab and others, we characterized a little-studied mechanism of NMDAR inhibition by memantine. Our data suggest that memantine can inhibit NMDARs by entering the plasma membrane and transiting to the NMDAR ion channel through a membrane-to-channel fenestration. We revealed that several NMDAR blockers in addition to memantine inhibit NMDARs through the same fenestration-dependent mechanism.

Table of Contents

List of Tables

List of Figures

List of Equations

Preface

I am very grateful for the kind faculty and staff at the University of Pittsburgh Center for Neuroscience and the members of the Johnson lab who have assisted my progress to PhD completion. I would like to thank my mentor Dr. Jon Johnson for his many teachings over the past 6 years. I also want to thank my committee, Drs. Elias Aizenman, Tija Jacob and Thanos Tzounopoulos, Dr. Steve Meriney, and my outside examiner Dr. Kasper Hansen for their support. I also have had a wealth of support in my personal life including support from my parents Alison and Malcolm, sister Naomi, my partner Neil, and many friends near and far.

1.0 General Introduction to Chemical Excitatory Neurotransmission

Every thought we think and sensation we experience arises from the nervous system. The nervous system contains billions of neurons: specialized cells that transmit information throughout the body. Neurons communicate with one another to give rise to both conscious and unconscious aspects of being. Synapses, which allow efficient chemical transmission of information between neurons, can form where the axon of one neuron meets the dendrite of another. Axon terminals release chemical signals called neurotransmitters from the presynaptic region onto dendrites in the postsynaptic region. Postsynaptically, dendrites contain many neurotransmitter receptors across the synaptic cleft from the axon terminal, prepared to react to presynaptic signals. Binding of released neurotransmitters to postsynaptic neurotransmitter receptors can initiate depolarizing electrical potentials in the postsynaptic cell that spread into the neuronal cell body. These depolarizing potentials can initiate a propagating action potential that causes the release of neurotransmitters from the depolarized cell's axon terminals. This mechanistic loop of neuronal communication is at the heart of all experience.

Neurotransmitter binding to postsynaptic receptors causes receptors to open and pass ions across the cellular membrane. Numerous neurotransmitter receptors are present in the postsynaptic region, including ionotropic glutamate receptors (iGluRs). iGluRs are ligand-gated ion channels that open in response to glutamate binding. When iGluR channels are open, cations can flow through them to transport messages across membranes. iGluRs mediate fast excitatory transmission in the brain and are present at most excitatory synapses in the mammalian central nervous system (CNS).

There are three main classes of iGluRs: kainate receptors, alpha-amino-3-hydroxy-5-methyl-4-isoxazolepropionic acid (AMPA) receptors and N-methyl-D-aspartate (NMDA) receptors. AMPA receptors (AMPARs) and NMDA receptors (NMDARs) are found ubiquitously in the brain, while kainate receptors (KARs) have a more restricted expression pattern. NMDARs, AMPARs and KARs have been implicated in synaptic plasticity, which is thought to be one of the most important substrates of learning and memory. NMDARS have many unique and physiologically important characteristics among iGluRs that make them paramount to the initiation of many types of synaptic plasticity. The work discussed in this dissertation focuses predominantly on NMDARs.

1.1 Physiological Roles of NMDA Receptors

Upon activation, NMDARs pass positively charged ions including Ca^{2+}, Na^{+}, and K^{+} through their pores. Ca^{2+} is a central signaling molecule in the CNS and acts to regulate many cellular processes (Traynelis et al., 2010b). Intracellular Ca^{2+} is maintained at low concentrations by physiological buffers, ion pumps and exchangers. When Ca^{2+} enters the cell through channels or receptors, it can cause various changes in cell status. While most AMPARs and KARs have low permeability to Ca^{2+}, NMDAR Ca^{2+} permeability is relatively high. NMDARs are inhibited by membrane voltage (V_m)-dependent Mg^{2+} block at cellular resting potentials. By combining agonist-dependent entry of Ca^{2+} into cells with V_m-dependent Mg^{2+} block, NMDARs act as "coincidence detectors". Significant ion flux occurs only when agonist binds and relief of V_m-dependent Mg^{2+} block occurs. NMDARs activate when two co-agonists, glutamate and glycine (or D-serine), bind (Traynelis et al., 2010b). Since the glycine binding sites are often occupied by

ambient glycine, glutamate binding is typically the limiting step in NMDAR activation (McNamara and Dingledine, 1990). Therefore, the ion channels (pores) of postsynaptic NMDARs open when glutamate is released from presynaptic terminals. Relief of V_m-dependent Mg^{2+} block requires depolarization of the postsynaptic cell, which can occur with postsynaptic activity. Thus, NMDARs pass ions, including the important signaling ion Ca^{2+}, during simultaneous pre- and post-synaptic activity.

1.2 NMDARs in Learning and Memory

The coincidence detecting capability of NMDARs is crucial to their function in long-term potentiation (LTP) and long-term depression (LTD) of synaptic efficacy, which are important for many types of memory. NMDARs allow significant Ca^{2+} into cells when presynaptic stimulation is coupled with postsynaptic depolarization (Nicoll, 2017). This pairing of conditions mimics the physiological requirements for NMDARs to pass significant current: (1) binding of glutamate, and (2) relief of Mg^{2+} block. These conditions are typically induced experimentally by a strong tetanus (e.g. 100 Hz for 1 s). The large influx of Ca^{2+} through NMDARs during a tetanus activates postsynaptic Ca^{2+}-dependent proteins that promote an increase in synaptic strength through numerous proposed mechanisms including AMPAR phosphorylation (Lee, 2006), insertion of AMPARs into the postsynaptic density (PSD) (Luscher and Malenka, 2012) and modulation of protein transcription (Sacktor, 2008). These processes increase synaptic efficacy and sustain it over a long period of time (i.e. LTP). In addition to LTP, LTD is critical for learning and memory. NMDAR-dependent LTD is typically induced through low-frequency presynaptic stimulation that does not induce large postsynaptic depolarization (Luscher and Malenka, 2012). This allows for

glutamate binding to NMDARs without significant Mg^{2+} unblock, which leads to a small amount of Ca^{2+} influx through NMDARs (due to incomplete Mg^{2+} block of NMDARs). Repeated low-level Ca^{2+} influx through NMDARs leads to AMPAR removal from the PSD, reducing synaptic efficacy (Nicoll, 2017).

1.3 NMDARs in Disease

Due to the critical role of NMDARs in the mammalian CNS, alterations in NMDAR function often induce or exacerbate pathogenesis. In recent years, mutations in NMDAR subunits have been linked to numerous neurodevelopmental (Burnashev and Szepetowski, 2015, Chen et al., 2017, Fedele et al., 2018, Vyklicky et al., 2018, Yuan et al., 2014) and seizure disorders (Addis et al., 2017, Gao et al., 2017, Vyklicky et al., 2018, Yuan et al., 2014) in humans. NMDAR dysfunction is implicated in many disorders including Parkinson's Disease (Oh et al., 1998, Calon et al., 2002, Nash and Brotchie, 2002, Tikhonov et al., 2006), fragile X syndrome (Toft et al., 2016, Lau and Tymianski, 2010), and stroke (Wu and Tymianski, 2018, Li and Wang, 2016). Involvement of NMDARs in several prevalent conditions is detailed below to illustrate the importance of NMDARs in disease.

1.3.1 Alzheimer's disease

Alzheimer's disease is the sixth leading cause of death in the United States (US). In 2018, long-term care and hospice services for Alzheimer's disease patients cost the US an estimated $277 billion (Alzheimer's Association (2018)). While NMDARs are critical for synaptic plasticity,

overactive NMDARs cause excessive Ca^{2+} influx and excitotoxicity. Excitotoxicity is central to the pathogenesis of Alzheimer's disease. NMDAR localization (synaptic vs. extrasynaptic) also seems to play a role in Alzheimer's disease pathogenesis. Activation of synaptic NMDARs is linked to cell survival, while activation of extrasynaptic NMDARs is associated with cell death and correlates with the pathological changes that occur in Alzheimer's disease (Hardingham and Bading, 2010, Wang and Reddy, 2017). Increases in extracellular glutamate have also been shown to occur in Alzheimer's disease and may contribute to overactivation of NMDARs and cell death (Wang et al., 2013). Additional evidence indicates that aβ oligomers and overexpression of tau protein, which are consistently tied to pathogenesis in Alzheimer's disease, cause dysregulation of NMDARs (Wang and Reddy, 2017, Liu et al., 2019, Zhao et al., 2017). In a sort of vicious cycle, activation of extrasynaptic NMDARs drives tau overexpression, which subsequently promotes the activity of GluN2B-containing receptors (Liu et al., 2019). aβ oligomers have been shown to activate NMDARs in neurons (Ferreira et al., 2012) and heterologous expression systems (Texido et al., 2011, Domingues et al., 2007). aβ oligomers have also been shown to induce synaptic depression, promoting LTD and preventing LTP, which may contribute to dementia in Alzheimer's disease (Liu et al., 2019).

Memantine is an NMDAR inhibitor and a Food and Drug Administration (FDA)-approved treatment for moderate-to-severe Alzheimer's disease (Thomas and Grossberg, 2009). Evidence suggests that memantine preferentially inhibits NMDARs exposed to high intracellular Ca^{2+}, which may partially explain its clinical efficacy (Glasgow et al., 2017). Additionally, memantine preferentially inhibits GluN2C and GluN2D-containing receptors in physiological Mg^{2+} (Kotermanski and Johnson, 2009). GluN2C and GluN2D-containing receptors in the cortex are preferentially expressed on adult interneurons (Rudolf et al., 1996, Yamasaki et al., 2014, Standaert et al., 1996), which suggest that memantine may act through promoting cortical disinhibition (Povysheva and Johnson, 2016).

1.3.2 Schizophrenia

Schizophrenia is a disabling mental condition that affects nearly 1% of the world's population (Balu, 2016) and is influenced by both environmental and genetic factors (Moran et al., 2016). NMDAR dysfunction has long been implicated in the development of schizophrenia pathology. Mutations in NMDARs and PSD proteins are linked to heritable schizophrenia (Harrison and Weinberger, 2005, Kirov et al., 2012) and hypofunction of NMDARs is proposed to be critical to schizophrenic pathogenesis (Snyder and Gao, 2013). The NMDAR hypofunction hypothesis of schizophrenia is supported by numerous findings. Administration of several NMDAR open-channel blockers including ketamine and phencyclidine (PCP) to healthy individuals results in psychotomimetic (schizophrenia-like) symptoms (Javitt and Zukin, 1991, Krystal et al., 1994). Low doses of NMDAR inhibitor that do not produce psychotomimetic effects in healthy individuals reproduce other physiological changes seen in schizophrenia such as eye-tracking abnormalities and increased subcortical dopamine release (Radant et al., 1998, Kegeles

et al., 2000). Inhibition of NMDARs by PCP causes schizophrenia-associated neurochemical alterations in animal models of schizophrenia (Morris et al., 2005) and NMDAR dysregulation is frequently observed in postmortem tissue of schizophrenic individuals (Snyder and Gao, 2013).

1.3.3 Depression

Major depression is among the most ubiquitous mental disorders in the United States. Excessive NMDAR activation is implicated in depression, and several classes of NMDAR inhibitors have shown efficacy in depression treatment (Ates-Alagoz and Adejare, 2013). Glycine-site antagonists, allosteric NMDAR inhibitors, and open-channel blockers including ketamine have been suggested to improve depressive symptoms in pre-clinical studies (Kiss et al., 2012, Maj et al., 1994, Paul et al., 1992, Maj et al., 1992, Trullas and Skolnick, 1990). Despite potential unwanted side effects at therapeutic doses (e.g. psychotomimetic effects, see Section 1.3.2), mounting evidence suggests that ketamine is effective in the treatment of depression (Schwartz et al., 2016, Duman, 2018). The FDA recently approved a ketamine-containing nasal spray for treatment-resistant depression (2019). However, it is unclear whether ketamine's efficacy stems from inhibition of NMDARs or separate effects (Duman, 2018, Zanos et al., 2016).

1.4 Properties of NMDARs

All functional NMDARs are composed of four subunits (i.e. "tetrameric"). Two of the four subunits in functional NMDARs are GluN1 subunits, which bind glycine. The other two subunits can be any combination of the GluN2(A-D) or GluN3(A-B) subunits. GluN2 subunits bind

glutamate, while GluN3 subunits bind glycine. Therefore, GluN1/3 receptors (receptors containing two GluN1 and two GluN3 subunits) are glycine-gated, and GluN1/2 receptors (receptors containing two GluN1 and two GluN2 subunits) are glycine-and-glutamate-gated. NMDARs that contain two GluN1 subunits and two of the same GluN2 or GluN3 subunits are referred to as diheteromers (e.g. GluN1/2A), while NMDARs that contain two GluN1 subunits and two different GluN2 or GluN3 subunits are called triheteromers (e.g. GluN1/2A/3A). This dissertation focuses specifically on GluN1/2 diheteromers and does not include significant discussion of triheteromeric or GluN3-containing NMDARs. However, the topics discussed in this work may have important implications for triheteromeric and GluN3-containing NMDARs. Recently, new expression techniques have assisted research into triheteromeric NMDARs (Hansen et al., 2014, Stroebel et al., 2014). For review, see Stroebel et al (Stroebel et al., 2018).

1.4.1 GluN1 subunit expression

NMDAR subunit expression varies throughout development. GluN1 mRNA expression begins as early as embryonic day (E) 14 in rats, peaks around the third postnatal week, and then declines slightly into adulthood (Monyer et al., 1992). GluN1 is present in 8 splice variants: GluN1-1a, GluN1-1b, GluN1-2a, GluN1-2b, GluN1-3a, GluN1-3b, GluN1-4a and GluN1-4b (Dingledine et al., 1999). GluN1 splice variants have different combinations of three alternatively spliced exons: exon 5 in the amino terminal domain (NTD) and exons 21 and 22 in the C-terminal Doman (CTD), referred to as C1 and C2 cassettes, respectively (Figure 1). Exon 22 contains an alternative splice site that can lead to splicing out part of exon 22 and the inclusion of the C2' cassette. The eight GluN1 splice variants are diagrammed in Figure 1. The "a" label indicates exon 5's absence, and "b" indicates its presence (Dingledine et al., 1999). GluN1 splice variants that

lack exon 5 (GluN1-a) are expressed widely throughout the brain, while GluN1 splice variants that include exon 5 (GluN1-b isoforms) are restricted to specific areas including the sensorimotor cortex and thalamus. The GluN1-2a and GluN1-2b are also widely expressed throughout the brain, while the GluN1-1a and GluN1-2b isoforms are in rostral brain and GluN1-4a and GluN1-4b isoforms are in caudal brain. GluN1-3 expression it is barely detectable at birth and remains at low levels in cortex and hippocampus into adulthood (Ewald and Cline, 2009). Splice variants can imbue NMDARs with unique properties including susceptibility to NMDAR modulators (see Section 1.6).

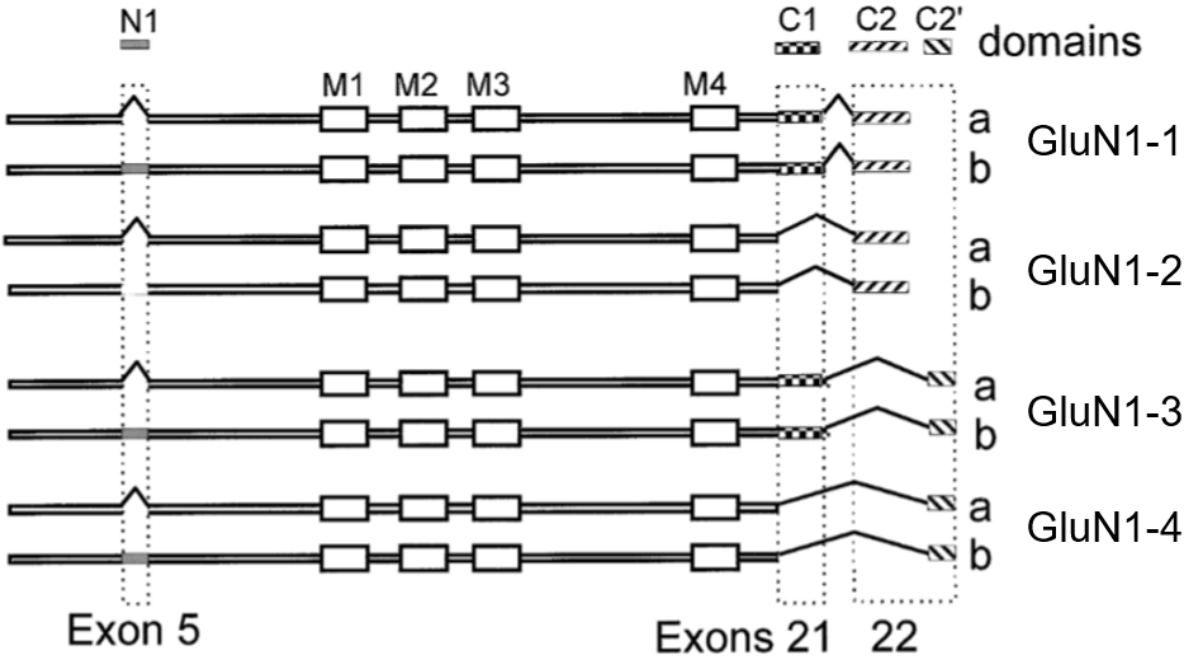

Figure 1 GluN1 splice variants

Diagram of the eight GluN1 splice variants and their corresponding names. GluN1 splice variant expression varies with developmental stage and brain region, and can influence NMDAR properties, along with the GluN2 or GluN3 subunits present in an intact receptor. Figure adapted from (Dingledine et al., 1999).

1.4.2 GluN2 subunit expression

Like GluN1 splice variant expression, GluN2 subunit expression varies with brain region and developmental stage (Monyer et al., 1994). GluN2B and GluN2D receptor mRNAs are present prenatally in rat CNS. GluN2B mRNA expression peaks around postnatal day (P) 12, GluN2D expression peaks around P7, and both decline as the animal reaches adulthood. Expression of GluN2A mRNA begins postnatally, with significant expression apparent by P7. GluN2A

expression increases into animal adulthood, when it plateaus. Similarly, GluN2C mRNA expression begins shortly after birth and increases until it reaches a plateau in mature animals. GluN2C and GluN2D expression are more spatially restricted than GluN2A and GluN2B, with GluN2C present mainly in the cerebellum and GluN2D present mainly in the midbrain. However, GluN2C and GluN2D receptors are present in interneuron subtypes in the adult hippocampus (Monyer et al., 1994).

1.4.3 NMDAR structure

In the intact NMDAR, GluN1 and GluN2 or GluN3 subunits are arranged in an alternating arrangement (Figure 2A) with GluN1 subunits across from one another and GluN2 subunits across from one another (Karakas and Furukawa, 2014, Riou et al., 2012). Each subunit contains an extracellular NTD and agonist binding domain (ABD), a transmembrane domain (TMD), and intracellular CTD (Figure 2B,C).

The TMD of each subunit is structured similarly, with three transmembrane helices (M1, M3, M4), and a re-entrant loop (M2) that lines the ion channel (Figure 2B,C). The M3 regions compose the channel gate and M2 regions form the ion selectivity filter. The M2 and M3 regions together form the ion conduction pathway in NMDARs. The M1 and M4 regions sit external to M2 and M3 regions (see Section 1.5 for more information on the TMD).

The ABD lies atop the TMD, while the NTD is the most extracellular portion of the receptor. The ABD and NTD in intact NMDARs are each composed of four subunits in a “dimer of dimers” organization (Traynelis et al., 2010b). Interestingly, domain swapping occurs between the NTD and ABD: the subunits composing dimers in the ABD are different from those composing dimers in the NTD, though each layer maintains a GluN1-GluN2-GluN1-GluN2 arrangement

(Karakas and Furukawa, 2014, Lee et al., 2014). The NTD of each subunit is composed of an upper (R1) and lower (R2) lobe that, together, resemble a clamshell. The S1 and S2 amino acid segments form most of the upper (D1) and lower (D2) lobe, respectively, of the clamshell-like LBD. S1 connects to the M1 domain and S2 forms a large loop that joins the M3 and M4 regions (Figure 2B) (Traynelis et al., 2010b).

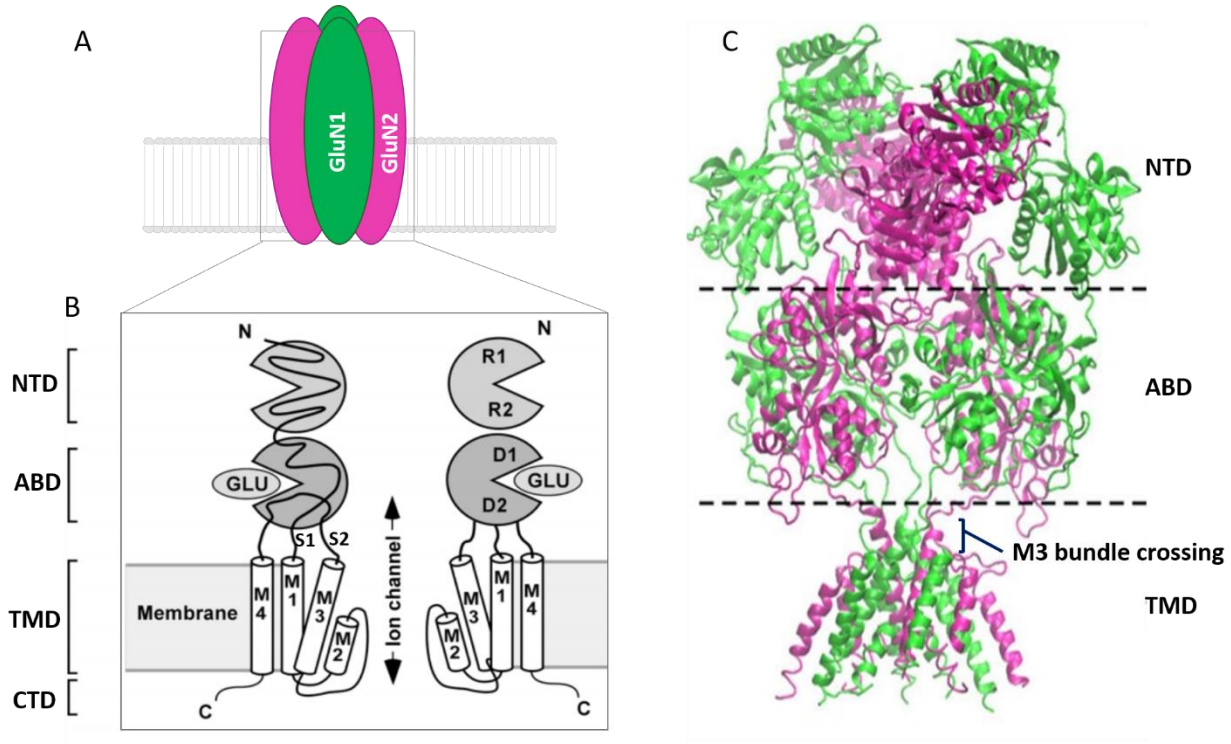

Figure 2 Structure of NMDARs

A, diagram of an NMDAR composed of two GluN2 and two GluN2 subunits showing the alternating GluN1-GluN2-GluN1-GluN2 arrangement of subunits. B, blow-up of cross section showing two GluN2 subunits in the membrane. NTD, amino terminal domain; ABD, agonist binding domain; TMD, transmembrane domain; CTD, C-terminal domain. Within the TMD, transmembrane helices M1, M3, and M4, and re-entrant loop M2 are shown. M2 regions from all four subunits line the pore in intact NMDARs. S1 connects to M1 and forms most of the lower lobe of the ABD. S2 connects to M3 and forms most of the upper lobe of the ABD. R1 and R2 are the upper and lower lobes of the NTD, respectively. C, crystal structure of GluN1/2B NMDAR (PBD 4PE5) with receptor domains labelled. The M3 bundle crossing within the TMD (proposed channel gate) is also labelled. The crystal structure does not contain the CTD. Image in B was adapted from (Siegler Retchless et al., 2012); image in C was adapted from (Glasgow et al., 2015).

1.4.4 Subtype dependence of NMDAR properties

The GluN2 subunits present in an intact NMDAR imbue receptors with specific properties. Many of the properties of NMDARs can be categorized into "gating and ligand-binding properties" and "channel properties" (Figure 3). Gating and ligand-binding properties include the probability of the receptor being open (P_{open}), agonist potency, Zn^{2+} sensitivity, proton sensitivity, and ifenprodil sensitivity (Zn^{2+}, proton, and ifenprodil sensitivity are discussed in detail in section 1.6). Channel properties include Mg^{2+} sensitivity, selective permeability to Ca^{2+}, single-channel conductance and inherent membrane voltage (V_m) dependence of gating.

1.4.5 Gating and ligand binding properties

Gating and ligand binding properties vary with the GluN2 subunits present in the intact NMDAR (Figure 3B). GluN1/2A receptors have the highest maximal P_{open}, about 0.5, GluN1/2B receptors have a maximal P_{open} of about 0.1, GluN1/2C and GluN1/2D receptors have a maximal P_{open} of about 0.01 (Wyllie et al., 1998, Erreger et al., 2005, Chen et al., 1999, Dravid et al., 2008b, Gielen et al., 2009, Yuan et al., 2009, Glasgow et al., 2015). Glutamate potency increases from GluN1/2A to GluN1/2D receptors (glutamate EC_{50} GluN1/2A = 3.3 μM; GluN1/2B = 2.9 μM; GluN1/2C = 1.7 μM; GluN1/2D = 0.51 μM) (Traynelis et al., 2010b). Glycine potency varies similarly between receptor subtypes (glycine EC_{50} GluN1/2A = 1.1 μM; GluN1/2B = 0.72 μM; GluN1/2C = 0.34 μM; GluN1/2D = 0.13 μM) (Traynelis et al., 2010b). Subtype dependence of glutamate and glycine potency and maximal probability of being open (max P_{open}) are influenced by the GluN2D NTD and NTD-LBD linker (Figure 3A) (Yuan et al., 2009, Gielen et al., 2009). The weighted time constant (τ_w) of deactivation following rapid glutamate removal also varies

significantly with the identity of the GluN2 subunits. GluN1/2A receptors have the fastest τ_w (~50-130 ms), followed by GluN1/2B and GluN1/2C (~300-400 ms), and GluN1/2D subunits (>1 second) (Yuan et al., 2009, Monyer et al., 1992, Vicini et al., 1998, Wyllie et al., 2013, Monyer et al., 1994). The τ_w of NMDARs plays an important role in determining the time course of excitatory post synaptic potentials (EPSCs), along with total charge transfer when NMDARs are activated (Lester et al., 1990, Tovar and Westbrook, 2012, Dingledine et al., 1999).

1.4.6 Channel properties

NMDARs can be split into two categories with regard to channel properties: GluN1/2A-like and GluN1/2D-like (Figure 3B). GluN1/2B receptors, which have similar channel properties to GluN1/2A receptors, are considered GluN2A-like; GluN1/2C receptors, which have similar channel properties to GluN1/2D receptors, are considered GluN1/2D-like. GluN1/2A-like receptors show higher potency of Mg^{2+} block (IC_{50} at -65 mV ~45 μM) than GluN1/2D-like receptors (IC_{50} at -65 mV ~200 μM) (Siegler Retchless et al., 2012). Siegler Retchless et al. examined the relative Ca^{2+} permeability of NMDAR subtypes by calculating reversal potentials in various concentrations of extracellular Ca^{2+}. Ca^{2+} permeability was found to be greater in GluN1/2A-like receptors than GluN1/2D receptors (Burnashev et al., 1995, Schneggenburger, 1996). GluN1/2A-like and GluN1/2D-like receptors show differences in single channel conductance (Burnashev et al., 1995, Schneggenburger, 1996, Siegler Retchless et al., 2012). GluN1/2D-like receptors show a main conductance state ~35 pS and subconductance state of ~20 pS while GluN1/2A-like receptors show a main conductance single-channel conductance of ~50 pS, with a ~40 pS subconductance (Siegler Retchless et al., 2012, Stern et al., 1992, Stern et al.,

1994, Wyllie et al., 1996). Inherent V_m dependence of gating occurs in NMDARs and was found to be larger in GluN1/2A and GluN1/2B receptors compared to GluN1/2D receptors (Siegler Retchless et al., 2012, Clarke et al., 2013, Clarke and Johnson, 2008). Siegler Retchless et al. identified a site in GluN2 subunits, called the "GluN2 S/L site" that dictates the subtype dependence of channel properties including single-channel conductance, Ca^{2+} permeability, Mg^{2+} inhibition (Figure 3A). Subsequent work revealed that the subtype dependence of inherent V_m dependence of gating also depends on the GluN2 S/L site (Clarke et al., 2013). The GluN2 S/L site is a serine (S) in GluN2A and GluN2B receptors, and a leucine (L) in GluN2C and GluN2D receptors. Astoundingly, mutation of the GluN2 S/L site in GluN2A receptors (GluN2A(S632)) to leucine results in a nearly complete switch of GluN2A-like channel properties to GluN2D-like channel properties.

A

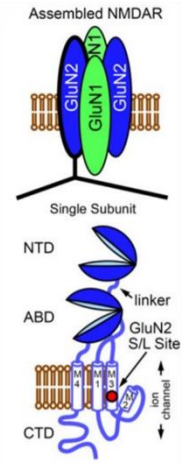

B

NMDAR Subtype	Gating and Ligand-Binding Properties: GluN2 NTD-Dependent						Channel Properties: GluN2 S/L Site-Dependent			
	Maximal P_{open}	Agonist Potency	Deactivation Kinetics	Zn^{2+} Sensitivity	Proton Sensitivity	Ifenprodil Sensitivity	Mg^{2+} Sensitivity	Ca^{2+} Permeability	Single-Channel Conductance	Inherent V_m Dependence
	Low - High	Low - High	Slow - Fast	Low - High	Low - High	Low - High	Low - High	Low - High	Low - High	None - Strong
GluN1/2A										
GluN1/2B										
GluN1/2C										
GluN1/2D										

Figure 3 NMDAR structure and subtype dependent function

A, cartoon of NMDAR GluN1/2 receptor in membrane (top). Bottom, schematic of a single GluN2 subunit with the GluN2 S/L site, NTD – ABD linker, and ion channel labelled. B, table of subtype-dependent NMDAR gating and ligand-binding properties, which are GluN2 NTD-dependent, and subtype-dependent channel properties, which depend on the GluN2 S/L site. Figure adapted from (Glasgow et al., 2015).

1.5 The Structural and Functional Role of the TMD

As outlined in Section 1.4.3, the TMD contains three transmembrane helices M1, M3 and M4, and a re-entrant loop M2 that lines the ion channel (Figure 1A-C, Figure 4). The TMD is central to NMDAR function and its structural components contribute to receptor gating, Mg^{2+} block, and Ca^{2+} permeability.

1.5.1 Determinants of gating

The M3 transmembrane helices from each subunit in an assembled receptor form a "bundle crossing" near the extracellular side of the membrane (Figure 3C, 4A). The M3 bundle crossing is thought to act as the channel gate. When the tips of the M3 regions are huddled together near the extracellular side of the membrane, they form a physical block between the extracellular space and the ion channel (Song et al., 2018). The M3 regions splay apart during receptor activation and allow access between the extracellular solution and the channel. The M3 regions are linked to the ABD through a short linker, which plays an important role in coupling agonist binding with channel opening.

The M3s house an important amino acid motif, SYTANLAAF, that is almost fully conserved in animal iGluRs (Hansen et al., 2018). This highly conserved region is located near the bundle crossing in intact receptors. Mutation of the eighth residue in the nine-residue SYTANLAAF motif, Alaine (A), to threonine (T) ("A8T") in the δ2 glutamate receptor was found to cause lurching ataxic movements in mice containing a single copy (called "*lurcher"* mice) (Phillips, 1960, Zuo et al., 1997). Mice homozygous for the A8T mutation died at birth. The A8T mutation was found to cause constitutive (i.e. agonist-independent) activation of δ2 receptors that resulted in cerebellar neurodegeneration and ataxia (Zuo et al., 1997). Similarly, modification of several locations in the SYTANLAAF motif in NMDARs generate constitutively open channels (Sobolevsky et al., 2007, Kashiwagi et al., 2002, Jones et al., 2002, Yuan et al., 2005, Beck et al., 1999). The extreme conservation of the SYTANLAAF motif, along with decoupling of agonist binding and gating in NMDAR SYTANLAAF mutant receptors suggest that this motif is critical for normal NMDAR function. Recent evidence suggests that the SYTANLAAF motif may interact

with the pre-M1 (Figure 4B,C) and pre-M4 regions located just extracellular to the TMD to influence gating (Chen et al., 2017, Fedele et al., 2018).

Work by Amin et al. has revealed that the M4 segment also plays an important role in receptor gating. A conserved glycine on the extracellular side of the M4 region was found to be crucial for receptor activation, serving as a hinge that allows pore opening (Amin et al., 2018). In GluN1 and GluN2 subunits, mutations at the conserved glycine increased mean closed times and altered receptor deactivation. In a separate study, Amin et al. conducted a tryptophan scan of the GluN1 and GluN2A M4 regions. The introduction of a large, bulky tryptophan at many regions in the M4 resulted in substantially altered gating, and mutation of residues at the extracellular end of the M4 resulted in receptors that failed to gate altogether. This suggests that the M4 region participates in important gating interactions (Amin et al., 2017).

Investigation of NMDAR inhibition by ethanol suggested that intersubunit interfaces in the TMD are important for gating. Ethanol modulates NMDAR gating (Peoples et al., 1997, Wright et al., 1996). Ren et al. identified residues along the GluN1 M3 – GluN2A M4 and GluN1 M4 – GluN2A M3 interfaces that are critical to ethanol sensitivity (Ren et al., 2012). Functional residue interactions that influence ethanol sensitivity and receptor deactivation were found between the GluN1(G638) and GluN2A(M823), GluN1(F639) and GluN2A(M823), GluN1(M818) and GluN2A(P636), and GluN1(L819) and GluN2A(F636) positions. The last pair was also found to influence desensitization. Similarly, six pairs of residues at the GluN1 M3 – GluN2B M4 and GluN1 M4 – GluN2B M3 interfaces were found to influence ethanol sensitivity in GluN1/2B receptors (Zhao et al., 2016). Additionally, work by Buck et al. suggested a role for GluN1 M2 – GluN2 M3 interface in NMDAR gating. Mutation of GluN1(W611), predicted to face the GluN2

M3 region (Siegler Retchless et al., 2012), to leucine caused increased channel mean open time (Buck et al., 2000).

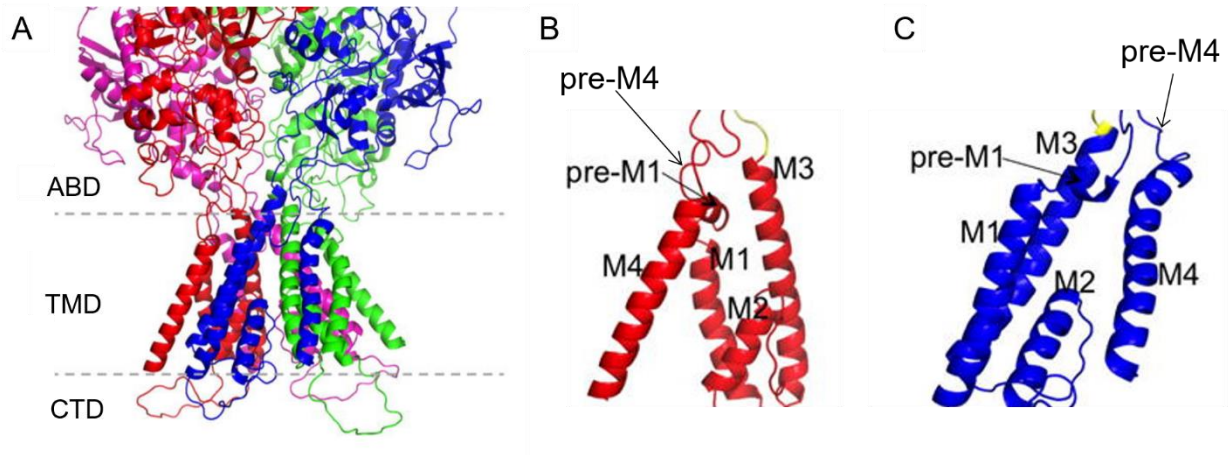

Figure 4 Arrangement of TMD regions

A, TMD of NMDAR from PDB 4TLM (Lee et al., 2014) with residues missing in the TMD modeled (Amin et al., 2017). GluN1 subunits are in blue and magenta; GluN2B subunits are in red and green. "Bundle crossing" where M3 regions come together near the extracellular (ABD-proximal) end of the TMD of the membrane is shown from the side. B, View of organization within the GluN2B TMD showing the relative arrangement of the M1-M4, pre-M1 and pre-M4 regions. C, View of organization within the GluN1 TMD showing the relative arrangement of the M1-M4, pre-M1 and pre-M4 regions. Figure adapted from Pang et al (Pang and Zhou, 2017).

1.5.2 Determinants of Mg^{2+} block and Ca^{2+} permeability

The M2 reentrant loop is composed of a helical segment and an extended region. The extended region greatly influences ion permeation and block in NMDARs. The extended region

of each subunit contains a residue called the Q/R/N site, which is a critical determinant of Ca^{2+} permeability (Burnashev et al., 1992a, Burnashev et al., 1992b, Egebjerg and Heinemann, 1993), single-channel conductance (Swanson et al., 1997, Swanson et al., 1996, Traynelis and Wahl, 1997), and channel block of iGluRs (Burnashev et al., 1992b, Mori et al., 1992, Kashiwagi et al., 2002, Bowie and Mayer, 1995). NMDARs have an asparagine at the Q/R/N site, called the N-site in NMDARs. The asparagines at the N-site in GluN1 and GluN2 subunits, and at the neighboring N+1 site in GluN2 subunits, have been shown to be critical for Mg^{2+} block and Ca^{2+} permeability (Burnashev et al., 1992b, Kashiwagi et al., 2002, Kuner and Schoepfer, 1996, Mesbahi-Vasey et al., 2017).

In addition to residues in the selectivity filter, non-pore-lining residues are important for Mg^{2+} bock. The GluN2 S/L site that dictates subtype-dependence of channel properties (Figure 2A, Section 1.4.6) is located on the GluN2 M3 region facing toward the GluN1 M2. It was initially surprising that a single residue facing away from the pore could be the key determinant of subtype-dependent channel properties. Siegler Retchless et al. sought to understand the mechanism through which the GluN2 S/L site mediated its effects. The results of mutant cycle analysis revealed that the residue at the GluN2A S/L site (GluN2A(S632)) interacts with a tryptophan (GluN1(W608)) predicted to lie across the intersubunit interface to influence Mg^{2+} IC_{50}. The tryptophan at position GluN1(608) is conserved at the homologous location in GluN2A-D subunits, suggesting that maintaining tryptophan at this site is functionally important. Interestingly, mutation of the homologous tryptophan in GluN2B (GluN2B(W607)) nearly abolishes Mg^{2+} block. Williams et al. found that mutation of GluN2B(W607) to non-aromatic residues (residues excluding phenylalanine and tyrosine) resulted in reduced Mg^{2+} potency, increased Ba^{2+} permeation, and increased Mg^{2+} permeation (Williams et al., 1998). Kashiwagi et al. observed that mutation of

GluN2B(W607) to non-aromatic residues influenced pore block by drugs in addition to Mg^{2+} (Kashiwagi et al., 2002). Evidence suggests that GluN2B(W607) plays a role in supporting NMDAR channel structure that can only be fulfilled by an aromatic residue (McMenimen et al., 2006). Recently, GluN2B(W607C) was identified as a disease-associated mutation in human NMDARs that causes decreased Mg^{2+} block of NMDARs in addition to decreased surface expression and agonist potency (Vyklicky et al., 2018). Structural and modeling evidence indicate that GluN2B(W607) likely faces toward the GluN1 M3 region, suggesting that M2 – M3 interfaces between adjacent subunits are important for channel permeation and block (Vyklicky et al., 2018, Mesbahi-Vasey et al., 2017, Song et al., 2018, Fedele et al., 2018).

Much like Mg^{2+} block, Ca^{2+} permeation is influenced by residues in addition to the N and N+1 sites at the selectivity filter. Residues in the GluN1 subunit form an interesting amino acid motif (DRPEER) that lies just extracellular to the channel gate in assembled receptors (see Section 1.5.2). Residues within the DRPEER motif are important influencers of Ca^{2+} permeability. The DRPEER amino acid motif is thought to bind Ca^{2+} in the external vestibule and promote its entry into the pore (Watanabe et al., 2002). Neutralization of the negatively charged residues aspartate (D) and glutamate (E) results in NMDARs with reduced Ca^{2+} permeability without affecting block by Mg^{2+} (Watanabe et al., 2002). Recently, a conserved glycine residue, which is linked to genetic disorders when mutated, was also shown to be critical to Ca^{2+} permeability (Amin et al., 2018). The conserved glycine lies near the extracellular region of the M4 helix in GluN1 and GluN2 subunits and its mutation caused reduced Ca^{2+} influx by preventing the expansion of the selectivity filter.

1.6 Modulators of NMDAR Function

Numerous modulators of NMDAR function exist, and act through several different pathways. Orthosteric antagonists, commonly referred to as competitive antagonists, bind in the NMDAR agonist binding pockets to inhibit the receptor. Positive allosteric modulators (PAMs) of NMDARs enhance the activity of the receptor through binding to non-orthosteric sites (Hackos and Hanson, 2017). Negative allosteric modulators (NAMs) decrease the activity of the receptor through binding to non-orthosteric sites. A recurring theme in NMDAR modulation is the receptor's immense allostery, which allows functional communication between distant regions. Further, stereotyped configurations of receptor domains, particularly the NTD and ABD, seem to consistently affect NMDAR function. Several intriguing NMDAR modulators that lend insight into NMDAR structure and function are detailed below.

1.6.1 Orthosteric antagonists

Glutamate and glycine site antagonists share structural similarity with glutamate and glycine and were very useful in early investigation of NMDAR structure and function. Evidence from orthosteric site agonists and antagonists suggests that agonists induce closure of the ABD clamshell, whereas antagonists stabilize open-clamshell states (Zhu et al., 2016, Zhou, 2017, Paganelli et al., 2013, Romero-Hernandez et al., 2016). LBD clamshell closure may initiate M3 splaying, causing opening of the bundle crossing. Two well-known orthosteric antagonists are the glutamate site antagonist 2-amino-5-phosphonovalerate (APV) and the glycine site antagonist 7-chlorokynurenic acid (7CK). APV was discovered in the 1980s and used to push forward knowledge about the role of NMDARs in LTP, epilepsy, and pain (Davies et al., 1981, Lodge et

al., 2019). In 1988, 7CK was developed and found to be a competitive glycine site antagonist (Kemp et al., 1988). Both 7CK and APV were used to predict that the NMDAR bound two glutamate and two glycine molecules decades before structural information was available (Benveniste and Mayer, 1991).

1.6.2 Inhibition by protons

GluN1-a/2A and GluN1-a/2B receptors are ~50% inhibited by protons at pH 7.3, while GluN1-a/2D receptors are ~50% inhibited by protons at pH 7.2. GluN1/2C receptors are less sensitive to proton inhibition, and are ~50% inhibited by protons at pH 6.2 (Traynelis et al., 1995). In addition to GluN2 subunit identity, GluN1 splice variants influence proton sensitivity. Receptors composed of exon 5-containing GluN1 subunits are less sensitive to proton inhibition than receptors with exon 5-lacking subunits, showing 50% inhibition of response at pH 6.6 – 6.7 in GluN1/2A, GluN1/2B, and GluN1/2D receptors. Mutation of residues in exon 5 revealed that substitution of lysine 211 greatly reduced the effect of exon 5 on proton inhibition (Traynelis et al., 1995). This suggests that exon 5 acts as a pH-sensitive modulator of receptor function.

Recently, structures of GluN1/2A receptors at pH 6.3 and 7.8 were resolved by cryo-electron microscopy (cryo-EM) (Zhang et al., 2018). Through comparison of the structures at different pH's the authors concluded that protons act primarily on the NTD. Low pH resulted in NTD clamshell closure stemming from increased distance between the R2 lobes (Figure 5). This is in agreement with electrophysiological experiments that have linked NTD clamshell closure to inhibition and NTD clamshell opening to potentiation (Yuan et al., 2009, Gielen et al., 2008). Closure of the NTD clamshell is thought to induce changes in gating through inter and intra-subunit interfaces with the ABD.

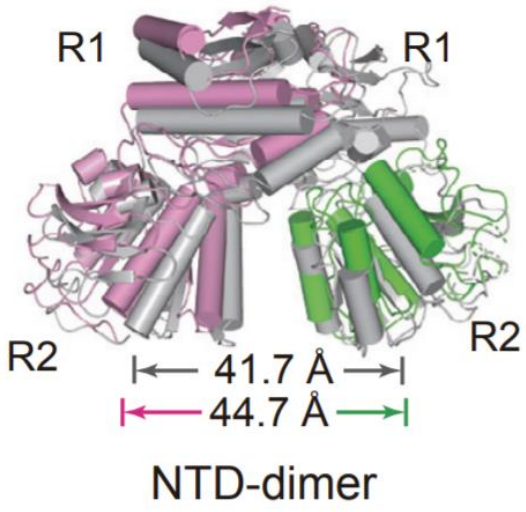

Figure 5 pH-dependent changes in the NMDAR NTD

Overlay of NTD structures at pH 6.3 and 7.8. The pH 6.3 structure shows the GluN1 subunit in pink and the GluN2A subunit in green. The pH 7.8 structure shows the GluN1 and GluN2A subunits in gray. The distance between the R2 lobes is larger at pH 6.3 than pH 7.8, consistent with clamshell closure. Figure from (Zhang et al., 2018).

1.6.3 GluN2A and GluN2B subunit-specific negative allosteric modulators

Zn^{2+} selectively inhibits GluN1/2A receptors through an NTD-mediated mechanism (Legendre and Westbrook, 1990, Christine and Choi, 1990, Karakas et al., 2009). GluN1-1b/2A receptors are inhibited by Zn^{2+} with lower potency than GluN1-1a/2A receptors. Site-directed mutagenesis of exon 5 revealed that lysine 211 mediates the effect of exon 5 on Zn^{2+} inhibition (Traynelis et al., 1995). The same residue was implicated in proton inhibition of NMDARs. Further exploration of GluN1 residues outside of exon 5 revealed that several residues important for proton

inhibition of NMDARs are also important for Zn^{2+} inhibition of NMDARs. Therefore, Zn^{2+} is thought to inhibit NMDARs by increasing their pH sensitivity (Choi and Lipton, 1999, Traynelis et al., 1995, Zheng et al., 2001). Evidence suggests that Zn^{2+} binds in the cleft of the GluN2A NTD and induces closure of the GluN2A NTD clamshell (Romero-Hernandez et al., 2016, Karakas et al., 2009). Stabilization of the closed conformation of the GluN2A NTD induces allosteric changes in the ABD that favor channel closure (Gielen et al., 2008, Romero-Hernandez et al., 2016). Of note, Zn^{2+} also causes subtype-independent V_m-dependent inhibition of NMDAR receptors at high concentrations (μM) relative to GluN2A-selective inhibition. This is thought to occur through Zn^{2+} occupancy of a binding site in the pore (Mayer and Vyklicky, 1989, Christine and Choi, 1990, Legendre and Westbrook, 1990).

Phenylethanolamines are GluN2B-specific inhibitors that bind in the NTD at the interface of the GluN1 R1 and GluN2B R2 lobes (Karakas et al., 2011). Ifenprodil exemplifies the effects of phenylethanolamines on GluN1/2B receptors (Gallagher et al., 1996, Williams, 1993). Several NMDAR structures with ifenprodil bound have become available in recent years (Karakas et al., 2009, Karakas and Furukawa, 2014). Analogous to Zn^{2+} in GluN2A-containing receptors, ifenprodil binds in the GluN2B NTD region (Karakas et al., 2009). Comparing ifenprodil-bound with the apo NTD structures reveals that ifenprodil causes the NTD R2 domains to splay apart, initiating clamshell closure (Tajima et al., 2016). Like Zn^{2+} inhibition of GluN1/2A receptors, ifenprodil inhibition is pH-dependent. Ifenprodil is more potent at lower pH (Pahk and Williams, 1997), and may enhance the inhibitory effects of protons (Mott et al., 1998). Unlike Zn^{2+}, ifenprodil inhibits NMDARs approximately equally in the presence and absence of exon 5.

1.6.4 GluN2B-specific positive allosteric modulators

Spermine and other polyamines show subtype-dependent potentiation of NMDARs. Spermine potentiates NMDAR responses in conditions of saturating glycine (glycine-independent potentiation) (Benveniste and Mayer, 1993, Lerma, 1992, Rock and MacDonald, 1992) and also in conditions of non-saturating glycine (glycine-dependent potentiation) through different mechanisms (Benveniste and Mayer, 1993, McGurk et al., 1990). Glycine-dependent potentiation involves an increase in NMDAR affinity for glycine. Glycine-independent potentiation occurs only at GluN1/2B receptors that contain exon 5-lacking GluN1 subunits (e.g. GluN1-1a). As with inhibition of NMDARs by Zn^{2+} and ifenprodil, evidence suggests that spermine acts through regulating proton inhibition of NMDARs (Traynelis et al., 1995). By shielding negative charges present on GluN1 and GluN2B NTD R2 regions, spermine and other polyamines may allow the NTD lower lobes to remain close to one another, discouraging NTD clamshell closure (Mony et al., 2011). Separate from its mechanism of GluN2B-specific potentiation, spermine also blocks NMDARs in a V_m-dependent manner (Araneda et al., 1999, Benveniste and Mayer, 1993).

1.6.5 Actions of steroids at NMDARs

Numerous neurosteroids and steroid precursors exist in the brain and may modulate NMDAR function. Pregnenolone sulfate (PS) is a hydrophobic neurosteroid well-known for endogenous antagonism of $GABA_A$ receptor function (Wang, 2011, Shen et al., 2000, Chen et al., 2019). Data suggest that PS also has complex and varied effects on NMDARs. PS was initially shown to modulate NMDARs in a subtype-dependent manner, potentiating GluN1/2A and GluN1/2B receptors and inhibiting GluN1/2C and GluN1/2D receptors (Malayev et al., 2002). The

basis of subtype dependence of PS action was proposed to stem from differences in the GluN2 ABD (Jang et al., 2004, Horak et al., 2006). At GluN1/2A and GluN1/2B receptors, PS increases the NMDAR current at saturating agonist concentrations, and increases glutamate and glycine potency at subsaturating agonist conditions (Malayev et al., 2002). One publication proposed that PS induces Ca^{2+} influx through GluN1/2A and GluN1/2B receptors in the absence of agonist, although the NMDAR dependence of PS-induced Ca^{2+} influx has not been directly tested (Adamusova et al., 2013). Work by Chopra et al. suggests that Ca^{2+} and the intracellular milieu are powerful mediators of PS action. Heterologously expressed GluN1/2A receptors in cells with intact intracellular milieu (perforated patch technique) show greater modulation in response to PS than dialyzed cells. Interestingly, in both dialyzed and perforated patched cells, GluN1/2A receptors responses can be either potentiated *or* inhibited by the same concentration of PS, depending on external Ca^{2+} concentration (Chopra et al., 2015) .

Another neurosteroid, pregnanolone sulfate (PAS), inhibits NMDARs in a use-dependent and voltage-independent manner (Vyklicky et al., 2015). PAS inhibits NMDARs by increasing occupancy of desensitized states (Kussius et al., 2009). A synthetic analog of PAS (PAS-6) and similar molecules exhibit unusually slow kinetics of NMDAR inhibition, atypical for molecular interactions with the NMDAR in aqueous solution (Borovska et al., 2012). Recovery from inhibition by PAS-6-like molecules was accelerated by cyclodextrin, which was used to alter the cholesterol content of the plasma membrane (Borovska et al., 2012). Additionally, the membrane capacitance was found to increase in response to application of PAS, and return to baseline after PAS washout. These experiments suggest that PAS may affect NMDARs by first partitioning into the membrane. Other experiments found that binding of negatively charged PAS analogs is disrupted by mutations to the SYTANLAAF motif (Vyklicky et al., 2015), suggested binding to

regions near the NMDAR bundle crossing. Interestingly, positively-charged PAS analogs show V_m-dependent inhibition, much like positively charged open-channel blockers (Vyklicky et al., 2015).

Physiological cholesterol modulates NMDARs. Cholesterol depletion from NMDAR-containing plasma membranes decreased NMDAR P_{open} and increased entry into desensitized states (Korinek et al., 2015, Sibarov et al., 2018). Physiological NMDAR modulation by cholesterol and its breakdown products may be quite complex. Cholesterol breakdown product 24-S-hydroxycholesterol appears to potentiate NMDARs independent of subtype, while 25-S-hydroxcholesterol antagonizes the effects of 24-S-hydroxycholesterol (Linsenbardt et al., 2014). Additionally, although oxysterols are thought to partition into the plasma membrane to act on NMDARs, application of oxysterols to the intracellular space was found to have no effect on NMDAR function (Linsenbardt et al., 2014).

1.6.6 Inhibition by open channel blockers

Open channel blockers are another class of drugs that inhibit NMDARs. The mechanism of action of these molecules is well-described by their name: they enter open NMDAR channels. Several open-channel blockers are very useful therapeutically. Memantine is an NMDAR open-channel blocker widely used for the management of Alzheimer's disease, and is also being explored for treatment of Huntington's disease and ischemia (Witt et al., 2004, Emre et al., 2010, Kafi et al., 2014, Okamoto et al., 2009, Dau et al., 2014). Ketamine, a recently FDA-approved treatment for depression, is also an open channel blocker. Open channel blockers are described in detail in the next section.

1.7 Mechanisms of Open Channel Block

Open channel blockers are NMDAR inhibitors that bind in the pore, and require opening of the NMDAR channel to bind and unbind from their binding site (MacDonald et al., 1991, Wong et al., 1986). They are typically thought to reach their binding site from the extracellular space, though inhibition by intracellular open-channel blockers is also known to occur (Berretta and Jones, 1996). Open channel blockers can be further categorized as "foot-in-the-door" blockers and trapping blockers. Foot-in-the-door blockers bind in a manner that occludes the flow of ions while preventing channel closure. Examples of NMDAR foot-in-the-door blockers include 9-aminoacridine (Benveniste and Mayer, 1995), tetrahydroaminoacridine (Vorobjev and Sharonova, 1994), tetrapentylammonium (Sobolevsky, 2000, Sobolevsky et al., 1999) and bupivacaine (Paganelli and Popescu, 2015). Trapping blockers allow channel closure while bound, causing the blocker to become trapped inside closed receptors. Examples of well-known and mechanistically interesting open channel blockers are described below.

1.7.1 Memantine

Memantine is a rare clinical success story among NMDAR antagonists: it is tolerated very well, with few side effects (Muir, 2006, Gladstone et al., 2002). Memantine is typically administered orally and has 100% bioavailability (Robinson and Keating, 2006). Memantine is excreted intact in urine (Robinson and Keating, 2006), suggesting that memantine itself, rather than its breakdown products, mediates therapeutic efficacy. Memantine's binding site in the pore resides near the selectivity filter where 6 asparagine residues are clustered (Kashiwagi et al., 2002, Chen and Lipton, 2005, Kotermanski et al., 2009). This binding site is accessible from the

extracellular space when agonist is present and the channel is open, and is thought to overlap with the Mg^{2+} binding site (Glasgow et al., 2018, Kotermanski et al., 2009, Kotermanski and Johnson, 2009).

Memantine is a partial trapping channel blocker (Blanpied et al., 1997, Kotermanski et al., 2009, Mealing et al., 1999, Sobolevsky et al., 1998), which means that a fraction of memantine unbinds from closed NMDARs. Memantine was shown to have several unique properties, including stabilization of Ca^{2+}-dependent desensitized states (Glasgow et al., 2017). This results in memantine preferentially inhibiting receptors exposed to high intracellular Ca^{2+}, which may contribute to its therapeutic efficacy in Alzheimer's disease. Although memantine is subtype independent in the absence of Mg^{2+}, it inhibits GluN1/2C and GluN1/2D receptors more potently than GluN1/2A and GluN1/2B receptors in the presence of physiological Mg^{2+} (Kotermanski and Johnson, 2009). Therapeutic brain concentrations of memantine are low compared to the GluN1/2A and GluN1/2B memantine IC_{50}s in the presence of physiological Mg^{2+}, suggesting that some of memantine's therapeutic actions may be mediated by GluN1/2C and GluN1/2D receptors (Povysheva and Johnson, 2016).

Interestingly, when concentrations of memantine several fold higher than its channel blocking IC_{50} are applied in the absence of agonist and briefly washed away, subsequent agonist application shows NMDAR inhibition. NMDAR inhibition following memantine application in the absence of agonist has been attributed to the binding of memantine to two sites: the site in the pore that gives rise to open-channel block ("the deep site") and a "superficial site" that is accessible in closed receptors (Blanpied et al., 1997, Sobolevsky and Koshelev, 1998, Sobolevsky et al., 1998, Chen and Lipton, 2005, Kotermanski et al., 2009). Reported memantine IC_{50} at the superficial site is quite high, ranging from 79-179 μM (Kotermanski et al., 2009, Blanpied et al.,

1997). It is currently unclear whether memantine acting through two mechanisms is significant to its clinical utility.

1.7.2 Ketamine

Like memantine, ketamine is a clinically useful NMDAR inhibitor. Ketamine has been used as a pediatric anesthetic and analgesic (Durrmeyer et al., 2010, Hall and Shbarou, 2009), and more recently, as an anti-depressant (Schwartz et al., 2016). However, ketamine administration requires physician oversight because it can cause dissociative effects and psychotomimetic behavior. Ketamine is suggested to bind near the selectivity filter in the pore, overlapping with the Mg^{2+} binding site (Johnson et al., 2015, MacDonald et al., 1991). However, it is unclear whether ketamine's antidepressant effects are due to NMDAR inhibition or other targets of ketamine or ketamine breakdown products (Zanos et al., 2016).

1.7.3 MK-801

MK-801's open-channel block mechanism was discovered over three decades ago (Huettner and Bean, 1988, Foster and Wong, 1987, Wong et al., 1986) and MK-801 has been used to block NMDARs in many experiments ever since. Recovery of NMDARs from block by MK-801 in the presence of agonist was found to be extremely slow at negative voltages (order of minutes), making MK-801 useful for "irreversible" NMDAR inhibition on the timeline of many experiments. MK-801 unblock occurs much faster at positive voltages (Huettner and Bean, 1988). NMDAR recovery from MK-801 inhibition in the presence of agonist was found to be accelerated by Mg^{2+} and memantine, suggesting that the slow unbinding of MK-801 arises partially from the

subsequent unbinding and re-binding of MK-801 to the NMDAR (McKay et al., 2013). MK-801 binds in the pore with its positive charge facing the 6 asparagines (Song et al., 2018, Reynolds and Miller, 1988). Recent structural data suggest that during MK-801 pore block, two aromatic rings of MK-801 lie near the GluN1 M3 region, close to GluN1(V642), while the methyl substituent lies near GluN2B(L640) (Song et al., 2018). Mutation of GluN1(V642) eliminates MK-801 binding.

MK-801 also inhibits NMDARs from the intracellular space, though at high concentrations (mM) relative to the IC_{50} of external MK-801 (nM). (Berretta and Jones, 1996, Sun et al., 2018). MK-801 is seemingly too large to reach its binding site through direct diffusion into the pore from the intracellular region, suggesting that NMDAR inhibition by intracellular MK-801 may occur through a more complex mechanism. Sun et al. found that the intracellular MK-801 has an affinity for NMDARs ~30,000 times less potent than extracellular MK-801, suggesting that it behaves very differently from extracellular MK-801 at NMDARs (Sun et al., 2018).

1.8 Dissertation Contents

The work discussed in this dissertation centers around the NMDAR TMD. I began work in the Johnson lab shortly after the publication of their work on the GluN2 S/L site detailing its critical role in influencing subtype-dependent properties (Siegler Retchless et al., 2012). My first project in the lab involved exploring the functional role of intersubunit interactions in the TMD, and in particular, the role of a conserved M2 tryptophan that, in GluN1, interacts with the GluN2A S/L site (Chapter 2). I then performed experiments on the mechanism of "superficial site" block by memantine, which were included in a publication by former graduate student Nathan Glasgow

(Chapter 3) (Glasgow et al., 2018). Intrigued by the unique mechanism of memantine binding to the “superficial site”, I continued to explore non-traditional actions of open-channel blockers (Chapter 4).

2.0 Role of a Conserved Tryptophan at Intersubunit Interfaces in NMDA Receptors

2.1 Summary

My coauthors and I examined the role of a tryptophan residue in NMDA receptors (NMDARs) that is conserved in ionotropic glutamate receptor (iGluR) subunits and similar proteins. This conserved tryptophan lies at an intersubunit interface in the transmembrane domain (TMD). In a previous publication the tryptophan in GluN1 (GluN1(W608)) was found to interact with GluN2A(S632) to influence NMDAR subtype-dependent channel properties. We examined whether GluN1(W608) and GluN2A(S632) are in close physical proximity, as predicted by structural models, by mutating both residues to cysteine and probing for intersubunit disulfide linkages. Using Western blot and tandem mass spectrometry, we confirmed that GluN1(W608C) and GluN2A(S632C) crosslink, and therefore, are in close proximity. Examining the cysteine mutant receptors electrophysiologically, we noted slowed deactivation kinetics in GluN1(W608C)/2A receptors. Through mutant cycle analysis we discovered that the GluN1(608) and GluN2A(632) positions couple to influence deactivation kinetics. Therefore, intersubunit interfaces in the TMD can influence receptor kinetics as well as permeation properties. We next examined the homologous tryptophan in GluN2A subunits. Using molecular modeling, we predicted that GluN2A(W606) lies across the intersubunit interface from, and in close proximity to, GluN1(M634). We mutated GluN1(M634) and GluN2A(W606) to cysteine and examined the mutant receptors electrophysiologically. We found that GluN1(M634C) interacts with GluN2A(W606C) to influence Mg^{2+} IC_{50}. However, we found no evidence of biochemical crosslinking between GluN1(M634C) and GluN2A(W606C). Last we examined the conserved

tryptophan in GluN2B subunits. We examined whether, as in GluN1/2A receptors, a cysteine introduced at the site of the conserved tryptophan in GluN2B subunits interacts with GluN1(M634C) to influence Mg^{2+} IC_{50}. Surprisingly, GluN2B(W607C)-containing receptors showed potentiation in response to Mg^{2+} at negative potentials. After compensating for the large Mg^{2+} potentiation in GluN2B(W607C)-containing receptors we identified that block by Mg^{2+} occurs in GluN1/2B(W607C) and GluN1(M634C)/2B(W607C) receptors, though it is less potent and less efficacious than in wildtype GluN1/2B receptors. Interestingly, while the GluN2B(W607C) mutation increases Mg^{2+} IC_{50} in GluN1/2B receptors and the GluN1(M634C) mutation does not, the opposite is true at the homologous residues in GluN1/2A receptors. This reveals a striking role reversal in the effect on Mg^{2+} block of mutating GluN1(M634) and the GluN2 conserved tryptophan in GluN1/2A and GluN1/2B receptors. Thus, residues at intersubunit interfaces in the NMDAR TMD are critical to gating and block, but the effects of interface mutations are strongly subtype dependent.

2.2 Introduction

NMDA receptors (NMDARs) are ionotropic glutamate receptors (iGluRs) that are central to learning and memory (Nicoll, 2017, Li and Tsien, 2009), and also implicated in neurological disease and neurodegeneration (Kayser and Dalmau, 2011, Hallett and Standaert, 2004, Zhou and Sheng, 2013, Zhang et al., 2016, Balu, 2016). NMDARs are composed of two GluN1 and two GluN2(A-D) or GluN3(A,B) subunits (Traynelis et al., 2010b). Each subunit contains an amino-terminal domain (NTD), agonist binding domain (ABD), transmembrane domain (TMD), and C-terminal domain (CTD). The NTD and ABD are extracellular, while the CTD is intracellular.

Linking extra- and intracellular domains is the membrane-embedded TMD. The GluN1 and GluN2 subunits share high sequence homology (Monyer et al., 1992) and have very similar structures in the TMD (Traynelis et al., 2010b). The TMD of each subunit contains three transmembrane helices (M1, M3, M4) and a re-entrant loop (M2) that lines the ion channel. The M2 region is composed of an alpha helix and an extended region, which forms the selectivity filter. In the extended region of the M2, asparagines (N) at the Q/R/N site and the adjacent N+1 site have been found to be critical to block of NMDARs by Mg^{2+} and other channel blockers (Burnashev et al., 1992b, Kashiwagi et al., 2002, Kuner and Schoepfer, 1996, Wollmuth et al., 1998). These asparagines have been suggested to coordinate Mg^{2+} in the channel, giving rise to V_m-dependent Mg^{2+} block of NMDARs (Mesbahi-Vasey et al., 2017, Burnashev et al., 1992b, Kashiwagi et al., 2002, Kuner and Schoepfer, 1996, Wollmuth et al., 1998).

In the fully assembled NMDAR, subunits are in an alternating GluN1-GluN2-GluN1-GluN2 conformation (Traynelis et al., 2010b, Karakas and Furukawa, 2014, Lee et al., 2014). Therefore, within each receptor there are four intersubunit interfaces in the TMD. At these locations, the GluN1 M2 and GluN2 M3, and GluN1 M3 and GluN2 M2 regions come into close contact. Several previous studies have explored the roles of residues at these interfaces. Williams et al. demonstrated that mutation of a GluN2B tryptophan (W; GluN2B(W607)) to non-aromatic residues decreased Mg^{2+} block, increased Mg^{2+} permeation, and decreased Ba^{2+} permeation (Williams et al., 1998). Interestingly, mutation of the homologous residue in GluN1 (GluN1(W608)) and GluN2A (GluN2A(W606)) had little-to-no effect on Mg^{2+} block. Williams et al. speculated that GluN2B(W607) participated in Mg^{2+} coordination and was positioned at the narrow part of the channel constriction. Several years later, Kashiwagi et al. revealed that GluN2B(W607) mutations alter NMDAR block by several channel-blocking molecules with

binding sites that overlap the Mg^{2+} binding site, including memantine, MK-801, and TB-3-4 (Kashiwagi et al., 2002). Like Williams et al. (1998), Kashiwagi et al. suggested that GluN2B(W607) may reside at the narrow construction of the channel. However, Kashiwagi et al. also speculated that GluN2B(W607) could instead form a structural backbone that influences the structure of the pore. In 2006, work by McMenimen et al. confirmed that GluN2B(W607) is involved in maintaining the structure of the pore, possibly through interactions with the GluN1 M3 region (McMenimen et al., 2006).

Siegler Retchless et al. identified a single GluN2 residue at a TMD intersubunit interface that determines the subtype dependence of NMDAR channel properties (Siegler Retchless et al., 2012). GluN1/2A and GluN1/2B receptors show similar channel properties, including Mg^{2+} block, single channel conductance, and selective permeability to Ca^{2+}. The residue, serine (S) in GluN1/2A and GluN1/2B receptors and leucine (L) in GluN1/2C and GluN1/2D receptors (the "GluN2 S/L site"), determines whether NMDAR channel properties are "GluN1/2D-like"or "GluN1/2A-like" (Siegler Retchless et al., 2012). Siegler Retchless et al. used molecular modeling to predict that the GluN2 S/L site faces away from the pore toward the neighboring GluN1 subunit and identified nearby residues through which the GluN2 S/L site could mediate its effect. Mutant cycle experiments were performed by swapping the residues of interest in the GluN1 and GluN2A subunits and examining the Mg^{2+} IC_{50}s of the resulting subunit combinations. Mutant cycle analysis suggested that the GluN2A subunit S/L site (GluN2A(S632)) interacts functionally with GluN1(W608) (which is homologous to GluN2A(W606) and GluN2B(W607)) to produce subtype dependent Mg^{2+} block.

We were intrigued by the conservation of the M2 tryptophan in GluN2, GluN2A, and GluN2B receptors (Figure 1A), as well as residue-residue interactions at intersubunit interfaces in

the TMD. In this work, we set out to explore NMDAR properties mediated by the conserved tryptophan at the TMD intersubunit interface in GluN1, GluN2A, and GluN2B subunits, and to identify interacting residues. We used a molecular model of the NMDAR TMD to identify residues that may interact with the conserved tryptophan in the GluN1, GluN2A, and GluN2B subunits. We then mutated the conserved tryptophan within each subunit, and potential interacting residues, to cysteine (C). We examined whether the introduced mutations interact with one another in GluN1/2A and GluN1/2B receptors through cysteine substitution and Western blotting, electrophysiological mutant cycle analysis, and tandem mass spectrometry. Our results reveal that interactions at intersubunit interfaces in the NMDAR TMD are crucial for determining both receptor gating and channel properties.

2.3 Methods

2.3.1 Cell culture and transfection

Experiments were performed on the tsA201 cell line (The European Collection of Authenticated Cell Cultures), a variant of the HEK 293 cell line. tsA201 cells were maintained as previously described (Glasgow and Johnson, 2014) in DMEM supplemented with 10% fetal bovine serum and 1% GlutaMAX (Thermo Fisher Scientific). 1×10^5 cells/dish were plated in 35 mm petri dishes containing 15 mm glass coverslips treated with poly D-lysine (0.1 mg/ml) and rat-tail collagen (0.1 mg/ml, BD Biosciences). 12–24 h after plating, cells were transiently co-transfected using FuGENE6 Transfection Reagent (Promega) with mammalian expression plasmids that contained cDNAs encoding enhanced green fluorescent protein (EGFP

in pRK7) for identification of transfected cells, the rat GluN1-1a subunit (hereafter GluN1; GenBank X63255 in pcDNA3.1), the rat GluN2A subunit (GenBank M91561 in pcDNA1), or the rat GluN2B subunit (GenBank M91562 in pcDNA1). In some experiments we used cells transfected with GluN1 and an EGFP:pIRES:GluN2A construct, which was a kind gift from Dr. Kasper Hansen (Hansen, unpublished) (Glasgow et al., 2017). Mutagenized with the Stratagene Quik-Change XL sited-directed mutagenesis kit NMDAR subunit cDNAs from isolated colonies were sequenced from 100–200 bases upstream to 100–200 bases downstream of each mutation (University of Pittsburgh Genomics and Proteomics Core Laboratories). cDNA ratios used in transfection were 1:1:1 (EGFP, GluN1, and GluN2A), 1:1 (GluN1 and EGFP:pIRES:GluN2A), or 1:1:2 (EGFP, GluN1, and GluN2B). Following transfection, 200 μM of the competitive NMDAR antagonist D,L-2-amino-5-phosphonopentanoate was added to the media to prevent NMDAR-mediated cell death.

2.3.2 Solutions

The extracellular bath solution contained (in mM): 140 NaCl, 2.8 KCl, 0.1 $CaCl_2$, 10 HEPES, 0.1 glycine, 0.01 EDTA, and osmolality adjusted to 290 ± 10 mOsm with sucrose. Extracellular solution pH was balanced to 7.2 ± 0.05 with NaOH. Intracellular solution contained (in mM) 130 CsCl, 10 HEPES and 10 EGTA with pH balanced to 7.2 ± 0.05 with CsOH and an osmolality of 280 ± 10 mOsm. Tris(2-carboxyethyl)phosphine (TCEP; Sigma), L-glutamate (Sigma) and MgCl (Sigma) were added to solutions on the day of experiments as indicated. Whole cell voltage-clamp recordings were obtained from transfected tsA201 cells 12–48 h after transfection. Pipettes were pulled from borosilicate capillary tubing (Sutter Instruments) on a Sutter Instruments-Flaming Brown P-97 glass puller and polished using a heated filament to a

resistance of 2–5 MΩ. Whole-cell recordings were made from cells expressing EGFP identified by epifluorescence illumination on an inverted Zeiss Axiovert microscope. Cells were held at a membrane potential of −60 mV (corrected for a liquid junction potential of −6 mV) unless otherwise indicated (e.g. +50 mV in Figure 6). For experiments in which high concentrations of Mg^{2+} were used ($[Mg^{2+}] > 2$ mM) the bath was grounded using a flowing KCl bridge. Whole-cell currents were recorded using an Axopatch 200B patch-clamp amplifier (Molecular Devices), low-pass filtered at 5 kHz and sampled at 10 or 20 kHz in pClamp10 (Molecular Devices). Series resistance was compensated 80–90% with prediction and correction circuitry in all experiments. Solutions were delivered to cells attached to the coverslip using a ten-barrel fast perfusion system with 27 ms time constant of solution exchange (Glasgow et al., 2017).

2.3.3 Analysis

All data were analyzed with Clampfit 10.7 (Molecular Devices) or GraphPad Prism 7. For experiments in which Mg^{2+} IC_{50} was measured, steady-state response to glutamate application before and after application of $[Mg^{2+}]$. Experiments in which recovery was <80% were excluded from analysis.

The weighted time constant of deactivation (τ_w) was calculated by fitting a double exponential curve to the deactivation time course following the glutamate wash off after currents reached steady-state using the following formula:

$$\tau_w = \tau_1\left(\frac{A_1}{A_1 + A_2}\right) + \tau_2\left(\frac{A_2}{A_1 + A_2}\right) \qquad \textit{Equation 1}$$

Where A_1 and A_2 are the amplitudes, and τ_1 and τ_2 are time constants, resulting from each of two exponential fits.

IC_{50} was calculated using the following equation:

$$\frac{I_{Mg^{2+}}}{I_{Control}} = A_1 + \frac{(1 - A_1)}{1 + \left(\frac{[Mg^{2+}]}{IC_{50}}\right)^n} \qquad \textbf{Equation 2}$$

Where $\frac{I_{Mg^{2+}}}{I_{Control}}$ is the normalized steady-state current following application of $[Mg^{2+}]$ (concentration of Mg^{2+}) in the presence of agonist, A_1 is the value at saturating Mg^{2+} and n is the Hill coefficient. Data from cells at each $[Mg^{2+}]$ were averaged and a fit was performed to average data to obtain the IC_{50} value.

The mutant cycle coupling coefficient, Ω, was calculated as follows using τ_w:

$$\Omega = \frac{\tau_w GluN1(m)/2A * \tau_w GluN1/2A(m)}{\tau_w GluN1(m)/2A(m) * \tau_w GluN1/2A} \qquad \textbf{Equation 3}$$

Where *(m)* indicates that a subunit contains a mutated residue. **Ω** resulting from mutant cycle analysis of Mg^{2+} IC_{50} was calculated similarly, except using Mg^{2+} IC_{50} values in place of τ_w values.

2.3.4 Plasma membrane preparation and Western blot

Cell lysates were prepared from tsA201 cells transfected with the indicated plasmids. A plasma membrane protein extraction kit (Abcam) was used to isolate proteins expressed at the cell surface. Resolved mixtures were run on a 7.5% polyacrylamide gel, for ~1.5 hours at 100 V before transferring to a polyvinylidene difluoride (PVDF) membrane. We blocked membranes with proprietary blocking buffer (LI-COR biosciences) for 1 hour at room temperature. Then the membrane was incubated with mouse anti-pan-GluN1(1:1000) (Millipore, catalog # 05-432) or rabbit anti-GluN2A (1:1000) (Millipore, catalog # 04-901) primary antibody with the proprietary blocking buffer at 4°C overnight. We revealed specific bands by incubating with appropriate secondary antibody (goat anti-mouse or goat anti-rabbit, from LI-COR Biosciences) conjugated to a fluorophore (with excitation wavelength of 680 or 800 nm) for 1 hour at room temperature. Membranes were imaged with a LI-COR Odyssey CLx. To compare diheteromer content between lanes, densitometry was used to quantify the diheteromer and GluN1 monomer bands and calculated the diheteromer/monomer ratio. Densitometry analysis was done in ImageJ 1.50i (National Institutes of Health).

2.3.5 Mass spectrometry

Gel bands were washed with 50:50 methanol: 50 mM ammonium bicarbonate twice for 40 min with gentle agitation (VWR Thermal Shake Touch, 900 rpm). Gel bands were dehydrated by adding 500 μL acetonitrile for 20 minutes. Acetonitrile was removed and gel bands were dried in an Eppendorf 5301 Vacufuge Concentrator for approximately 15 minutes. Trypsin solution (10 μL at 20 μg/mL in 50 mM ammonium bicarbonate) was added to gel bands and incubated on ice for

15 minutes, then incubated overnight at 37˚C with gentle agitation (VWR Thermal Shake Touch, 900 rpm). The pH was adjusted to ~2 (5M HCl) and pepsin solution (10 μL at 1 mg/mL in H_2O (pH~3)) was added. Tubes were incubated overnight at 37˚C with gentle agitation. Digested peptides were extracted into supernatant and transferred to VWR non-stick microcentrifuge tubes. Digested peptides were further extracted by incubating gel bands twice for 30 minutes in 500 μL of 0.1 % formic acid in 50:50 acetonitrile:H_2O. The resulting supernatant was collected and combined with the supernatant collected immediately following the overnight incubation. Digest extract solution was dried in an Eppendorf 5301 Vacufuge Concentrator. Dried extract was reconstituted in 50 μL of 0.1% formic acid in H_2O for 30 minutes with gentle agitation. The reconstituted peptides were run through liquid chromatography-mass spectrometry (LCMS). Electrospray ionization quadrupole time-of-flight mass spectrometry (ESI-Q-TOF MS) was done on the extracted peptides and measurements were taken using an Agilent 6530 Q-TOF-MS with an Agilent HPLC-Chip II G4240-62006 ProtID-Chip-150. The mobile phase was created by combining varying percentages of Solvent A (95 % H_2O, 5 % ACN, 0.1 % Formic acid) and Solvent B (95 % ACN, 5 % H_2O, 0.1 % Formic acid). The nanoflow elution gradient was developed as follows at 0.50 μl/min of Solvent A (minute, percent A): 0.00, 95 %; 4.00, 10 %; 6.00, 70 %; 9.00,: 50 %; 11.50, 95 %; 13.00, 95 %. The mass-to-charge (m/z) ratio range was 200-1700 m/z for MS analysis and 100-2000 m/z for MSMS analysis. Data were processed using Agilent Qualitative Analysis Software 6.0 using the following parameters: 2 missed enzymatic cleavages, 20 ppm precursor ion/ 0.1 Da product ion cutoff, and peptide modifications (oxidation and acrylamidation). For MS/MS analysis, the extracted peptide samples were run again on the Agilent 6530 Q-TOF-MS, targeting the specific m/z ratio, charge, and retention time (RT) of the cross-linked peptides identified in MS analysis. Collision-induced dissociation (CID) was used for

MS-MS fragmentation following a linear increase in collision energy by m/z using the equation: y = 3.7x + 2.5. CID was performed at ± 0.2 min from initial MS scan RT of each crosslinked precursor ion identified. Measurements were taken in triplicate from distinctive gel bands at molecular weights of crosslinked dimers. Precursor/product ion pairing identified in ≥2 of 3 trials of mass ions unique to crosslinked diheteromer gel band and not identified in controls (single subunit and enzymatic solution gel band) were considered as evidence of diheteromer formation.

2.3.6 Statistics

Statistical tests were performed in GraphPad Prism 7. Student's t-test and two-way ANOVA with Tukey's post-hoc test were used where indicated and p-values of <0.05 were considered statistically significant. Statistical significance of mutant cycles was tested using a two-way ANOVA with the identity of the residue at each mutated site as factors. A significant interaction between factors was taken to reflect significant coupling between the mutated sites. Error bars indicate ± standard error of the mean (SEM). Mg^{2+} IC_{50} error is the standard error reported in the curve fit to determine Mg^{2+} IC_{50}.

2.3.7 Molecular modeling, sequence alignment and image creation

To identify residues of interested at intersubunit interfaces in the TMD, we utilized the published all-atom GluN1/2A TMD model (Mesbahi-Vasey et al., 2017). We achieved the sequence alignment shown in Figure 6A using NCBI BLAST (https://blast.ncbi.nlm.nih.gov/Blast.cgi). Images of NMDAR TMD model used in figures were created using Pymol software.

2.4 Results

2.4.1 GluN1(W608C) and GluN2A(S632C) form a disulfide linkage

We began our exploration of the conserved tryptophan in GluN1, GluN2A, and GluN2B subunits (Figure 6) with GluN1(W608). Based on the observation by Siegler Retchless et al. that GluN1(W608) and GluN2A(S632) interact to mediate the effects of the GluN2 S/L site, we created GluN1(W608C) and GluN2A(S632C) mutants to explore whether the introduced cysteines are in close physical proximity, as predicted (Siegler Retchless et al., 2012). We hypothesized that we could detect GluN1(W608C) - GluN2A(WS632C) disulfide bond formation in non-reducing Western blots by probing for GluN1/2A diheteromers. Cysteine residues near one another share the ability to crosslink, resulting in formation of a covalent disulfide bond (Anfinsen and Haber, 1961). Observation that a disulfide bond can form between a pair of introduced cysteines suggests that their α-carbons come within 7 Å of each other (Katz and Kossiakoff, 1986). Based on known NMDAR structure, naturally-occurring intersubunit disulfide bonds should not occur in properly-assembled GluN1/2A receptors. In agreement with this, non-reducing western blots of membrane proteins isolated from *Xenopus* oocytes show no diheteromerization in WT GluN1/2A receptors (Talukder and Wollmuth, 2011). Non-reducing western blots of whole-cell extracts in tsA201 and HEK293 cells, however, do show faint diheteromer bands in WT GluN1/2A lanes that are eliminated by inclusion of a reducing agent in the protein sample (Lee and Gouaux, 2011, Xu et al., 2015). Nonfunctional proteins located in ribosomes (Pechmann et al., 2013), likely present in whole-cell extracts, could be responsible for the observed inter-subunit disulfide bonds. Therefore, we performed Western blots on proteins isolated from the surface of tsA201 cells to obtain a sample with minimal misfolded or improperly assembled protein (Riou et al., 2012) expecting that

any observed diheteromers would correspond to crosslinking between GluN1(W608C) and GluN2A(S632C). To our surprise, even after isolation of the plasma membrane fraction, we consistently observed a faint diheteromer signal in WT GluN1/2A lanes. This could arise due to imperfect separation of the plasma membrane and cytosolic fractions or may be ascribed to association of integral membrane proteins with NMDAR subunits even in the presence of detergents. We observed that GluN1(W608C)/2A(S632C) receptors showed a diheteromer/monomer ratio (30.7 ± 5.3 %) several-fold larger than in GluN1/2A receptors (8.93 ± 1.80, p = 0.017), suggesting that crosslinking occurs between GluN1(W608C) and GluN2A(S632C) (Figure 7B,C).

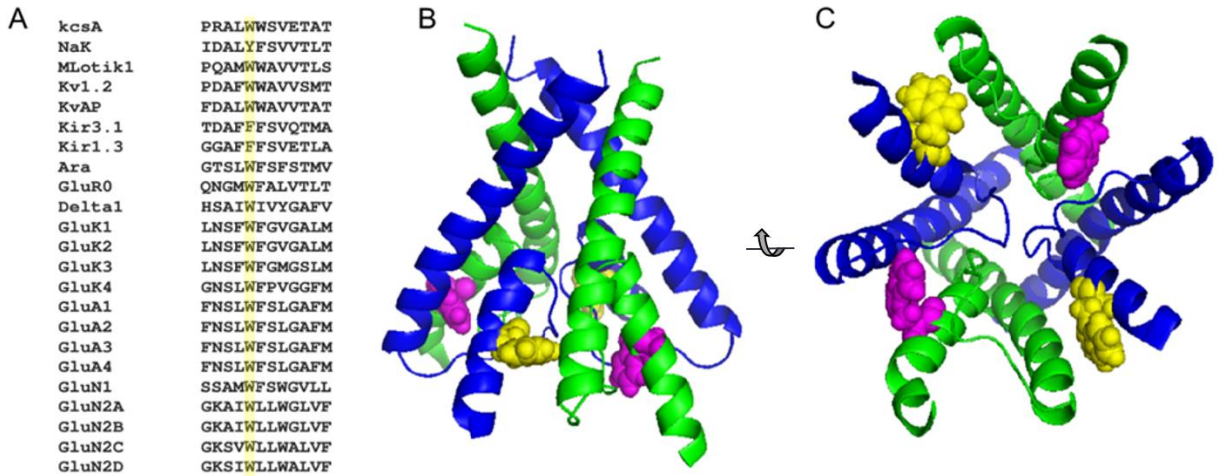

Figure 6 A conserved tryptophan in NMDARs

A, a conserved tryptophan (W) emerges from an alignment of p-loops of glutamate receptor and K^+ channel subunits from a wide range of organisms. KcsA, prokaryotic K^+ channel from *Streptomyces lividans*; NaK, bacterial action channel from *Bacillus cereus*; MlotiK1, prokaryotic

K^+ channel from *Mesorhizobium loti*, KvAP archaebacterial K^+ channel from *Aeropyrum Pernix; Ara,* glutamate binding protein from the plant Arabidopsis; GluR0, prokaryotic glutamate receptor from *Synechocystis;* Kv1.2, Kir 3.1, Kir 1.3: mammalian K^+ channels; delta1, GluK1-4, GluA1-4, GluN1, GluN2A-D: mammalian glutamate receptors. B, molecular model of GluN1/2A M2 and M3 segments of the TMD (Mesbahi-Vasey et al., 2017) showing the conserved tryptophans. GluN1 is green and GluN2A is blue. GluN1(W608) residues are in magenta and GluN2A(W606) residues are in yellow. C, same as B, but viewed from below.

To further explore whether our Western blot contained diheteromers due specifically to crosslinking of GluN1(W608C) and GluN2A(S632C), we performed electrospray ionization quadrupole time-of-flight mass spectrometry (ESI-Q-TOF MS) on excised gel slices. ESI-Q-TOF MS allowed us to specifically identify mass-shifted diheteromer derived disulfide linked GluN1-GluN2A peptides arising from the introduced cysteines. Tandem-MS studies were conducted on three independently prepared samples. Mass coverage of GluN1(W608C) and GluN2A(632C) ranged from 50 – 65% in our trials. Given the potential steric hindrance of the disulfide linkage as well as the raggedness of pepsin cleavage (Gorman et al., 2002), results with two missed cleavages, as well as oxidation and acrylamidation, were analyzed. Overall, in the three trials 10 different precursor ions were identified within 20 ppm mass error of mass-shifted disulfide-linked peptides consistent with linked diheteromers. In all cases, tandem MS studies showed *a*, *b*, and *y* product ion fragmentation patterns. In 6 of these cases, the intact disulfide linkage, which is labile to collision-induced dissociation (which also leads to cleavage of more than one bond) (Clark et al., 2011), was observed amongst the product ions. A representative MS/MS scan with assigned fragmentation pattern is provided in Figure 8. For simplicity only single CID cleavages to either the diheteromer or the free GluN1 or GluN2A peptide were assigned. These experiments revealed

that a disulfide bond formed between GluN1(W608C) and GluN2A(S632C) in agreement with our Western blot results.

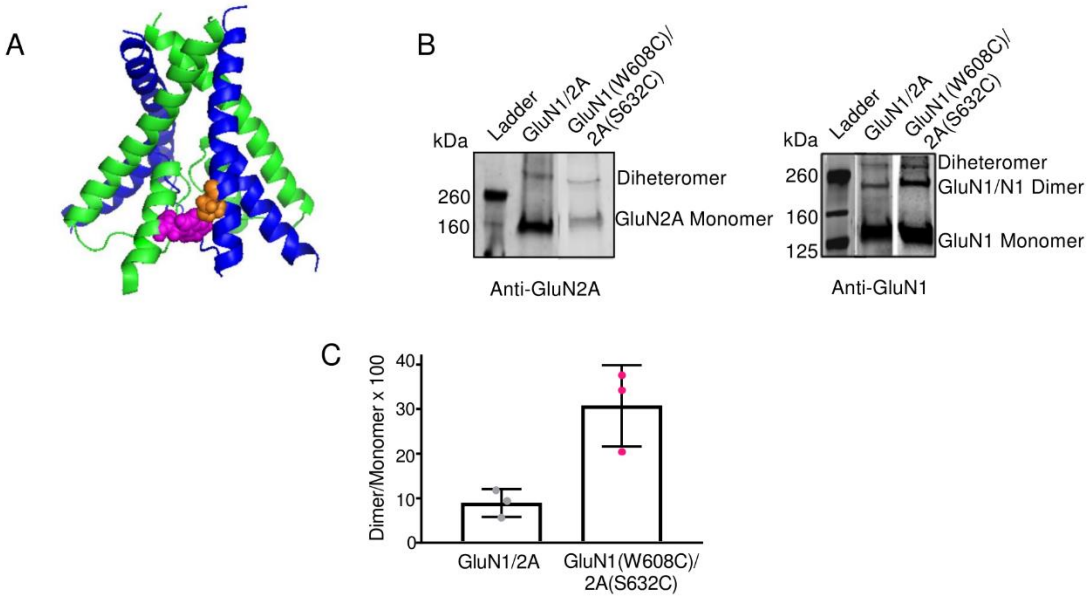

Figure 7 GluN1(W608C) and GluN2A(S632C) form a disulfide bond in assembled receptors

A, image of GluN1 (green) and GluN2A (blue) M2 and M3 regions (Mesbahi-Vasey et al., 2017) showing GluN1(W608) in magenta and GluN2A(S632) in orange. B, Western blot of surface NMDARs probed with anti-GluN2A and anti-GluN1. Diheteromer (~300 kDa), GluN1/N1 dimer (~240 kDa), GluN2A monomer (~175 kDa), and GluN1 monomer bands (~125 kDa) are labelled. C, plot of intensity of the diheteromer band divided by the intensity of the GluN1 monomer band, multiplied by 100, for GluN1/2A and GluN1(W608C)/2A(S632C) receptors (n = 3 Western blots).

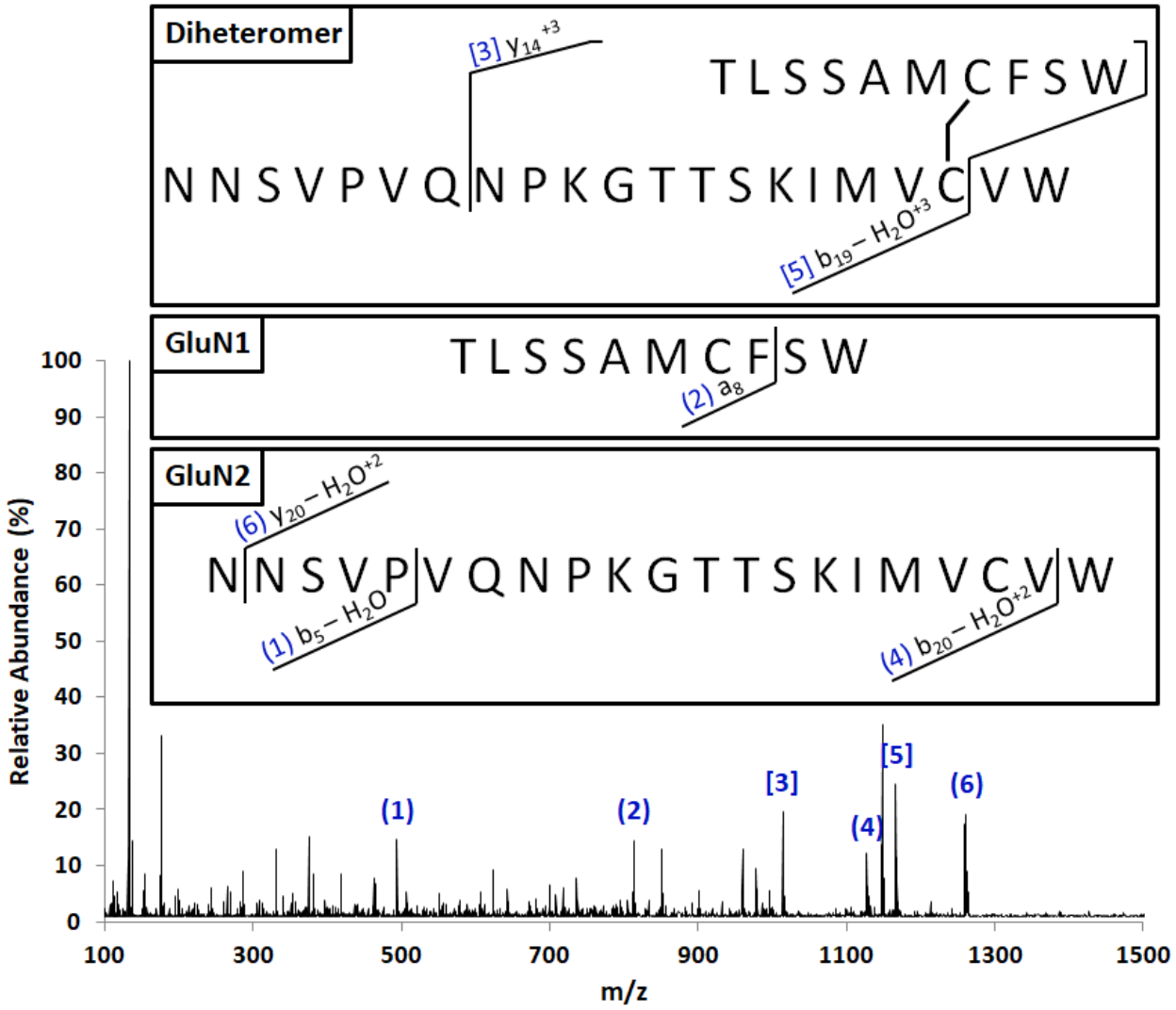

Figure 8 MS analysis of crosslinked diheteromer

Representative tandem MS-MS fragmentation scan of precursor m/z corresponding to crosslinked peptide pair produced from enzymatic double digestion. Fragmented *a*, *b* and *y* product ions (labeled 1-6) stemming from the crosslinked peptide pair precursor ion were assigned to product ions containing the disulfide crosslink between GluN1 and GluN2 (Diheteromer) as well as product ions assigned to individual GluN1 and GluN2 peptides due to CID of the disulfide linkage.

2.4.2 GluN1(W608C) and GluN2A(S632C) interact to influence deactivation kinetics

Next we examined the electrophysiological effects of the GluN1(W608C) and GluN2A(S632C) mutations on receptor function. We noticed that GluN1(W608C)/2A receptors showed remarkably slow deactivation, similar to that of GluN1/2D receptors (Traynelis et al., 2010b). In further experiments, we found that the effect of the mutation on deactivation depended on the redox state of the receptor: deactivation kinetics were modulated by the membrane-impermeable reducing reagent TCEP. To examine the effect of the GluN1(W608C) mutation on deactivation in a uniform population of NMDARs we measured the time constant of deactivation (τ_w) in the presence of 5 mM TCEP. GluN1(W608C)/2A receptors showed drastically slowed deactivation (τ_w = 3390 ± 628 ms) compared to WT GluN1/2A receptors (τ_w = 140 ± 20 ms, $p < 0.0001$, one-way ANOVA) in 5 mM TCEP. τ_w of GluN1/2A(S632C) receptors was not different from WT GluN1/2A receptors ($p > 0.99$). GluN1(W608C)/2A(S632C) receptors showed τ_w slower than WT GluN1/2A receptors (1550 ± 180 ms, $p = 0.017$) but faster than GluN1(W608C)/2A receptors ($p = 0.004$).

We were intrigued by evidence of proximity between GluN1(W608C) and GluN2A(S632C) residues (Figures 7,8) as well as published evidence that GluN1(W608) and GluN2A(S632) couple to influence Mg^{2+} IC_{50} (Siegler Retchless et al., 2012). We decided to examine whether the GluN1(W608) and GluN2A(S632) positions also couple to influence receptor gating. Mutant cycle analyses involve comparing the effect of each of two single mutations (e.g. GluN1(W608C)/2A and GluN1/2A(S632C) receptors) on a parameter of interest (e.g. τ_w) with the effect induced by both mutations simultaneously (GluN1(W608C)/2A(S632C)). If the mutated residues do not interact, the fractional change in τ_w between GluN1/2A and

GluN1(W608C)/2A receptors should be equal to the fold change in τ_w between GluN1/2A(S632C) and GluN1(W608C)/2A(S632C) receptors. If the mutated residues are coupled, the fractional change in τ_w between GluN1/2A(S632C) and GluN1(W608C)/2A(S632C) receptors will be greater than or less than the fractional change between GluN1/2A and GluN1(W608C)/2A receptors. A coupling coefficient, **Ω**, is often used as a measure of residue coupling (equation 3, Methods). If **Ω** = 1, there is no evidence for residue coupling, while **Ω** < 1 or **Ω** > 1 suggests that residues are coupled. Based on the average τ_w for each receptor type, we calculated the Ω value of the GluN1(W608C)/2A(S632C) mutant cycle. We found that Ω was greater than 1 (Ω = 2.0), suggesting that the GluN1(608) and GluN2A(S632) positions interact to influence deactivation kinetics (Figure 9C). The interaction between the GluN1(W608) and GluN2A(S632) was statistically significant ($p = 0.0001$) using two-way ANOVA, supporting the idea that the residues interact to influence receptor deactivation kinetics.

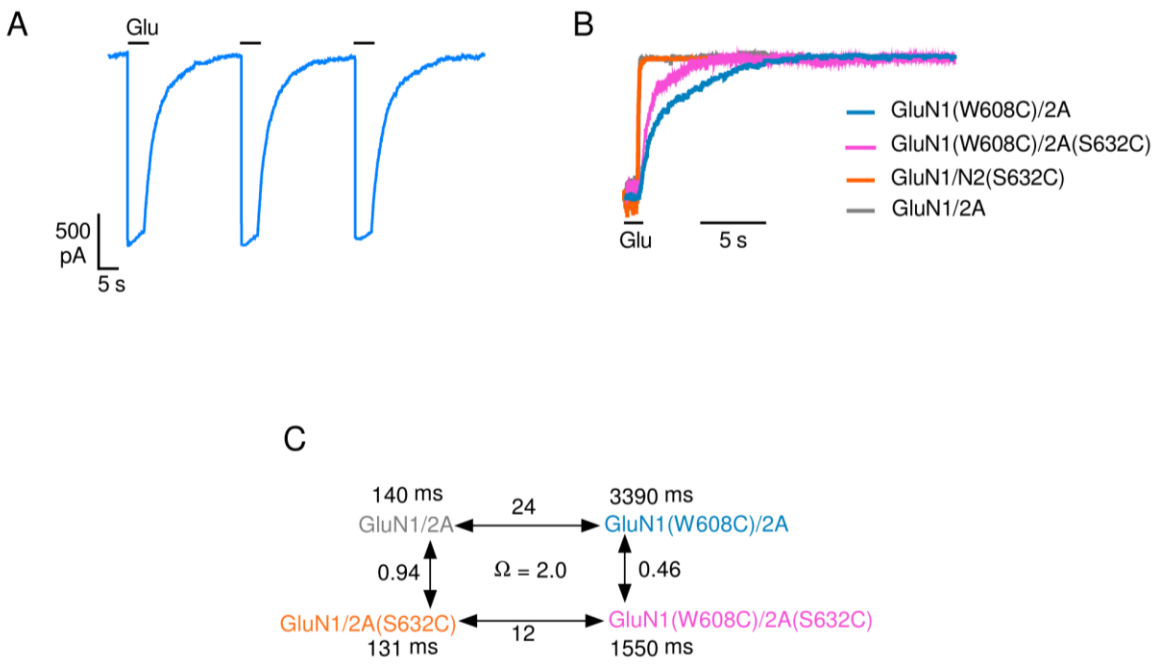

Figure 9 GluN1(W608C)/2A receptors show slowed deactivation kinetics; GluN1(W608) interacts functionally with Glun2A(S632) to influence receptor gating

A, example trace of GluN1(W608C)/2A receptors showing slow deactivation in response to 5 s glutamate (Glu) applications. B, overlay of mutant and WT receptor normalized currents showing receptor deactivation. C, mutant cycle analysis diagram based on average τ_w of receptors (n = 4-5 cells per receptor type). Numbers beside arrows indicate the fold change in τ_w between the indicated receptors. The mutant cycle τ_w value is shown in the center. The interaction between the GluN1(608) and GluN2A(632) positions with respect to τ_w was tested using two-way ANOVA and was found to be statistically significant (p = 0.0001)

2.4.3 GluN2A(W606C) interacts with GluN1(M634C) to influence Mg^{2+} IC_{50}

We next examined the role of GluN2A(W606) and residues it may interact with (Figure 10). Using an all-atom NMDAR TMD model (Mesbahi-Vasey et al., 2017) we noticed \ that GluN1(M634) is positioned for interaction with GluN2A(W606) (Figure 10A). Interestingly, GluN1(M634) is homologous to GluN2A(S632) (Tikhonov, 2007, Siegler Retchless et al., 2012). We mutated GluN2A(W606) and GluN1(M634) to cysteine and examined the resulting receptors electrophysiologically (Figure 10). We found that the Mg^{2+} IC_{50} was significantly greater for GluN1(M634C)/2A receptors (385 ± 224 μM) than for GluN1/2A receptors (69.4 ± 7.1 μM, $p = 0.021$) (Figure 10C). We decided to explore whether GluN1(M634C) and GluN2A(W606C) interact by performing mutant cycle analysis using Mg^{2+} IC_{50} as a readout of potential residue coupling. We measured Mg^{2+} IC_{50} in GluN1/2A(W606C) and GluN1(M634C)/2A(W606C) receptors and found that, while GluN1(M634C)/2A(W606C) receptors showed IC_{50} (1.45 ± 0.19 mM) different from GluN1/2A receptors ($p < 0.0001$), GluN1/2A(W606C) receptors did not (59.2 ± 19.3 μM, $p = 0.99$). We calculated the mutant cycle **Ω** using Mg^{2+} IC_{50} values and found that **Ω** = 0.23) suggesting that GluN1(M634C) and GluN1A(W606C) interact functionally to influence Mg^{2+} IC_{50} (Figure 10D)($p = 0.023$ by two-way ANOVA). We next examined whether GluN1(M634C) and GluN2A(W606C) receptors were in close physical proximity, as predicted by the NMDAR TMD model. We isolated plasma membrane receptors and performed non-reducing Western blots to examine whether crosslinking occurred between the introduced cysteines. Examining surface GluN1/2A and GluN1(M634C)/2A(W606C) receptors for evidence of intersubunit crosslinking, we found that diheteromeric signal above WT levels was not present in GluN1(M634C)/2A(W606C) lanes. Therefore, the results of the Western blots suggest that GluN1(M634C) and GluN2A(W606C) do not form disulfide bonds.

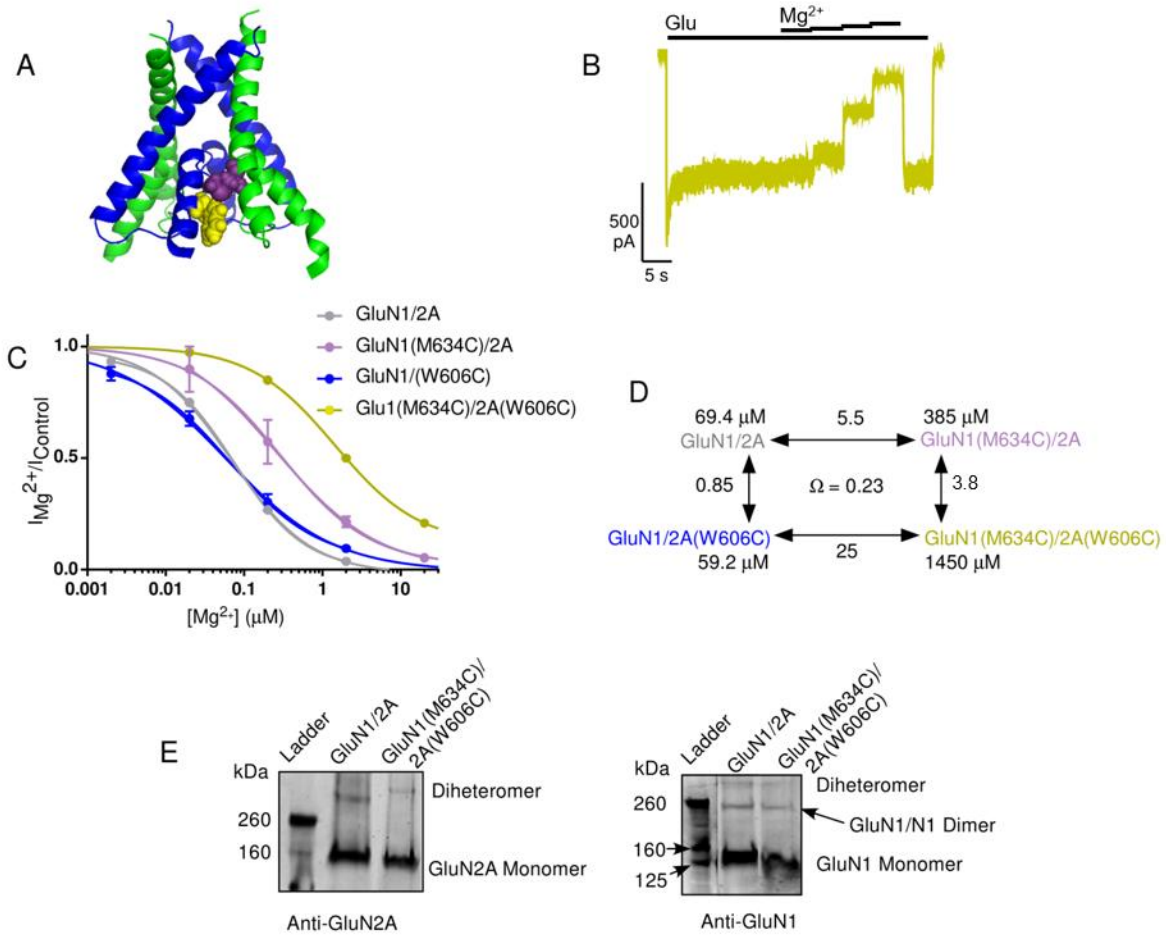

Figure 10 GluN1(M634C) and GluN2A(W606C) interact functionally but not biochemically

A, image of GluN1 (green) and GluN2A (blue) M2 and M3 regions (Mesbahi-Vasey et al., 2017) showing GluN1(M634C) in yellow and GluN2A(W606C) in purple. B, example trace of Mg^{2+} IC_{50} data from GluN1(M634C)/2A(W606C) receptors with glutamate and increasing [Mg^{2+}]s applied as indicated. C, [Mg^{2+}]-inhibition curves for mutant and WT receptors tested for mutant cycle (n = 4-5 cells per receptor type). D, mutant cycle analysis diagram based on Mg^{2+} IC_{50} of receptors. Numbers beside arrows show the fold change in IC_{50} between the indicated receptors. The interaction between the GluN1(634) and GluN2A(606) positions with respect to

Mg^{2+} IC_{50} was tested using a two-way ANOVA, which revealed a significant interaction ($p < 0.0001$).” E, Western blot of surface NMDARs. Left, probed with anti-GluN2A, GluN2A monomer bands are apparent at about 160 kDa and faint diheteromer bands are seen in the GluN1/2A and GluN1(M634C)/2A(W606C) receptor lanes. Right, same blot probed with anti-GluN1 showing GluN1/N1 dimers and GluN1 monomers.

2.4.4 No evidence of interaction between GluN1(W607C) and GluN1(M634C) to influence Mg^{2+} inhibition

Based on the similarity of the GluN2A and GluN2B subunits in the M2 and M3 regions, we examined electrophysiologically whether the residue in GluN2B homologous to GluN2A(W606) (GluN2B(W607)) interacts with GluN1(M634) in GluN1/2B receptors. Intriguingly, we noticed potentiation of current when [Mg^{2+}] was applied to cells expressing GluN1/2B(W607C) and GluN1(M634C)/2B(W607C) receptors (Figure 11A,B). These experiments were done with GluN1-1a/2B receptors (see Methods), which are sensitive to voltage and glycine-independent potentiation by Mg^{2+} (Paoletti et al., 1995, Wang and MacDonald, 1995). Mg^{2+} potentiation of WT GluN1-1a/2B receptors was reported to be maximal (approximately three-fold) at 10 mM, the highest [Mg^{2+}] examined, and absent at GluN1-1a/2A receptors (Paoletti et al., 1995). While Mg^{2+} potentiation is voltage-independent, it is occluded by V_m-dependent Mg^{2+} block in WT GluN1-1a/2B receptors. Therefore, we isolated Mg^{2+} potentiation by applying Mg^{2+} at +50 mV, where V_m-dependent Mg^{2+} block is minimal. We examined whether Mg^{2+} potentiation at GluN1/2B(W607C) and GluN1(M634C)/2B(W607C) receptors differed from potentiation of GluN1/2B receptors at +50 mV (Figure 11C). At several Mg^{2+} concentrations tested, GluN1(M634C)/2B(W607C) receptors showed significantly more potentiation than GluN1/2B

receptors. It was previously shown that the presence of exon 5 in the GluN1 subunit (e.g. GluN1-1b) eliminates potentiation of GluN1/2B by Mg^{2+}. We examined Mg^{2+} potentiation in GluN1/2B receptors with NTD-lacking GluN1 subunits (GluN1(ΔNTD)). Paoletti et al., 1995, showed that exon 5 in the GluN1 NTD controls Mg^{2+} potentiation. Our data show little-to-no potentiation in GluN1(ΔNTD)/2B receptors, indicating that the NTD is critical for Mg^{2+} potentiation.

To determine whether Mg^{2+} inhibition occurs in addition to Mg^{2+} potentiation in GluN1/2B(W607C) and GluN1(M634C)/2B(W607C) receptors, we normalized $I_{Mg^{2+}}/I_{Control}$ values at -60 mV ($I_{Mg^{2+}}/I_{Control}$(-60mV)) to $I_{Mg^{2+}}/I_{Control}$ values at + 50 mV ($I_{Mg^{2+}}/I_{Control}$(+50mV)). We found that V_m-dependent Mg^{2+} inhibition occurs at GluN2B(W607C)-containing receptors but is masked by Mg^{2+} potentiation (Figure 11D). We fit $I_{Mg^{2+}}/I_{Control}$(-60mV))/ $I_{Mg^{2+}}/I_{Control}$(+50mV) data from GluN2B(W607C)-containing receptors with Equation 2 to determine Mg^{2+} IC_{50}. Mg^{2+} block was incomplete in GluN2B(W607C)-containing receptors. In GluN1/2B and GluN1(M634C)/2B receptors, Mg^{2+} potentiation was either small or absent at the [Mg^{2+}]s used to determine the Mg^{2+} IC_{50}. Therefore, Mg^{2+} IC_{50} values in these receptors were measured using unnormalized data collected at -60 mV. Mg^{2+} IC_{50}s were similar in GluN1/2B (26.9 ± 3.3 μM) and GluN1(M634C)/2B (20.1 ± 1.0 μM) receptors ($p = 0.99$). We found that both GluN1/2B(W607C) (264 ± 18 μM, $p = 0.0006$) and GluN1(M634C)/2B(W607C) receptors (365 ± 180 μM, $p < 0.0001$) showed higher Mg^{2+} IC_{50} than GluN1/2B receptors. Using the measured IC_{50} values, we calculated the mutant cycle Ω. We found that Ω = 0.53, and that the interaction between the GluN1(634) and GluN2B(607) positions was not significant by two-way ANOVA ($p = 0.12$). Therefore, we did not find evidence that GluN1(M634) and GluN2B(W607) interact to influence Mg^{2+} IC_{50}.

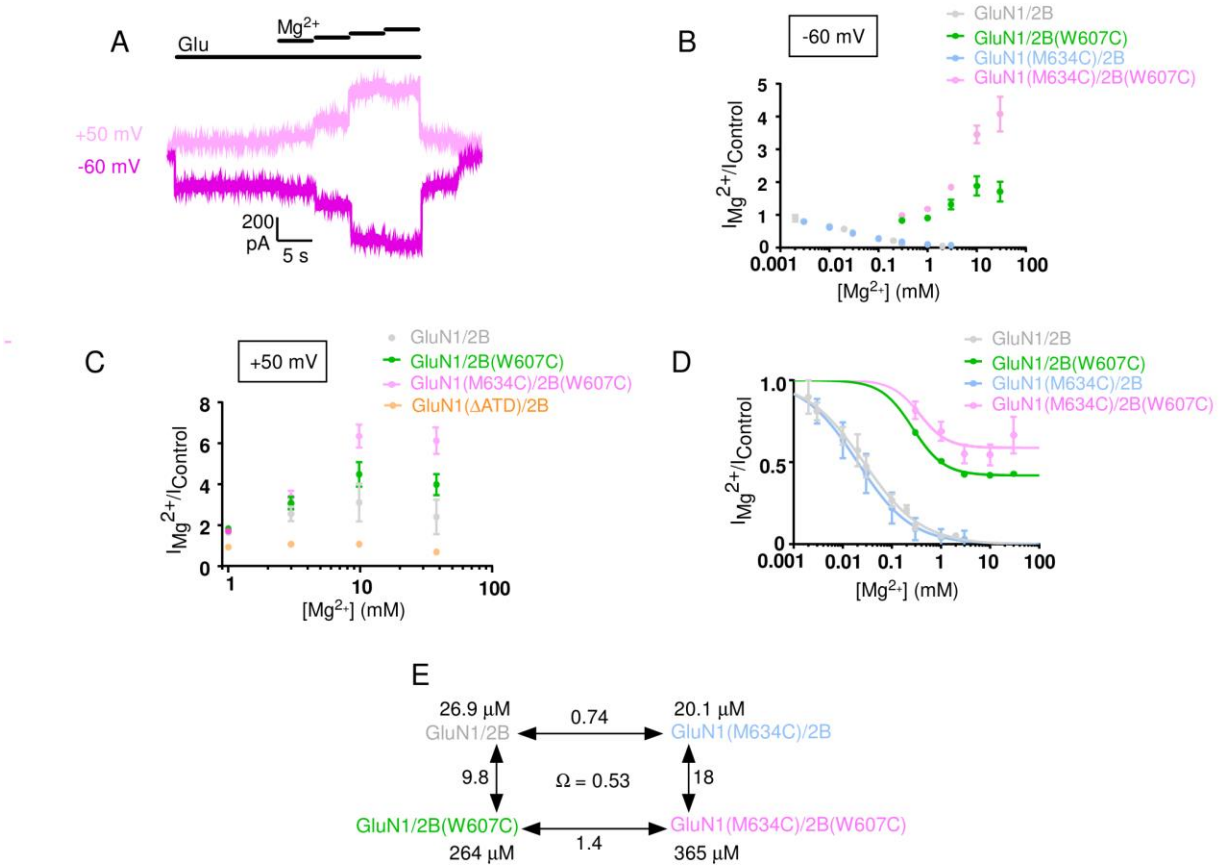

Figure 11 No evidence for interaction of GluN1(M634C) and GluN2B(W607C) to influence Mg2+ IC50

A, example trace of responses of GluN1(M634C)/2B(W607C) receptors to varying [Mg^{2+}] at -60 mV (dark pink, bottom trace) and +50 mV (light pink, top trace). Traces at -60 mV and +50 mV are from two different cells. B,C, Plotted response of WT and mutant receptors to varying [Mg^{2+}] at -60 mV (B; n=4-8 cells per receptor type) and +50 mV (C; n = 4-5 cells per receptor type). C also shows the absence of potentiation in GluN1(ΔNTD)/2B receptors. D, IC_{50} values of WT and mutant receptors. GluN1(M634C)/2B and GluN1/2B receptor IC_{50}s were determined from recordings at -60 mV, while GluN1/2B(W607C) and GluN1(M634C)/2B(W607C) IC_{50}s were

obtained by fitting responses to [Mg^{2+}] at -60 mV normalized to responses to the same [Mg^{2+}] at +50 mV. E, mutant cycle analysis diagram based on Mg^{2+} IC_{50} of receptors. Numbers beside arrows indicate the fold change in IC_{50} between the indicated receptors. **Ω** is shown in the center. The interaction between GluN1(M634) and GluN2B(W607) with respect to Mg^{2+} IC_{50} determined using two-way ANOVA was not statistically significant ($p = 0.12$).

2.5 Discussion

In this work we investigated the role of a conserved tryptophan in the TMD of GluN1, GluN2A and GluN2B subunits and its interaction with residues predicted to be nearby across the intersubunit interface. We began by studying the conserved tryptophan in GluN1 subunits. GluN1(W608) was previously shown to couple with GluN2A(S632), predicted to across the interface from GluN2A(S632), with respect to Mg^{2+} IC_{50} (Siegler Retchless et al., 2012). To test whether GluN1(W608) and GluN2A(S632) are in close proximity, we created the GluN1(W608C) and GluN2A(S632C) mutations and probed for crosslinking between the introduced cysteines by examining diheteromer formation in membrane proteins (Figure 7). Western blotting identified diheteromers in both WT GluN1/2A and GluN1(W608C)/2A(S632C) membrane proteins. The ratio of diheteromer to GluN1 monomer was significantly higher in GluN1(W608C)/2A(S632C) than in WT receptors, suggesting that crosslinking occurred between GluN1(W608C) and GluN2A(S632C). We further probed for crosslinking between GluN1(W608C) and GluN2A(S632C) using tandem mass spectrometry (Figure 8), which verified that crosslinking occurs between GluN1(W608C) and GluN2A(S632C). In accordance with predictions from molecular modeling (Siegler Retchless et al., 2012, Mesbahi-Vasey et al., 2017), our data suggest

that GluN1(W608) and GluN2A(S632) come into close proximity at the GluN1 M2 – GluN2A M3 interface.

The GluN2 S/L site, a position containing a serine (S) in WT GluN2A and GluN2B and leucine (L) in GluN2C and GluN2D influences NMDAR subtype-dependence of channel properties. We wanted to examine whether residues lining the GluN1 M2 – GluN2A M3 interface also influence receptor gating. Indeed, we detected altered gating in GluN1(W608C)/2A receptors electrophysiologically. GluN1(W608C)/2A receptors showed extremely slow deactivation kinetics. To explore whether GluN1(W608C) interacts with GluN2A(S632C) to affect deactivation kinetics we performed mutant cycle analysis using receptor τ_w (Figure 9). We discovered that positions GluN1(608) and GluN2A(632) interact to influence τ_w, suggesting functional coupling between these residues with respect to deactivation kinetics. Therefore, we suggest that residue-residue interactions at the GluN1 M2 – GluN2A M3 interface influence receptor gating as well as NMDAR channel properties (Siegler Retchless et al., 2012).

We next examined residues predicted to lie across the intersubunit interface from the conserved tryptophan in GluN2A (GluN2A(W606)). Using an NMDAR TMD model we identified that the residue homologous to GluN2A(S632C), GluN1(M634), lies directly across the GluN1 M3 – GluN2A M2 interface from GluN2A(W606). To investigate whether the GluN2A(W606) interacts functionally with the GluN1(M634) position, we examined GluN1/2A, GluN1(M634C)/2A, GluN1/2A(W606C), and GluN1(M634C)/2A(W606C) receptors electrophysiologically (Figure 10). We noted altered Mg^{2+} IC_{50} in GluN1(M634C)-containing receptors and performed mutant cycle analysis using Mg^{2+} IC_{50} to examine whether GluN1(M634) and GluN2A(W606) interact to influence Mg^{2+} block. Mutant cycle analysis revealed evidence of residue coupling to influence Mg^{2+} IC_{50}. We conclude that residues at the GluN1(M634) and

GluN2A(W606) positions can modulate NMDAR block by Mg^{2+}. Williams et al. observed that GluN1/2A(W606L) receptors showed slightly increased Mg^{2+} IC_{50} compared to GluN1/2A receptors, as well as increased permeability to Mg^{2+} (Williams et al., 1998). Interestingly, we did not observe decreased Mg^{2+} potency in GluN1/2A(W606C) receptors. The differences in Mg^{2+} block between GluN1/2A(W606L) and GluN1/2A(W606C) receptors may be explained by the differing effects produced by insertion of leucine, rather than cysteine, at GluN2A(W606). After finding evidence of functional coupling between GluN1(M634C) and GluN2A(W606C), we examined the physical proximity of the residues by probing for disulfide bond formation between GluN1(M634C) and GluN2A(W606C) in membrane receptors. Western blot experiments did not reveal evidence for intersubunit disulfide bond formation between GluN1(M634C) and 2A(W606C). However, several factors influence whether cysteine residues can crosslink, including access to solvent (Wang and Kaltashov, 2015). If the GluN1(M634C) or GluN2A(W606C) residues are not solvent-accessible, disulfide bond formation between the residues may be inhibited regardless of their physical proximity. Therefore, this result neither confirms nor rejects the hypothesis that GluN1(M634C) and GluN2A(W606C) are physically close.

We also examined whether, like GluN2A(W606C), GluN2B(W607C) interacts with GluN1(M634C) to influence Mg^{2+} IC_{50} (Figure 11). Interestingly, application of Mg^{2+} to GluN1/2B(W607C) and GluN1(M634C)/2B(W607C) receptors resulted in potentiation of responses at -60 mV. Noting that exon 5-lacking WT GluN1/2B NMDARs (like those used here; GluN1-1a/2B receptors) are potentiated by Mg^{2+}, we investigated whether increased Mg^{2+} potentiation could explain the potentiation seen with GluN2B(W607C)-containing receptors at -60 mV. Mg^{2+} potentiation of WT GluN1/2B receptors is most apparent at positive potentials, where

V_m-dependent Mg^{2+} block of receptors is minimal. Therefore, we compared the potentiation by Mg^{2+} of WT GluN1/2B receptors with GluN2B(W607C)-containing receptors at +50 mV. We found that Mg^{2+} potentiation was eliminated in GluN1/2B receptors that lack the GluN1 NTD (GluN1(ΔNTD)/2B receptors), consistent with Paoletti et al., 1995. GluN1/2B(W607C) and GluN1(M634C)/2B(W607C) receptors showed significantly more Mg^{2+} potentiation than GluN1/2B receptors, indicating that that mutation of a GluN2B M2 residue can influence distant NTD-mediated phenomena. This result confirms that, as others have noted (Hansen et al., 2018), NMDARs are highly allosteric with extensive coupling between its domains.

We then determined whether increased Mg^{2+} potentiation prevented us from observing V_m-dependent Mg^{2+} block in GluN2B(W607C)-containing receptors at -60 mV. To measure V_m-dependent Mg^{2+} block in GluN2B(W607C)-containing receptors, we divided normalized responses to [Mg^{2+}] at -60 mV by responses to the same [Mg^{2+}] at +50 mV. We found that GluN1/2B(W607C) and GluN1(M634C)/2B(W607C) were maximally ~50% and ~40% inhibited, respectively, by Mg^{2+} at -60 mV. Incomplete block by Mg^{2+} of GluN1/2B(W607C) and GluN1(M634C)/2B(W607C) receptors may be due to increased Mg^{2+} permeation, which was observed in other receptors with mutations at GluN2B(W607) (Williams et al., 1998). We calculated Mg^{2+} IC_{50} values of GluN1/2B, GluN1(M634C)/2B, GluN1/2B(W607C), and GluN1(M634C)/2B(W607C) receptors to examine interaction between GluN1(M634) and GluN2B(W607) to influence Mg^{2+} IC_{50}. The values obtained for Mg^{2+} IC_{50} of GluN1/2A and GluN1/2B were within the range of reported values at similar membrane potentials for GluN1/2A (Wrighton et al., 2008, Qian et al., 2005, Monyer et al., 1992, Yi et al., 2018, Paoletti and Neyton, 2007) and GluN1/2B (Williams et al., 1998, Siegler Retchless et al., 2012, Paoletti and Neyton, 2007). We found that the GluN2B(W607C) mutation resulted in a significantly larger Mg^{2+} IC_{50}

than in GluN1/2B receptors, while the GluN1(M634C) mutation did not affect Mg^{2+} IC_{50}. The interaction between GluN1(M634) and GluN2B(W607) residues to affect Mg^{2+} IC_{50} was not significant ($p = 0.12$), suggesting that GluN1(M634C) and GluN2B(W607C) do not couple to influence Mg^{2+} IC_{50}.

Our examination of the conserved tryptophan in GluN2A and GluN2B subunits reveals that the GluN1 M3 – GluN2 M2 interface powerfully influences GluN1/2A and GluN1/2B receptors. The GluN2A and GluN2B M1-M4 regions have identical sequences apart from three amino acids (Siegler Retchless et al., 2012, Tikhonov, 2007). However, our results suggest that the GluN2 conserved tryptophan may play different roles in GluN1/2A and GluN1/2B receptors. In GluN1/2A receptors, the GluN2A(W606C) mutation does not alter Mg^{2+} IC_{50} and the GluN1(M634C) mutation does. In GluN1/2B receptors, the opposite is true: the GluN1(M634C) mutation does not affect Mg^{2+} IC_{50}, while the GluN2B(W607C) does. This "role swapping" of homologous residues in the GluN2A and GluN2B subunits suggests that, despite the immense similarity between GluN2A and GluN2B subunit TMDs, there are functionally-important differences that may influence receptor function.

3.0 Effects of Mg^{2+} on Recovery of NMDA Receptors from Inhibition by Memantine and Ketamine Reveal Properties of a Second Site

Glasgow N.G, Wilcox M.R., Johnson, J.W. (2018). "Effects of Mg^{2+} on recovery of NMDA receptors from inhibition by memantine and ketamine reveal properties of a second site." Neuropharmacology 137: 344-358.

3.1 Overview

Memantine and ketamine are NMDA receptor (NMDAR) open channel blockers that are thought to act via similar mechanisms at NMDARs but exhibit divergent clinical effects. Both drugs act by entering open NMDARs and binding at a site deep within the ion channel (the deep site) at which the endogenous NMDAR channel blocker Mg^{2+} also binds. Under physiological conditions, Mg^{2+} increases the IC_{50}s of memantine and ketamine through competition for binding at the deep site. Memantine also can inhibit NMDARs after associating with a second site accessible in the absence of agonist, a process termed second site inhibition (SSI) that is not observed with ketamine. Here we investigated the effects of 1 mM Mg^{2+} on recovery from inhibition by memantine and ketamine, and on memantine SSI, of the four main diheteromeric NMDAR subtypes. We found that: recovery from memantine inhibition depended strongly on the concentration of memantine used to inhibit the NMDAR response; Mg^{2+} accelerated recovery from memantine and ketamine inhibition through distinct mechanisms and in an NMDAR subtype-dependent manner; and Mg^{2+} occupation of the deep site disrupted memantine SSI in a subtype-

dependent manner. Our results support the hypothesis that memantine associates with but does not inhibit at the second site. After associating with the second site, memantine can either slowly dissociate directly to the extracellular solution, or transit to the deep site, resulting in typical channel block. Memantine's relatively slow dissociation from the second site underlies the dependence of NMDAR recovery from inhibition on both memantine concentration and on Mg^{2+}.

3.2 Introduction

NMDA receptors (NMDARs) are a class of ionotropic glutamate receptors found at most fast excitatory synapses in vertebrate nervous systems (Iacobucci and Popescu, 2017a). NMDARs are implicated in many disorders of the central nervous system, driving sustained interest in therapeutically targeting NMDARs to treat disease (Paoletti et al., 2013, Parsons and Raymond, 2014). The clinical utility of two NMDAR channel blockers, memantine and ketamine, lend hope that continued development of drugs that modify NMDAR function may lead to new therapies for numerous disorders (Abdallah et al., 2015, Johnson et al., 2015, Parsons and Raymond, 2014). Despite sharing similar mechanisms of action at NMDARs, memantine and ketamine have strikingly divergent clinical profiles (Johnson et al., 2015, Parsons et al., 2007b, Abdallah et al., 2015). Memantine is approved for the treatment of moderate to severe Alzheimer's disease and is clinically well tolerated (Lipton, 2006, Parsons et al., 2007b, Parsons and Raymond, 2014). In contrast, ketamine was initially approved as an anesthetic and has shown efficacy as a rapid antidepressant and in treatment of pain, but causes psychotomimetic side effects at therapeutic doses (Abdallah et al., 2015, Persson, 2013, Krystal et al., 2003). A more thorough understanding

of the differential mechanisms of memantine and ketamine action may aid development of novel therapeutics for treatment of nervous system disorders.

NMDARs are glutamate- and glycine-gated ion channels that exhibit unique biophysical properties including highly V_m-dependent channel block by physiological concentrations (~1 mM) of Mg^{2+} (Mayer et al., 1984, Nowak et al., 1984). Mg^{2+} inhibition and other NMDAR biophysical properties vary substantially depending on the identity of the GluN2 subunits that constitute the receptor (Glasgow et al., 2015, Paoletti et al., 2013). NMDARs are heterotetramers typically composed of two GluN1 and two GluN2 subunits. One gene encodes the GluN1 subunit, whereas four genes encode four GluN2 subunits: GluN2A, GluN2B, GluN2C, and GluN2D (Iacobucci and Popescu, 2017a, Paoletti et al., 2013). The specific combination of subunits that make up an intact receptor defines the NMDAR subtype, of which there are many. For example, a GluN1/2A receptor subtype refers to an NMDAR that contains two GluN1 and two GluN2A subunits. Here we focus on the four GluN1/2 diheteromeric NMDAR subtypes: GluN1/2A, GluN1/2B, GluN1/2C, and GluN1/2D receptors. Due to NMDAR subtype-dependent structural differences, Mg^{2+} inhibition varies among NMDAR subtypes (Monyer et al., 1994, Kuner and Schoepfer, 1996, Siegler Retchless et al., 2012). Mg^{2+} exhibits similar inhibition of GluN1/2A and GluN1/2B receptors, and similar inhibition of GluN1/2C and GluN1/2D receptors, but Mg^{2+} inhibits GluN1/2A and GluN1/2B receptors more potently than GluN1/2C and GluN1/2D receptors.

Inhibition of all four GluN1/2 diheteromeric NMDAR subtypes by Mg^{2+}, memantine, and ketamine can be reduced or eliminated by mutation of critical asparagine residues at the N-site in the M2 pore-lining region of NMDARs (Yamakura et al., 1993, Kashiwagi et al., 2002, Burnashev et al., 1992b, Kuner and Schoepfer, 1996). These asparagine residues therefore are thought to play an essential role in forming the site, or overlapping sites, where channel blockers bind, referred to

here as the deep site. Because Mg^{2+} competes with organic NMDAR channel blockers for binding at the deep site, Mg^{2+} increases the IC_{50} of organic channel blockers, including memantine and ketamine (Kotermanski and Johnson, 2009, Nikolaev et al., 2012, Otton et al., 2011, Lerma et al., 1991). At a concentration of 1 mM, Mg^{2+} increases the memantine and ketamine IC_{50}s for inhibition of GluN1/2A and GluN1/2B receptors at -66 mV ~17-fold. However, 1 mM Mg^{2+} increases the memantine and ketamine IC_{50}s for inhibition of GluN1/2C and GluN1/2D receptors only ~3-fold because of the lower Mg^{2+} potency at these NMDAR subtypes (Kotermanski and Johnson, 2009). Therefore, in physiological Mg^{2+}, memantine preferentially inhibits GluN1/2C and GluN1/2D receptors, an effect proposed to impact strongly the clinical effects of memantine (Povysheva and Johnson, 2016). However, NMDAR subtype discrimination by memantine decreases with depolarization (Kotermanski and Johnson, 2009), inhibition of GluN1/2A receptors increases with increasing intracellular Ca^{2+} concentration (Glasgow et al., 2017), and low-dose memantine inhibition of GluN2A- and GluN2B-containing receptors reduces firing frequency *in vivo* (Szegedi et al., 2010). Thus, inhibition by memantine of all GluN1/2 receptor subtypes is likely to play important roles in the clinical actions of memantine.

Although the effects of Mg^{2+} on memantine and ketamine IC_{50}s are consistent with a competitive binding model, other data suggest a more complex interaction between Mg^{2+} and organic NMDAR channel blockers (Nikolaev et al., 2012). For example, Mg^{2+} can accelerate recovery from inhibition by MK-801 (McKay et al., 2013), an organic NMDAR channel blocker with a very slow time course of recovery (Huettner and Bean, 1988); if Mg^{2+} and MK-801 exhibited simple competitive binding, Mg^{2+} should not affect recovery from MK-801 inhibition. The effects of Mg^{2+} on the time course of recovery from inhibition by memantine and ketamine have not been explored. Indeed, most basic *in vitro* investigations of organic NMDAR channel

blockers have been conducted in the absence of extracellular Mg^{2+}. As a result, our ability to predict how organic NMDAR channel blockers act at NMDARs under physiological conditions, which may depend importantly on the effects of a physiological Mg^{2+} concentration (Gideons et al., 2014), is limited.

There are several differences between memantine and ketamine that may underlie their distinct clinical actions including binding to non-NMDAR targets (e.g. (Maskell et al., 2003, Lu et al., 2010)) and differences in pharmacokinetics (e.g. (Hesselink et al., 1999, Lord et al., 2013), but see (Kotermanski et al., 2013)). In addition to differences in non-NMDAR targets and pharmacokinetics, there is a prominent distinction between memantine and ketamine action at NMDARs: the ability of memantine (Blanpied et al., 1997, Chen and Lipton, 2005, Kotermanski et al., 2009, Sobolevsky and Koshelev, 1998), but not ketamine (Kotermanski et al., 2009), inhibit NMDARs via second site inhibition (SSI), a type of inhibition observed following drug association with a second site accessible in the absence of agonist. Although the clinical implications of memantine action at a second site are not clear, SSI has been suggested to contribute to the clinical safety of memantine (Parsons et al., 2007b, Chen and Lipton, 2005, Kotermanski et al., 2009). However, the effect of Mg^{2+} on memantine action at the second site has not been explored. Therefore, we investigated the effects of 1 mM Mg^{2+} both on the time course of recovery from inhibition by memantine and ketamine and on memantine SSI.

3.2.1 My contribution

Nathan G. Glasgow is the first author of this work, which is published in Neuropharmacology (Glasgow et al., 2018). As the second author, I designed some of the experiments in this paper, collected data (Figures 16,18), analyzed and interpreted data, and

assisted in writing the manuscript. This work is included as a chapter in my dissertation because it provides an informative introduction to SSI (later re-named membrane-to-channel inhibition; MCI, in Chapter 4). The findings in chapter 4 were rooted in discoveries that I contributed to in this paper.

3.3 Methods

3.3.1 Cell culture and transfection

Experiments were performed on the tsA201 cell line (The European Collection of Authenticated Cell Cultures), which is a variant of the HEK 293 cell line. tsA201 cells were maintained as previously described (Glasgow and Johnson, 2014) in DMEM supplemented with 10% fetal bovine serum and 1% GlutaMAX (Thermo Fisher Scientific), either with or without 100 IU/ml of penicillin and 100 mg/ml streptomycin (Corning). 1 x 10^5 cells/dish were plated on 15 mm glass coverslips treated with poly D-lysine (0.1 mg/ml) and rat-tail collagen (0.1 mg/ml, BD Biosciences) in 35 mm petri dishes. 12 to 24 hours after plating, the cells were transiently cotransfected using FuGENE 6 Transfection Reagent (Promega) with mammalian expression plasmids that contained cDNAs encoding enhanced green fluorescent protein (EGFP in pRK7) for identification of transfected cells, the rat GluN1-1a subunit (hereafter GluN1; GenBank X63255 in pcDNA3.1), and either the rat GluN2A subunit (GenBank M91561 in pcDNA1), the rat GluN2B subunit (GenBank M91562 in pcDNA1), the rat GluN2C subunit (GenBank M91563 in pcDNA1), or the rat GluN2D subunit (GenBank L31612 in pcDM8). For some experiments we used cells transfected with GluN1 and an EGFP:pIRES:GluN2A construct, which was a kind gift from Dr.

Kasper Hansen (Hansen, unpublished). Briefly, EGFP was inserted in pIRES (Clontech) under transcriptional control of the CMV promoter, and the open reading frame of rat GluN2A (GenBank D13211) was inserted after the IRES sequence. cDNA ratios used were 1:1:1 (EGFP, GluN1, and GluN2A); 1:1 (GluN1 and EGFP:pIRES:GluN2A); or 1:1:3 (EGFP, GluN1, and GluN2B, C, or D). cDNA for the GluN1(N616R) mutant subunit (residue numbering starting from initiating methionine) was a kind gift from Dr. Pierre Paoletti and was transfected at the same ratio as wild-type GluN1. Immediately after transfection, the culture medium was supplemented with the competitive NMDAR antagonists D,L-2-amino-5-phosphonopentanoate (200 μM) and 7-chlorokynurenic acid (200 μM) to prevent NMDAR-mediated cell death.

3.3.2 Solutions

The extracellular bath solution contained (in mM): 140 NaCl, 2.8 KCl, 1 CaCl2, 10 HEPES, 0.01 EDTA, and 0.1 glycine, balanced to pH 7.2 ± 0.05 with NaOH and osmolality raised to 290 ± 10 mOsm with sucrose. L-glutamate, MgCl2, memantine, and (R,S)-ketamine (hereafter, ketamine) were added to the extracellular solution as indicated from frozen concentrated stock solutions on the same day as experiments. The intracellular pipette solution contained (in mM): 130 CsCl, 10 HEPES, 10 BAPTA, and 4 MgATP balanced to pH 7.2 ± 0.05 with CsOH; solution osmolality was 280 ± 10 mOsm. Frozen aliquots of pipette solution were thawed and kept on ice until loaded into pipettes immediately before starting an experiment.

3.3.3 Electrophysiology

Whole-cell voltage-clamp recordings were performed on transfected tsA201 cells 12 – 72 hours after transfection. Pipettes were pulled from borosilicate capillary tubing (Sutter Instruments) on a Sutter Instruments-Flaming Brown P-97 microelectrode puller and fire polished to a resistance of 2 – 5 MΩ . Whole-cell recordings were made from cells expressing EGFP identified by epifluorescence illumination on an inverted Zeiss Axiovert microscope. Cells were held at a membrane potential (V_m) of -65 mV, unless otherwise indicated, corrected for an empirically determined liquid junction potential between the extracellular and intracellular solution of -6 mV. Whole-cell currents were amplified using an Axopatch 200B patch-clamp amplifier (Molecular Devices), low-pass filtered at 5 kHz and sampled at 20 kHz in pClamp10 (Molecular Devices). Series resistance was compensated 85-90% with the prediction and correction circuitry in all experiments.

Solutions were delivered to coverslip-attached cells through a ten-barrel fast perfusion system described previously (Glasgow et al., 2017). We determined the time course of solution exchange around whole cells by recording current relaxations following movements between two adjacent barrels. The initial barrel contained normal extracellular solution and 1 mM glutamate, and the barrel to which test movements were made contained extracellular solution with 50% NaCl and 1 mM glutamate. Solution exchange around a whole cell had a 10-90% rise time of 150 ± 35 ms (mean ± SD) and was well fit by a single exponential with a time constant of 27.4 ± 6.6 ms (mean ± SD).

Accurate measurement of the time course of recovery from inhibition by an inhibitory drug requires a rapid decrease of drug concentration to well below its IC_{50}. Effective drug washout can require multiple solution exchange time constants, especially with higher drug concentrations.

Therefore, some of our measurements of the τ_{fast} of recovery from drug inhibition may have been limited by the speed of solution exchange. For example, at a starting concentration of 100 μM drug, after 150 ms (~5 time constants) the drug concentration would be ~0.4 μM, which is still close to the IC_{50} for memantine or ketamine (Kotermanski and Johnson, 2009). However, measurements of the τ_{slow} of recovery from drug inhibition should have been unaffected by limitations of solution exchange around a whole cell, even at the highest drug concentrations used.

3.3.4 Analysis

All data were analyzed with Clampfit 10.3 or 10.7 (Molecular Devices), or GraphPad Prism 7. Time course of recovery from inhibition by memantine or ketamine were determined from drug concentration-inhibition relation experiments. Briefly, glutamate was applied for 10 – 20 s until current reached steady state, then glutamate with 1, 10, 100, or 1000 μM memantine or ketamine was applied for 10 – 40 s until a new steady-state current level was reached. Glutamate in the absence of drug was then reapplied for 20 – 60 s to allow recovery from inhibition. The time necessary to reach a steady level of inhibition and to allow recovery from inhibition depended on the NMDAR subtype, as expected for channel blockers. Experiments in which NMDAR-mediated current during recovery from inhibition did not reach at least 90% of steady-state NMDAR-mediated current preceding drug application were excluded from analysis.

Time course of recovery from memantine and ketamine inhibition was measured by performing least-squares fits of single or double exponential functions to current traces using Clampfit 10.3 or 10.7. The number of components used in exponential fits was determined by visual examination, using the fewest components required to obtain a satisfactory fit. For comparison with the time constant (τ) of single exponential fits, a weighted time constant (τ_w) was

calculated from the results of double exponential fits using the equation: $\tau_w = (\tau_{fast}*A_{fast} + \tau_{slow}*A_{slow})/(A_{fast} + A_{slow})$, where the faster component had time constant τ_{fast} and amplitude A_{fast} and the slower component had time constant τ_{slow} and amplitude A_{slow}. To compare amplitudes of the fast and slow components across cells irrespective of absolute current amplitude, normalized values of A_{fast} and A_{slow} were calculated by dividing each by $(A_{fast} + A_{slow})$.

SSI was measured using the following SSI protocol: (a) 1 mM glutamate was applied for 20 s, and control current before SSI ($I_{control1}$) was measured (see below); (b) normal extracellular solution was applied for at least 9 s to allow full deactivation of receptors; (c) memantine in the absence of glutamate was applied for 30 s; (d) memantine was washed away by a 1 s application of normal extracellular solution; (e) 1 mM glutamate was reapplied for 20 s for GluN1/2A receptors and for 40 s for GluN1/2C receptors, and current during SSI (I_{SSI}) was measured; (f) normal extracellular solution was applied for at least 40 s; (g) 1 mM glutamate was reapplied for 20 s and control current after SSI ($I_{control2}$) was measured. We chose to use a 1 s wash (>30-fold longer than the τ of solution exchange) in step (d) for ensure complete removal of memantine from the extracellular solution while still maintaining substantial SSI (τ of recovery from SSI is ~2 s) (Kotermanski et al., 2009).

The minimum fractional response after SSI (minimum $I_{SSI}/I_{control}$) was measured by comparing I_{SSI} to the average of $I_{control1}$ and $I_{control2}$ with a point-by-point ratio (Iacobucci and Popescu, 2017b) of $I_{SSI}/I_{control}$, where $I_{control} = ((I_{control1} + I_{control2})/2)$ (see Figure 16). Each of the currents was aligned to the time of glutamate application. We measured the minimum $I_{SSI}/I_{control}$ as the mean of $I_{SSI}/I_{control}$ over a 200 ms window centered on the minimum ratio value. The time constant of recovery from SSI ($\tau_{recovery}$ SSI) was measured by fitting a single exponential function

to recovery of $I_{SSI}/I_{control}$ (see Figure 16). SSI measurements were excluded if $I_{control2}$ did not recover to at least 80% of $I_{control1}$.

Cells with NMDAR currents > 2 nA were excluded from analysis due to large Ca^{2+}-dependent desensitization. Because of potent Mg^{2+} inhibition at -65 mV, for recordings in the continuous presence of 1 mM Mg^{2+} we chose cells with large NMDAR responses that exceeded our current amplitude cutoff in 0 Mg^{2+}. Therefore, separate cells were used for recordings performed in 0 Mg^{2+} and in the continuous presence of 1 mM Mg^{2+}.

3.3.5 Statistics

All statistical comparisons were performed in GraphPad Prism 7. We compared the τ or τ_w of recovery from drug inhibition across drug concentrations for each NMDAR subtype and Mg^{2+} concentration by repeated measures one-way ANOVA with Tukey's post hoc analysis; significance values are indicated in text. Individual pair-wise comparisons of the τ or τ_w of recovery from inhibition by the same drug concentration between 0 and 1 mM Mg^{2+} were made by two-tailed Student's t-test with the Bonferroni correction; significance values are indicated in text. We compared the minimum $I_{SSI}/I_{control}$ across all conditions within each NMDAR subtype by one-way ANOVA with Tukey's post hoc analysis; significance values are indicated in text. We compared the τ recovery SSI between GluN1/2A and GluN1/2C receptors and within each NMDAR subtype between $\tau_{recovery}$ SSI and τ_{slow} of recovery from memantine inhibition by one-way ANOVA with Tukey's post hoc analysis; significance values are indicated in text. All error bars indicate ± standard error of the mean (SEM). Current traces for presentation were refiltered offline in Clampfit 10.3 or 10.7 at 200 Hz.

3.4 Results

3.4.1 Recovery from inhibition by memantine, but not ketamine, exhibits strong dependence on drug concentration

To determine whether addition of 1 mM extracellular Mg^{2+} affects the time course of recovery from inhibition by memantine and ketamine, we first measured recovery from inhibition by memantine and ketamine in 0 Mg^{2+}. We used 1, 10 and 100 μM memantine or ketamine to assess the time course of recovery from inhibition for each drug with the four GluN1/2 diheteromeric NMDAR subtypes: GluN1/2A, GluN1/2B, GluN1/2C, and GluN1/2D receptors. Drug concentrations below 1 μM were not used because the small amount of inhibition prevented reliable measurements of recovery from inhibition. We assessed the time course of recovery from inhibition by comparing time constants of single (τ) or double exponential (τ_w) fits to current relaxations following rapid removal of drug in the continuous presence of agonists (see Methods). NMDARs were activated using 1 mM glutamate (applied at times indicated in figures) and 100 μM glycine (present in all extracellular solutions) to assure that all measurements were performed at saturating agonist concentrations (Traynelis et al., 2010a).

The time course of recovery from memantine and ketamine inhibition exhibited powerful NMDAR subtype dependence. At each memantine and ketamine concentration, recovery from inhibition was fastest for GluN1/2A receptors, slower for GluN1/2B receptors, and slowest for GluN1/2C and GluN1/2D receptors (Figure 12B; Figure 13B; Tables 1 and 2). These results are consistent with a defining characteristic of open channel blockers: recovery from inhibition occurs only when the channel is open, and thus speed of recovery from inhibition correlates with receptor maximal open probability (P_{open}), which is highest for GluN1/2A, lower for GluN1/2B, and lowest

for GluN1/2C and GluN1/2D receptors (Chen et al., 1999, Dravid et al., 2008a, Erreger et al., 2005, Wyllie et al., 1998).

We found in 0 Mg^{2+} that the time course of recovery from memantine inhibition of each NMDAR subtype depended strongly on the concentration of memantine used to inhibit the response (Figure 12B; Figure 14D; Table 1). Consistent with previous studies (Sobolevsky and Koshelev, 1998, Gilling et al., 2007), recovery from inhibition was slower at higher memantine concentrations, although we observed greater dependence of recovery time course on memantine concentration than reported previously (see Discussion). The τ_w of recovery from inhibition with 100 μM memantine was 11.7-fold slower than with 1 μM memantine for GluN1/2A receptors ($p = 0.0002$), 5.1-fold slower for GluN1/2B receptors ($p = <0.0001$), 2.5-fold slower for GluN1/2C receptors ($p = 0.04$), and 1.9-fold slower for GluN1/2D receptors ($p = 0.002$; Figure 12B; Figure 14D; Table 1). In sharp contrast, we found that the time course of recovery from ketamine inhibition was weakly concentration-dependent in GluN1/2A receptors and was not concentration-dependent in GluN1/2B, GluN1/2C, and GluN1/2D receptors (Figure 13B; Figure 15D; Table 2). These data are consistent with previous reports of no concentration dependence of recovery from ketamine inhibition (Parsons et al., 1995, MacDonald et al., 1991, Parsons et al., 1996). The τ_w of recovery from inhibition with 100 μM ketamine was only 1.6-fold slower than with 1 μM ketamine for GluN1/2A receptors ($p = 0.01$), which is ~10-fold less slowing than for memantine for GluN1/2A receptors. This small but significant increase could have resulted from limitations in the speed of solution exchange on washout of high drug concentrations (see Methods). Importantly, both τ_{slow} and A_{slow} (measurement of which should have been unaffected by speed of solution exchange; see Methods) increased substantially across all NMDAR subtypes between 1 and 100 μM for memantine (Table 1), but not ketamine (Table 2). Therefore, it appears implausible

that the robust concentration dependence of the time course of recovery from memantine inhibition could have resulted from limitations in the speed of solution exchange.

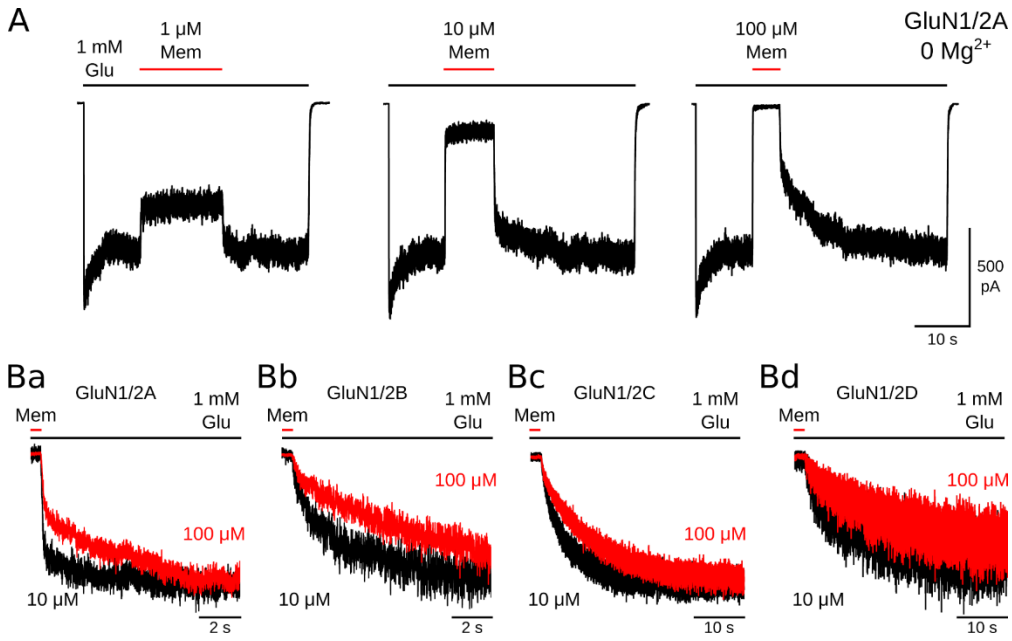

Figure 12 Time course of recovery from memantine inhibition is strongly concentration dependent

A, representative current traces used for measuring the time course of recovery from memantine inhibition of GluN1/2A receptors activated by 1 mM glutamate (Glu, black bars) in 0 Mg^{2+}. Memantine (Mem, red bars) was applied at the indicated concentrations. Traces are from the same cell. B, representative current traces illustrating memantine concentration dependence of recovery from memantine inhibition for GluN1/2A – GluN1/2D receptors (Ba-Bd). Current traces show recovery from memantine (red bars) inhibition in the continuous presence of glutamate (black bars) for GluN1/2A receptors (Ba; from cell used for panel A), or from similar experiments for GluN1/2B – GluN1/2D receptors (Bb-Bd). Pairs of traces at the indicated memantine concentrations are aligned at the time of memantine removal and scaled to the change in current

amplitude during recovery from inhibition. Results of exponential fits to recovery from memantine inhibition are shown in Figure 14 and Table 1.

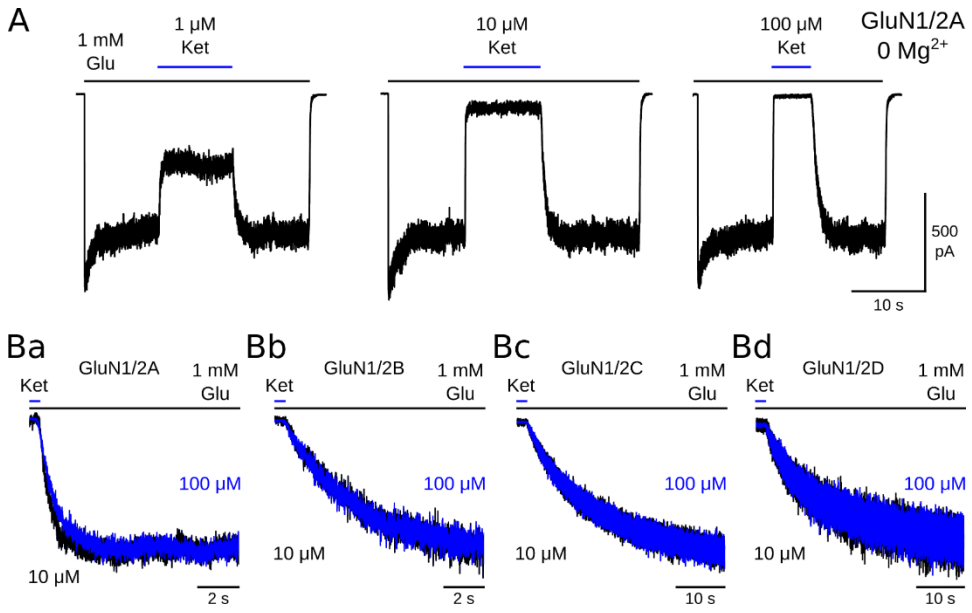

Figure 13 Time course of recovery from ketamine inhibition is largely independent of concentration

A, representative current traces used for measuring the time course of recovery from ketamine inhibition of GluN1/2A receptors activated by 1 mM glutamate (black bars) in 0 Mg^{2+}. Ketamine (Ket, blue bars) was applied at the indicated concentrations. Traces are from the same cell. B, representative current traces illustrating ketamine concentration independence of recovery from ketamine inhibition for GluN1/2A – GluN1/2D receptors (Ba-Bd). Current traces show recovery from ketamine (blue bars) inhibition in the continuous presence of glutamate (black bars) for GluN1/2A receptors (Ba; from cell used for panel A), or from similar experiments for GluN1/2B – GluN1/2D receptors (Bb-Bd). Pairs of traces at the indicated ketamine concentrations are aligned at the time of ketamine removal and scaled to the change in current amplitude during

recovery from inhibition. Results of exponential fits to recovery from ketamine inhibition data are shown in Figure 15D and Table 2.

Table 1 Components of the time course of recovery from memantine inhibition

Values represent means ± SEM, n = 5 – 7 cells per condition. Statistical significance of comparisons of τ_w values is displayed in Figure 14D.

NMDAR Subtype	[Mg^{2+}] (mM)	[Drug] (mM)	t_{fast} (ms)	± SEM	A_{fast}	± SEM	t_{slow} (ms)	± SEM	A_{slow}	± SEM	t_w (ms)	± SEM
GluN1/2A	0	1	67.2	8.07	0.71	0.06	591	205	0.29	0.06	240	82.8
		10	123	12.2	0.68	0.05	2385	402	0.32	0.05	857	204
		100	103	7.82	0.45	0.02	4942	404	0.55	0.02	2799	274
	1	10	107	14.9	0.74	0.04	1218	193	0.26	0.04	369	62.5
		100	110	9.75	0.67	0.03	2788	534	0.33	0.03	1012	207
		1000	249	70.9	0.43	0.03	6126	850	0.57	0.03	3459	309
GluN1/2B	0	1	254	42.4	0.30	0.04	1716	233	0.70	0.04	1167	191
		10	325	41.2	0.45	0.03	3275	303	0.55	0.03	1923	167
		100	262	33.7	0.24	0.03	7723	507	0.76	0.03	5947	459
	1	10	318	57.5	0.51	0.06	2218	608	0.49	0.06	1090	220
		100	373	35.6	0.56	0.02	5949	738	0.44	0.02	2861	367
		1000	329	36.8	0.32	0.02	9261	806	0.68	0.02	6357	533
GluN1/2C	0	1	1030	210	0.25	0.04	5423	499	0.75	0.04	4277	321
		10	1180	236	0.34	0.05	7029	872	0.66	0.05	5129	747
		100	722	159	0.19	0.02	12750	2078	0.81	0.02	10536	1809
	1	1	2569	388	0.54	0.07	11911	1389	0.46	0.07	6566	447
		10	2049	149	0.37	0.04	7671	423	0.63	0.04	5539	244
		100	1816	387	0.28	0.02	11953	1025	0.72	0.02	9159	783
		1000	752	299	0.10	0.03	14255	1211	0.90	0.03	13000	1308
GluN1/2D	0	1	1215	263	0.20	0.02	7880	822	0.80	0.02	6460	583
		10	1730	391	0.29	0.06	13020	1706	0.71	0.06	9383	858
		100	877	254	0.14	0.04	14224	997	0.86	0.04	12539	1119
	1	1	1390	496	0.20	0.04	7181	338	0.80	0.04	6062	219
		10	1697	561	0.26	0.08	9718	1329	0.74	0.08	7374	624
		100	629	162	0.09	0.00	13862	2353	0.91	0.00	12701	2128
		1000	488	133	0.11	0.02	16564	1552	0.89	0.02	14823	1385

Table 2 Components of the time course of recovery from ketamine inhibition

NMDAR Subtype	[Mg^{2+}] (mM)	[Drug] (mM)	T_{fast} (ms)	± SEM	A_{fast}	± SEM	t_{slow} (ms)	± SEM	A_{slow}	± SEM	t or t_w (ms)	± SEM
GluN1/2A	0	1	123	20.3	0.48	0.03	828	114	0.52	0.03	443	57.6
		10	340	40.7	0.64	0.10	1519	572	0.36	0.10	486	28.1
		100	294	60.0	0.40	0.06	1164	145	0.60	0.06	707	55.0
	1	10	259	18.4	0.64	0.07	1732	341	0.36	0.07	688	49.8
		100	345	43.9	0.59	0.06	1624	312	0.41	0.06	797	93.8
		1000	505	45.8	0.62	0.04	1836	191	0.38	0.04	988	90.5
GluN1/2B	0	1	1635	211	0.58	0.07	8165	1820	0.42	0.07	3703	451
		10	934	189	0.27	0.06	4197	472	0.73	0.06	3527	335
		100	1328	264	0.37	0.13	12767	5170	0.63	0.13	3781	426
	1	10	772	142	0.40	0.06	3435	418	0.60	0.06	2287	222
		100	858	178	0.43	0.12	4515	1284	0.57	0.12	2240	202
		1000	1157	144	0.55	0.06	4220	513	0.45	0.06	2327	130
GluN1/2C	0	1	3176	634	0.24	0.05	17502	1320	0.76	0.05	14012	739
		10	2784	770	0.16	0.04	15496	1569	0.84	0.04	13283	963
		100	2785	593	0.16	0.04	17183	1152	0.84	0.04	14754	707
	1	1	4060	1353	0.37	0.14	17412	3967	0.63	0.14	12265	1304
		10	4011	584	0.17	0.03	15951	1196	0.83	0.03	13853	677
		100	2591	619	0.15	0.04	15086	1338	0.85	0.04	13090	747
		1000	2458	617	0.17	0.04	15587	783	0.83	0.04	13300	310
GluN1/2D	0	1	3320	600	0.24	0.03	18779	1998	0.76	0.03	14287	1332
		10	3245	597	0.23	0.04	22074	1771	0.77	0.04	17474	959
		100	3828	963	0.23	0.06	21886	1801	0.77	0.06	17107	900
	1	1	3680	895	0.38	0.11	31316	9184	0.62	0.1	17295	1643
		10	4063	990	0.33	0.09	19422	2718	0.67	0.09	14060	597
		100	4023	214	0.31	0.03	20689	205	0.69	0.03	15546	398
		1000	4580	999	0.39	0.07	26379	2298	0.61	0.07	18165	1918

Values represent means ± SEM. Some cells displayed recovery from ketamine inhibition well fit by a single exponential, whereas other cells required a double exponential fit. Therefore, single exponential τ and double exponential τ_w values were combined when calculating the mean time constant value, with n = 4 – 7 cells per condition. The mean values for double exponential components have n = 2 – 7 cells per condition. Statistical significance of comparisons of τ and τ_w

values is displayed in Figure 15D. Mg^{2+} accelerates recovery from inhibition by memantine and ketamine in an NMDAR subtype-dependent manner

The presence of 1 mM Mg^{2+} causes an increase in the memantine and ketamine IC_{50} values ((Kotermanski and Johnson, 2009); see Introduction). To achieve similar fractional currents at each drug concentration in 1 mM Mg^{2+} as in 0 Mg^{2+} for GluN1/2A and GluN1/2B receptors, we used 10-fold higher memantine and ketamine concentrations (10, 100, and 1000 μM) when measuring the time course of recovery from inhibition in 1 mM Mg^{2+}. For GluN1/2C and GluN1/2D receptors in 1 mM Mg^{2+}, we used four memantine and ketamine concentrations (1, 10, 100, and 1000 μM).

We found that in 1 mM Mg^{2+}, the time course of recovery from memantine inhibition from each NMDAR subtype also exhibited strong concentration dependence (Figure 14A-B,D; Table 1). The τ_w of recovery with 1000 μM memantine was 9.5-fold slower than with 10 μM memantine for GluN1/2A receptors ($p = 0.0005$), 5.8-fold slower for GluN1/2B receptors ($p = 0.002$), 2.4-fold slower for GluN1/2C receptors ($p = 0.02$), and 2-fold slower for GluN1/2D receptors ($p = 0.002$; Figure 14B,D; Table 1). Recovery from ketamine inhibition was only weakly concentration-dependent in 1 mM Mg^{2+} for GluN1/2A receptors, and was concentration independent for GluN1/2B, GluN1/2C, and GluN1/2D receptors (Figure15A-B,D; Table 2), similar to results in 0 Mg^{2+}.

Interestingly, we found that recovery of GluN1/2A receptors from inhibition by 100 μM memantine and of GluN1/2B receptors from inhibition by 10 and 100 μM memantine was significantly faster in 1 mM than in 0 Mg^{2+} (Figure 14C-D; Table 1). Note that for GluN1/2A and GluN1/2B receptors, 10 and 100 μM memantine are the highest concentrations at which recovery from inhibition in 0 and 1 mM Mg^{2+} can be compared. In contrast, recovery from memantine

inhibition of GluN1/2C or GluN1/2D receptors was not faster in 1 mM than in 0 Mg^{2+}, and recovery of GluN1/2C receptors from inhibition by 1 μM memantine was slower in 1 mM than in 0 Mg^{2+} (Figure 14C-D; Table 1). Recovery of GluN1/2A receptors from inhibition by 10 μM ketamine was significantly slower in 1 mM than in 0 Mg^{2+}; recovery of GluN1/2B receptors from inhibition by 10 and 100 μM ketamine was significantly faster in 1 mM than in 0 Mg^{2+}; Mg^{2+} had no effect on recovery from ketamine inhibition of GluN1/2C and GluN1/2D receptors (Figure 15C-D; Table 2). The mechanism responsible for the small and variable slowing by Mg^{2+} of recovery from memantine and ketamine inhibition is not clear; one possibility is screening of surface potential ((Ascher and Nowak, 1988), but see (Zarei and Dani, 1994)) by Mg^{2+} (Isaev et al., 2012). However, the consistent and substantial acceleration by Mg^{2+} of recovery from memantine inhibition from GluN1/2A and GluN1/2B receptors is likely due to other mechanisms, as addressed below. Acceleration by Mg^{2+} of the time course of recovery of GluN1/2B receptors from ketamine inhibition is likely to result from Mg^{2+} potentiation of GluN1/2B receptor responses, which increases P_{open} (Paoletti et al., 1995) and therefore should accelerate the time course of recovery from inhibition; potentiation of GluN1/2B receptors by Mg^{2+} should also partially contribute to acceleration of the time course of recovery of GluN1/2B receptors from memantine inhibition.

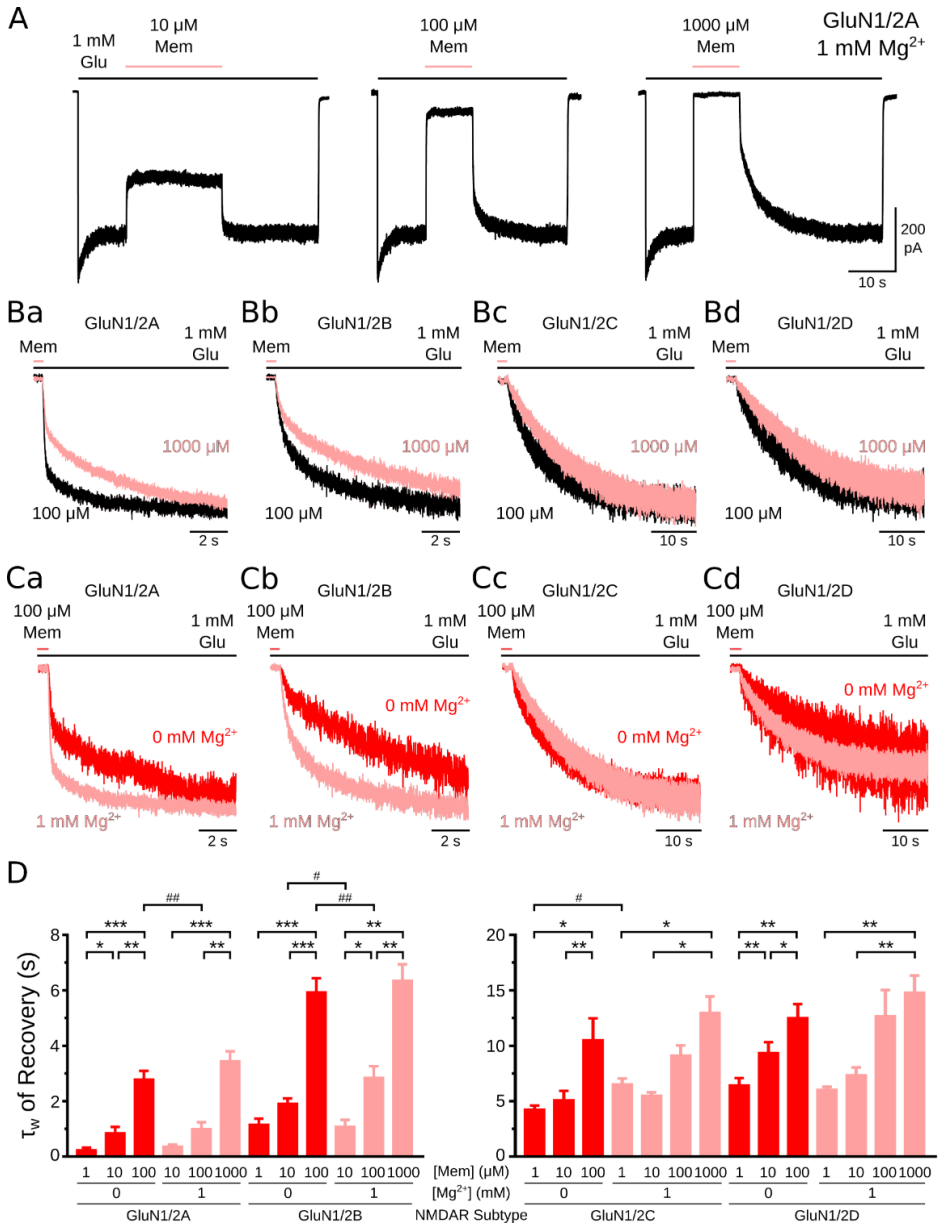

Figure 14 Mg2+ accelerates recovery from memantine inhibition of GluN1/2A and GluN1/2B receptor

A, representative current traces used for measuring the time course of recovery from memantine inhibition of GluN1/2A receptors in 1 mM Mg^{2+}. Receptors were activated by 1 mM glutamate (black bars). Memantine (pink bars) was applied at the indicated concentrations. Traces

are from the same cell. B, representative current traces illustrating memantine concentration dependence of recovery from memantine inhibition for GluN1/2A – GluN1/2D receptors (Ba-Bd) in 1 mM Mg^{2+}. Current traces show recovery from memantine (pink bars) inhibition in the continuous presence of glutamate (black bars) for GluN1/2A receptors (Ba; from cell used for panel A), or from similar experiments for GluN1/2B – GluN1/2D receptors (Bb-Bd). Pairs of traces at the indicated memantine concentrations are aligned at the time of memantine removal and scaled to the change in current amplitude during recovery from inhibition. C, representative current traces illustrate the effect of Mg^{2+} on recovery from 100 μM memantine inhibition of GluN1/2A – GluN1/2D receptors (Ca-Cd) in the continuous presence of glutamate. Pairs of traces in 0 Mg^{2+} (red traces, replotted from corresponding traces in Figure 12Ba-Bd) or 1 mM Mg^{2+} (pink traces, replotted from corresponding traces in Ba-Bd above) are aligned at the time of memantine removal, and scaled to the change in current amplitude during recovery from inhibition. D, Mean values of τ_w of recovery from memantine inhibition for indicated NMDAR subtype, Mg^{2+} concentration, and memantine concentration. Note the change in y-axis scale between GluN1/2A – GluN1/2B and GluN1/2C – GluN1/2D. Comparisons within NMDAR subtype and Mg^{2+} concentration were made by repeated measures one-way ANOVA with Tukey's post hoc analysis (* indicates $p < 0.05$; ** indicates $p < 0.01$; and *** indicates $p < 0.001$). Comparisons of the same memantine concentrations in 0 and 1 mM Mg^{2+} were made by two-tailed Student's t-test with Bonferroni correction for multiple comparisons (# indicates $p < 0.05$; ## indicates $p < 0.01$). n = 5 – 7 cells in each group.

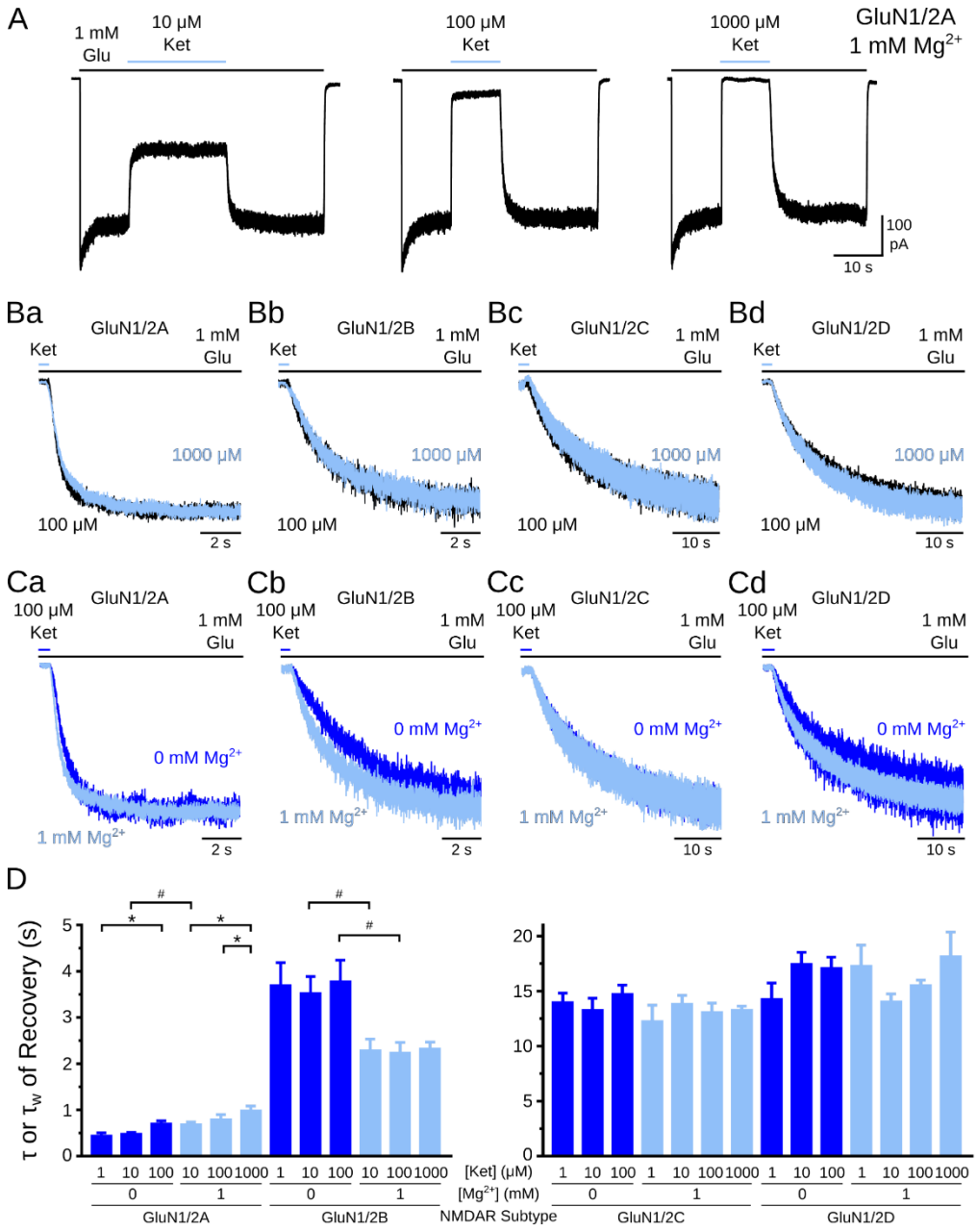

Figure 15 Mg2+ accelerates recovery from ketamine inhibition from GluN1/2B receptors

A, representative current traces used for measuring the time course of recovery from ketamine inhibition of GluN1/2A receptors in 1 mM Mg^{2+}. Receptors where activated by 1 mM glutamate (black bars). Ketamine (light blue bars) was applied at the indicated concentrations. Traces are from the same cell. B, representative current traces illustrating ketamine concentration

independence of recovery from ketamine inhibition for GluN1/2A – GluN1/2D receptors (Ba-Bd) in 1 mM Mg^{2+}. Current traces show recovery from ketamine (light blue bars) inhibition in the continuous presence of glutamate (black bars) for GluN1/2A receptors (Ba; from cell used for panel A), or from similar experiments for GluN1/2B – GluN1/2D receptors (Bb-Bd). Pairs of traces at the indicated ketamine concentrations are aligned at the time of ketamine removal and scaled to the change in current amplitude during recovery from inhibition. C, representative current traces illustrate the effect of Mg^{2+} on recovery from 100 μM ketamine inhibition of GluN1/2A – GluN1/2D receptors (Ca-Cd) in the continuous presence of glutamate. Pairs of traces in 0 Mg^{2+} (blue traces, replotted from corresponding traces in Figure 13Ba-Bd) or 1 mM Mg^{2+} (light blue traces, replotted from corresponding traces in Ba-Bd above) are aligned at the time of ketamine removal, and scaled to the change in current amplitude during recovery from inhibition. D, mean values of τ or τ_w of recovery from ketamine inhibition for indicated NMDAR subtype, Mg^{2+} concentration, and ketamine concentration. Note the change in y-axis scale between GluN1/2A – GluN1/2B and GluN1/2C – GluN1/2D. Comparisons within NMDAR subtype and Mg^{2+} concentration were made by repeated measures one-way ANOVA with Tukey's post hoc analysis (* indicates $p < 0.05$). Comparisons of the same ketamine concentrations in 0 or 1 mM Mg^{2+} were made by Student's t-test with Bonferroni correction for multiple comparisons (# indicates $p < 0.05$). n = 4 – 7 cells in each group.

3.4.2 Recovery from memantine SSI represents the slow component of recovery from memantine inhibition

Dependence of recovery from inhibition on memantine concentration is surprising if inhibition results from interaction of memantine with a single site. Concentration dependence of

the time course of drug *binding* (and thus of inhibition) is expected, since binding occurs in the presence of a varying drug concentration. In contrast, concentration dependence of drug unbinding kinetics (and thus recovery from inhibition) is atypical, since unbinding always occurs at the same drug concentration ([drug] = 0). Memantine concentration dependence of recovery from inhibition was proposed to reflect an ability of memantine to interact with two sites (Sobolevsky and Koshelev, 1998). However, the hypothesis that the site responsible for SSI (Blanpied et al., 1997, Chen and Lipton, 2005, Kotermanski et al., 2009) is involved in the memantine concentration dependence of recovery from inhibition has not been tested. Consistent with this hypothesis, memantine, but not ketamine, exhibits both SSI (Kotermanski et al., 2009) and strong concentration dependence of recovery from inhibition (data presented above). Previous data suggest that, paradoxically, the memantine SSI IC_{50} (~100 μM; (Blanpied et al., 1997, Kotermanski et al., 2009)) is much higher than the memantine IC_{50} for deep site inhibition (~1 μM; (Glasgow et al., 2017)), but the time course of recovery from memantine SSI is relatively slow (Kotermanski et al., 2009, Blanpied et al., 1997). High IC_{50} with slow recovery from inhibition is atypical because the speed of recovery of channel blockers generally increases as IC_{50} increases (Parsons et al., 2007b). Thus, we hypothesized that the slow component of recovery from memantine inhibition, which increases in relative amplitude as memantine concentration increased, reflects recovery from memantine SSI. We next evaluated this hypothesis by examining the time course of recovery from memantine SSI in 0 Mg^{2+}.

To assess memantine SSI, we used the SSI protocol described in Methods (see Figure 16A-B), which is similar to protocols used previously (Blanpied et al., 1997, Kotermanski et al., 2009, Sobolevsky and Koshelev, 1998). We used 100 μM memantine, which is near the previously estimated memantine SSI IC_{50} (80-180 μM (Blanpied et al., 1997, Kotermanski et al., 2009)). As

shown in Figure 14, the effects of Mg^{2+} on the time course of recovery from memantine inhibition are similar for GluN1/2A and GluN1/2B receptors and are similar for GluN1/2C and GluN1/2D receptors. We therefore examined NMDAR subtype dependence of memantine SSI here by comparing data from GluN1/2A and GluN1/2C receptors, first in 0 Mg^{2+} and later in 1 mM Mg^{2+}. We focus exclusively on memantine SSI because we previously showed that ketamine does not exhibit significant SSI (Kotermanski et al., 2009).

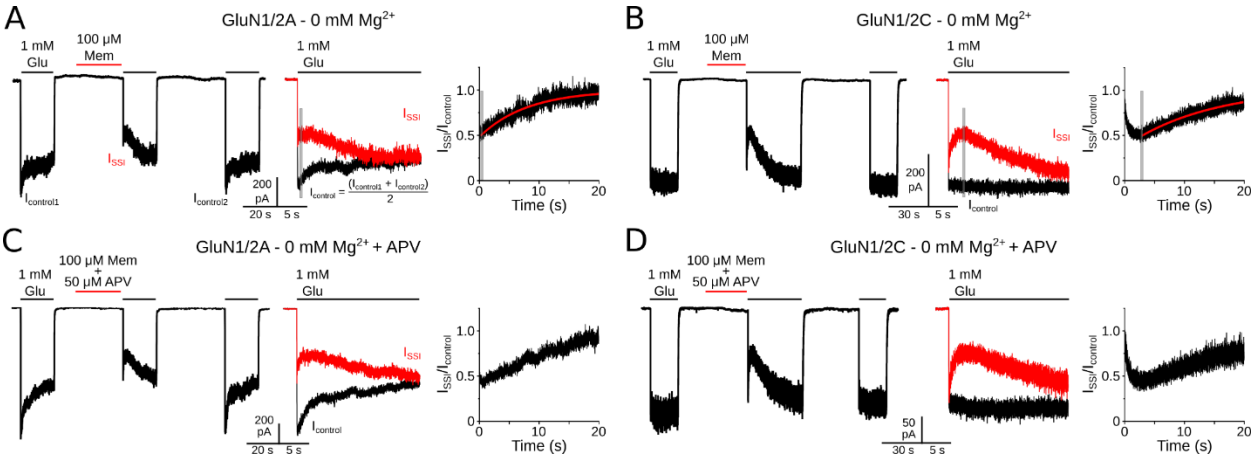

Figure 16 Recovery from memantine SSI represents the slow component of recovery from memantine inhibition

A-D, left, Representative current traces illustrate the memantine SSI protocol for GluN1/2A (A,C) or GluN1/2C (B,D) receptors in 0 Mg^{2+}. APV was present during memantine application only in C and D. Traces are from separate cells. A-D, center, Pairs of traces compare control ($I_{control}$; black) and SSI (I_{SSI}; red) currents aligned at the time of glutamate applications. A-D, right, Plot of $I_{SSI}/I_{control}$ of the example traces shown at left and center. Gray boxes in A and B center indicate the window over which the minimum $I_{SSI}/I_{control}$ was measured for GluN1/2A (A) and for GluN1/2C receptors (B). Red lines in A and B right show single exponential fits to the time course of recovery from SSI.

In 0 Mg^{2+}, we observed that 100 μM memantine induced robust SSI of GluN1/2C as well as GluN1/2A receptors. The minimum $I_{SSI}/I_{control}$ was slightly but significantly ($p = 0.035$) lower for GluN1/2C (0.44 ± 0.03) than for GluN1/2A receptors (0.56 ± 0.03; Figure 16A-B; Figure 17G). These data suggest that the potency of memantine SSI for GluN1/2A and GluN1/2C receptors is similar. The SSI protocol involves a 30-s application of 100 μM memantine in control solution. If our control solution contained a low concentration of contaminating glutamate, it may have permitted some memantine block to occur through open channels that we then misinterpreted as SSI. To control for this possibility, we repeated the SSI protocol while coapplying with memantine a competitive antagonist of glutamate binding (50 μM APV; Figure 16C-D). If a portion of the SSI we observed were due to memantine block of open NMDARs activated by contaminating glutamate, then coapplication of APV with memantine should increase the minimum $I_{SSI}/I_{control}$ (bring the minimum $I_{SSI}/I_{control}$ closer to 1, indicating less SSI). In contrast, when 50 μM APV was coapplied with 100 μM memantine, the minimum $I_{SSI}/I_{control}$ was not increased, but slightly decreased for GluN1/2A receptors (Figure 16C; minimum $I_{SSI}/I_{control}$: memantine, 0.56 ± 0.03; memantine + APV, 0.42 ± 0.02, $p = 0.01$) and was indistinguishable for GluN1/2C receptors (Figure 16D; minimum $I_{SSI}/I_{control}$: memantine, 0.44 ± 0.03; memantine + APV, 0.49 ± 0.03; $p = 0.84$). To determine whether complete unbinding of APV occurred during the 1 s wash following application of memantine and APV, we repeated the SSI protocol using a 30 s application of 50 μM APV alone (with no memantine). We observed no "SSI" using only 50 μM APV with GluN1/2A or GluN1/2C receptors (data not shown; minimum $I_{SSI}/I_{control}$: GluN1/2A, 1.02 ± 0.02; GluN1/2C, 1.04 ± 0.01). Thus, glutamate contamination of control solutions did not result in artefactual inhibition by memantine of open NMDARs. We conclude that SSI reflects a mechanism of memantine access to both GluN1/2A and GluN1/2C NMDARs distinct from

conventional open channel block, consistent with previous reports using neuronal NMDARs (Blanpied et al., 1997, Sobolevsky and Koshelev, 1998). The remaining SSI experiments were conducted without coapplication of APV.

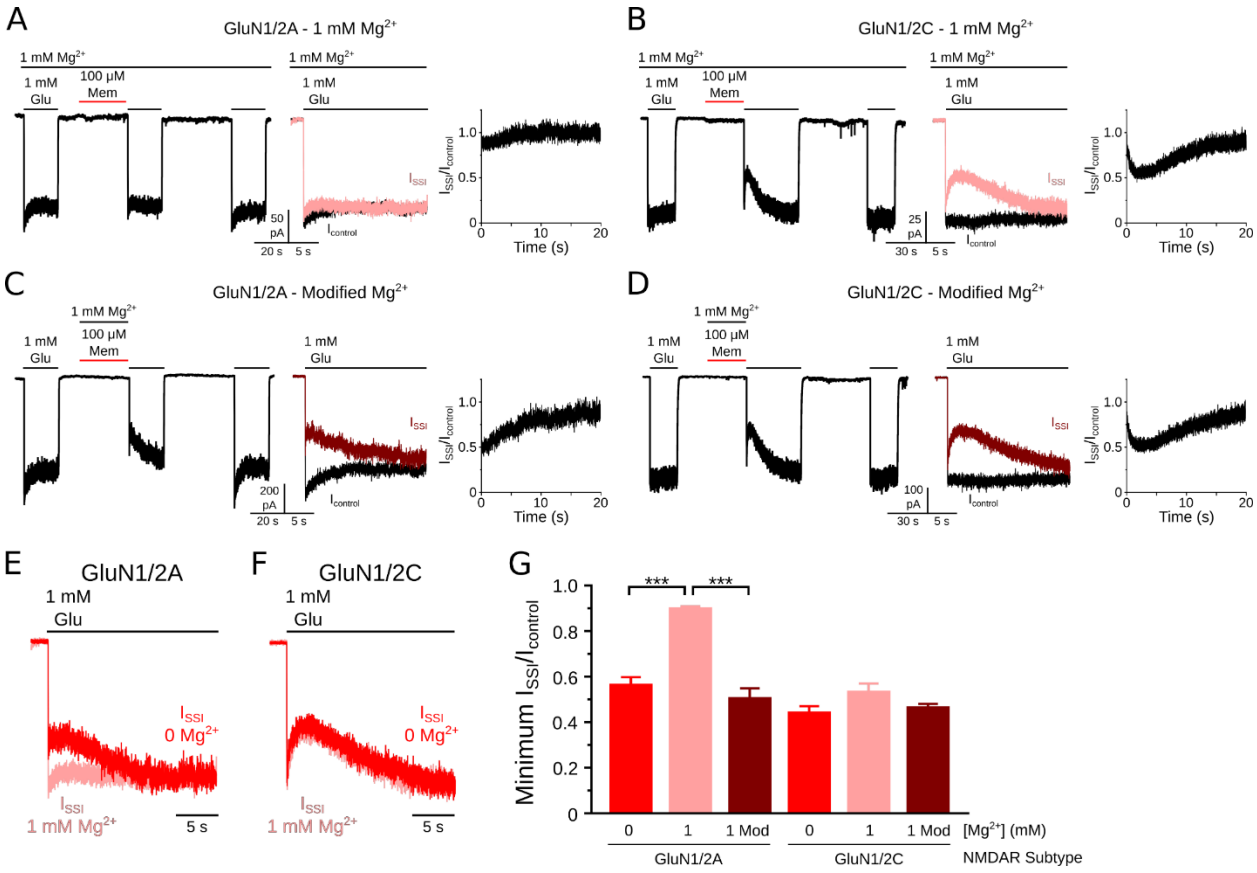

Figure 17 Mg2+ does not compete with memantine for association with the second site

(A-D, left) Representative current traces illustrate the memantine SSI protocol for GluN1/2A (A,C) or GluN1/2C (B,D) receptors in 1 mM Mg^{2+} (A,B) or with the Modified Mg^{2+} SSI protocol (C,D), where 1 mM Mg^{2+} was present only during memantine application. Traces are from separate cells. (A-D, center) Pairs of traces compare control ($I_{control}$; black) and SSI (I_{SSI}; pink and dark red) currents aligned at the time of glutamate applications. (A-D, right) Plot of $I_{SSI}/I_{control}$ of the example traces shown at left and center. (E,F) Representative current traces illustrate the

effect of Mg^{2+} on I_{SSI} for GluN1/2A (E) and GluN1/2C receptors (F). Traces in E are replotted from Figure 16A and 17A, middle; traces in F are replotted from Figure 16B and 17B, middle. Traces are aligned at the time of glutamate applications and scaled to the current amplitude of the steady-state response. (G) Mean minimum $I_{SSI}/I_{control}$ values measured during the window indicated by gray boxes in Figure 16A,B, right. 1 Mod indicates the Modified Mg^{2+} SSI protocol shown in C and D. *** indicate $p < 0.001$ by one-way ANOVA with Tukey's *post hoc* analysis. n = 4 – 6 cells in each group.

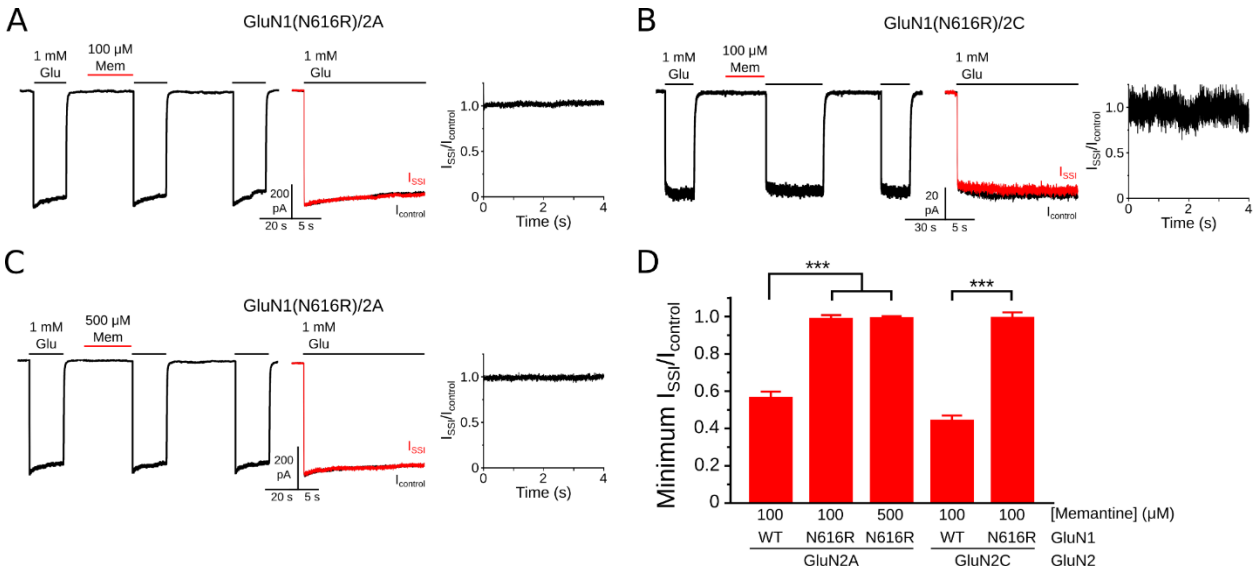

Figure 18 Deep site mutation eliminates memantine SSI

(A-C, left) Representative current traces illustrate the memantine SSI protocol for GluN1(N616R)/2A (A,C) or GluN1(N616R)/2C (B) receptors with 100 µM memantine (A,B) or with 500 µM memantine (C). Traces are from separate cells. (A-C, center) Pairs of traces compare control current ($I_{control}$; black) and current during SSI (I_{SSI}; red) aligned at the time of glutamate applications. (A-C, right) Plot of $I_{SSI}/I_{control}$ of the example traces shown at left and center. (D)

Mean minimum $I_{SSI}/I_{control}$ values measured during the time window indicated by gray boxes in Figure 16A,B, right. Mean values of the minimum $I_{SSI}/I_{control}$ for wild-type (WT) GluN1/2A and GluN1/2C receptors are replotted from Figure 17G. *** indicate $p < 0.001$ by one-way ANOVA with Tukey's *post hoc* analysis. n = 5 – 6 cells in each group.

Despite similar memantine SSI potency for GluN1/2A and GluN1/2C receptors, the time course of recovery from SSI appeared to be faster for GluN1/2A than for GluN1/2C receptors. To quantify the time course of recovery from SSI we measured the $\tau_{recovery}$ SSI (see Methods). We found that the time course of recovery from SSI was ~3-fold faster for GluN1/2A than for GluN1/2C receptors ($\tau_{recovery}$ SSI: GluN1/2A, 5.51 ± 0.33 s; GluN1/2C, 17.1 ± 1.4 s; $p < 0.0001$). It is unclear why the time course of recovery from SSI is faster for GluN1/2A than for GluN1/2C receptors. Possible explanations include dependence on NMDAR properties that differ between GluN1/2A and GluN1/2C receptors, such as P_{open}, gating kinetics or desensitization (Glasgow et al., 2015, Paoletti et al., 2013). As we hypothesized, the time course of recovery from SSI for GluN1/2A and GluN1/2C receptors is strikingly similar to the τ_{slow} of recovery from inhibition by 100 μM memantine in 0 Mg^{2+}, which also exhibits ~3-fold difference between GluN1/2A and GluN1/2C receptors (Table 1). Indeed, the $\tau_{recovery}$ SSI was indistinguishable from the τ_{slow} of recovery from inhibition by 100 μM memantine for GluN1/2A and GluN1/2C receptors (Table 1; $\tau_{recovery}$ SSI vs. τ_{slow} of recovery from inhibition by 100 μM memantine: GluN1/2A, $p = 0.99$; GluN1/2C, $p = 0.31$). These data strongly support our hypothesis that the slow component of recovery from memantine inhibition, which becomes more prominent as memantine concentration increases (Figure 12; Table 1), reflects recovery from SSI.

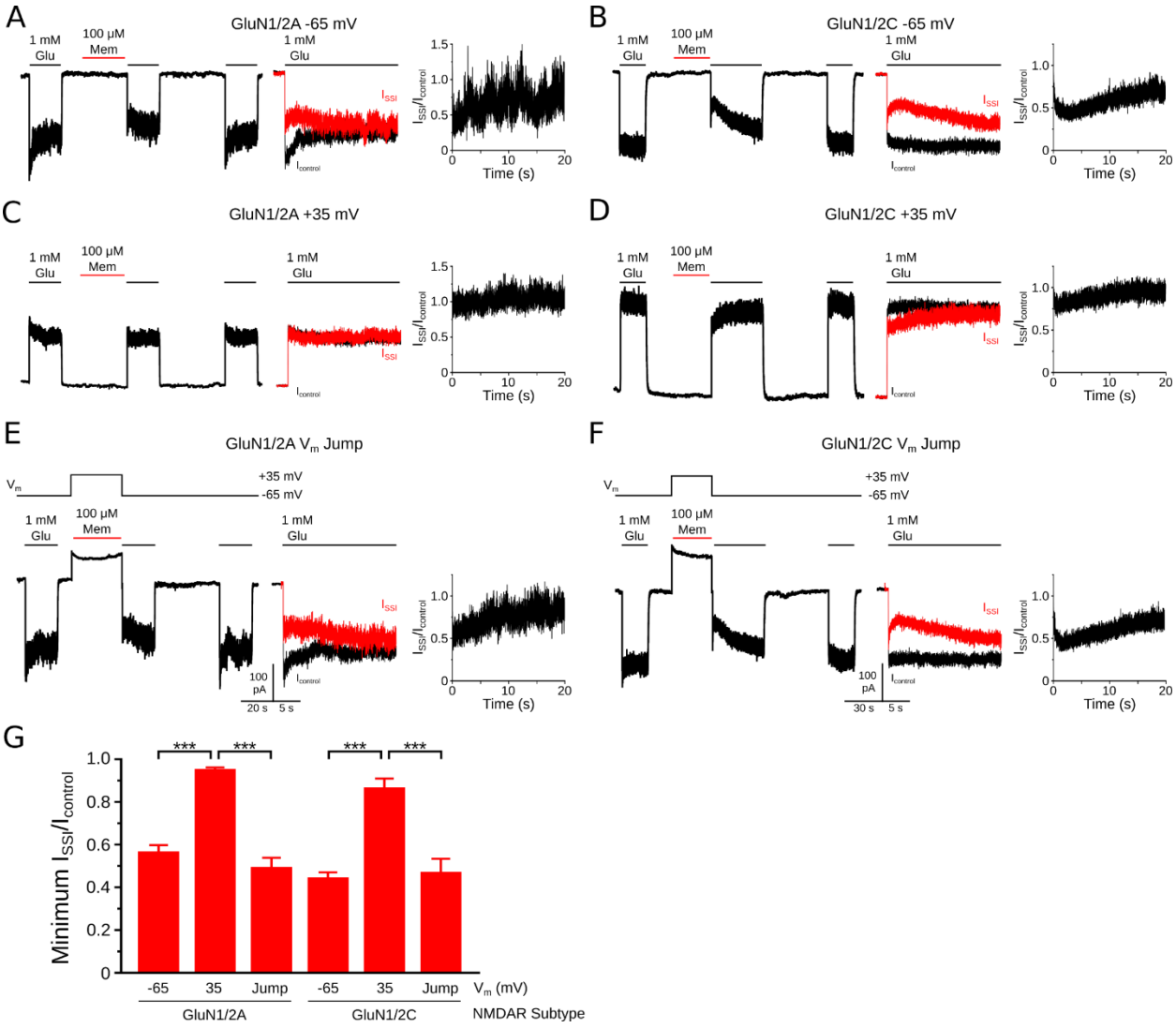

Figure 19 SSI requires memantine transit from the second site to the deep site

(A-F, left) Representative current traces illustrate the memantine SSI protocols in 0 Mg^{2+} for GluN1/2A (A,C,E) or GluN1/2C receptors (B,D,F) receptors. SSI protocols were performed at -65 mV (A,B), at +35 mV (C,D), or at -65 mV with a voltage jump to +35 mV from 0.5 s before to 0.5 s after memantine application (V_m Jump; E,F). Traces for GluN1/2A receptors (A,C,E) are from the same cell, and traces for GluN1/2C receptors (B,D,F) are from the same cell; mean data include cells where not all protocols were performed in the same cell. (A-F, center) Pairs of traces

compare control ($I_{control}$; black) and SSI (I_{SSI}; red) currents aligned at the time of glutamate applications. (A-F, right) Plot of $I_{SSI}/I_{control}$ of the example traces shown at left and center. (G) Mean minimum $I_{SSI}/I_{control}$ values during the time window indicated by gray boxes in Figure 16A,B, right. *** indicate $p < 0.001$ by one-way ANOVA with Tukey's *post hoc* analysis. n = 4 – 6 cells in each group. Mean values of the minimum $I_{SSI}/I_{control}$ for -65 mV in G are replotted from Figure 17G.

3.4.3 Mg^{2+} does not compete with memantine for association with the second site

Acceleration by Mg^{2+} of recovery from memantine inhibition (Figure 14; Table 1) could result from reduction by Mg^{2+} of the slow component of recovery from memantine inhibition for which SSI is responsible. Therefore, we next determined directly whether Mg^{2+} disrupts memantine SSI using the SSI protocol in the continuous presence of 1 mM Mg^{2+}. We found that in 1 mM Mg^{2+}, the minimum $I_{SSI}/I_{control}$ of GluN1/2A, but not of GluN1/2C receptors was significantly increased (Figure 17A,B,E-G). One possible explanation for these data is that Mg^{2+} competes with memantine for association with the second site of GluN1/2A receptors, but not for association with the second site of GluN1/2C receptors. To test this hypothesis more directly, we used a modified Mg^{2+} SSI protocol in which we coapplied 1 mM Mg^{2+} only during the application of 100 μM memantine (Modified Mg^{2+}; Figure 17C-D). If Mg^{2+} competes with memantine for association with the second site of GluN1/2A receptors, then the minimum $I_{SSI}/I_{control}$ should increase when measured using the Modified Mg^{2+} SSI protocol. Strikingly, we found that the minimum $I_{SSI}/I_{control}$ measured using the Modified Mg^{2+} SSI protocol was indistinguishable from the minimum $I_{SSI}/I_{control}$ measured in 0 Mg^{2+} for GluN1/2A receptors (and, not surprisingly, for

GluN1/2C receptors) (Figure 17C-D,G). These data suggest that Mg^{2+} does not compete with memantine for association with the second site.

If Mg^{2+} does not compete for association with the second site, how else might 1 mM Mg^{2+} reduce memantine SSI and accelerate recovery from memantine inhibition of GluN1/2A and GluN1/2B receptors, but not of GluN1/2C and GluN1/2D receptors? Interestingly, the NMDAR subtype dependence of Mg^{2+} IC_{50} (Kuner and Schoepfer, 1996, Monyer et al., 1994) results in a similar pattern of Mg^{2+} occupation of the deep site in 1 mM Mg^{2+}: there is much greater Mg^{2+} occupation of the deep site of GluN1/2A and GluN1/2B receptors than of GluN1/2C or GluN1/2D receptors. We therefore considered the hypothesis that Mg^{2+} competition with memantine for association with the deep site reduces memantine SSI of GluN1/2A receptors. This hypothesis suggests that memantine SSI may require transit of memantine from the second site to the deep site.

3.4.4 SSI requires memantine transit from the second site to the deep site

If memantine SSI requires transit of memantine from the second site to the deep site, then elimination of deep site binding by memantine should also eliminate memantine SSI. To test this prediction, we determined whether mutating the GluN1 N-site asparagine residue, which is critical to deep site binding by channel blockers, affects memantine SSI. We mutated the GluN1 N-site to an arginine (GluN1(N616R)), which greatly increases the memantine IC_{50} (Chen and Lipton, 2005, Kashiwagi et al., 2002).

We measured the minimum $I_{SSI}/I_{control}$ for GluN1(N616R)/2A and GluN1(N616R)/2C receptors (Figure 18A-B,D) using the SSI protocol as shown in Figure 16A-B. Strikingly, we found that SSI was completely abolished in GluN1(N616R)/2A and in GluN1(N616R)/2C receptors. We

also performed the SSI protocol with 500 μM memantine, a concentration that nearly saturates SSI in native NMDARs and in wild-type GluN1/2A receptors (Blanpied et al., 1997, Kotermanski et al., 2009). Even with 500 μM memantine, SSI was absent in GluN1(N616R)/2A receptors (Figure 18C-D). These data are consistent with the hypothesis that memantine association with the second site does not inhibit NMDARs, and that SSI requires transit of memantine from the second to the deep site. Inhibition would occur exclusively after memantine transits to the deep site, explaining why SSI was abolished by mutation of the deep site (Figure 18), and was reduced by Mg^{2+} occupation of the deep site (Figure 17).

We cannot rule out that the possibility that the GluN1(N616R) deep site mutation also may indirectly affect association of memantine with the second site. To further test our hypothesis that memantine SSI requires transit from the second site to the deep site in wild-type NMDARs, we next took advantage of the V_m dependence of memantine inhibition at the deep site (Blanpied et al., 1997, Bresink et al., 1996, Frankiewicz et al., 1996, Chen and Lipton, 1997). If SSI occurs via memantine transit from the second site to the deep site, then SSI should significantly decrease at depolarized voltage. SSI previously was found to be V_m-dependent, although less V_m-dependent than inhibition at the deep site (Blanpied et al., 1997). However, the previous experiments were interpreted assuming that occupation of the second site was sufficient to inhibit NMDAR responses. If SSI requires memantine transit from the second site to the deep site, then V_m dependence of SSI could result from the V_m dependence of dissociation from the deep site. In this case, occupation of the second site could exhibit negligible or no V_m dependence. We therefore determined whether occupation of the second site differed at -65 mV and 35 mV by comparing in 0 Mg^{2+} the results of three SSI protocols: (a) a protocol performed entirely at -65 mV (Figure 19A-B); (b) a protocol performed entirely at 35 mV (Figure 19C-D); (c) a protocol in which 100 μM

memantine was applied at 35 mV, but the rest of the protocol was performed at -65 mV (V_m Jump; Figure 19E-F). Experiments were performed using both GluN1/2A and GluN1/2C receptors; results described below apply to both NMDAR subtypes.

We found that when the entire SSI protocol was performed at 35 mV (protocol (b); Figure 19C-D,G), the minimum $I_{SSI}/I_{control}$ was significantly greater (reflecting weaker inhibition) than when the entire protocol was performed at -65 mV (protocol (a); Figure 19A-B,G), confirming that memantine SSI is V_m-dependent. However, when memantine was applied at 35 mV and the minimum $I_{SSI}/I_{control}$ measured at -65 mV (protocol (c); Figure 19E-G), the minimum $I_{SSI}/I_{control}$ was indistinguishable from the minimum $I_{SSI}/I_{control}$ at -65 mV, but was significantly less (reflecting greater inhibition) than the minimum $I_{SSI}/I_{control}$ at 35 mV. These results show that memantine association with the second site is voltage-independent, but that subsequent SSI depends on voltage. Protocol (c) (Figure 19E-F) demonstrates that when applied at 35 mV, memantine associated with the second site; protocol (b) (Figure 19C-D) demonstrates that memantine occupation of the second site did not result in NMDAR response inhibition. Thus, SSI is V_m-dependent, but only insofar as inhibition requires occupation of the deep site via memantine transit from the second site to the deep site.

3.5 Discussion

This study was initiated to investigate the effects of Mg^{2+} on the time course of recovery from inhibition by memantine and ketamine of the four main diheteromeric NMDAR subtypes, GluN1/2A – GluN1/2D receptors. Our results provide several new insights into mechanisms of

memantine and ketamine inhibition in the absence and presence of Mg^{2+}. We found that in 0 Mg^{2+}, the time course of recovery from memantine inhibition is ~2- to 10-fold slower following inhibition by 100 μM than following inhibition by 1 μM memantine (Figure 12; Figure 14D). The time course of recovery from ketamine inhibition, in contrast, demonstrated minimal dependence on ketamine concentration (Figure 13; Figure 16D). These data are consistent with the hypotheses that memantine inhibits via the deep site and via SSI, whereas ketamine inhibits via the deep site, but not via SSI (Blanpied et al., 1997, Chen and Lipton, 2005, Johnson et al., 2015, Kotermanski et al., 2009, Parsons et al., 2007b, Sobolevsky and Koshelev, 1998). The concentration dependence of recovery from memantine inhibition and the minimal concentration dependence of recovery from ketamine inhibition were maintained in 1 mM Mg^{2+} (Figure 14A-B,D; Figure 15A-B,D). We demonstrated that 1 mM Mg^{2+} accelerates recovery from memantine and ketamine inhibition in an NMDAR subtype-dependent manner (Figure 14C-D; Figure 15C-D). We inferred that Mg^{2+} accelerates recovery from memantine inhibition of GluN1/2A and GluN1/2B receptors by reducing SSI, a form of inhibition from which recovery is surprisingly slow (Figure 16A-B). In addition, it is likely that Mg^{2+} accelerates recovery from both memantine and ketamine inhibition of GluN1/2B receptors as a result of a Mg^{2+}-induced increase in P_{open} (Paoletti et al., 1995). We showed that Mg^{2+} reduces memantine SSI, but not as a result of Mg^{2+} competition for association with the second site (Figure 17). To test the alternative hypothesis that Mg^{2+} reduces memantine SSI by competing for binding to the deep site, we mutated the GluN1 asparagine essential to formation of the deep site. We found that mutation of the deep site also eliminated SSI (Figure 18). Examination of the V_m dependence of SSI and of memantine association with the second site further supported the conclusion that memantine occupation of the second site does not result in

NMDAR inhibition (Figure 19); inhibition only occurs after memantine transits from the second site to the deep site.

3.5.1 Determinants of the time course of recovery of NMDAR inhibition by memantine

Our finding that the time course of recovery from memantine inhibition depends strongly on the memantine concentration used to induce inhibition is inconsistent with previous studies that reported little or no concentration dependence (Frankiewicz et al., 1996, Gilling et al., 2009, Gilling et al., 2007, Parsons et al., 1993, Parsons et al., 1995). However, several previous studies did report an increase in the amplitude of the slow component of recovery from memantine inhibition with increasing drug concentration (Sobolevsky and Koshelev, 1998). We also saw an increase in the amplitude of the slow component of recovery from memantine inhibition. However, overall, we saw a greater dependence of recovery from inhibition on memantine concentration than has been reported previously. We believe our examination of single NMDAR subtypes and several aspects of our experimental conditions explain most of the differences between our results and those of previous studies.

We were able to study single NMDAR subtypes because our experiments were conducted in a heterologous expression system as opposed to neurons (Frankiewicz et al., 1996, Gilling et al., 2007, Parsons et al., 1993, Parsons et al., 1995, Sobolevsky and Koshelev, 1998, Blanpied et al., 1997), which contain a heterogeneous population of NMDAR subtypes, including triheteromeric NMDARs (Glasgow et al., 2015, Paoletti et al., 2013, Al-Hallaq et al., 2007, Luo et al., 1997). As the time course of recovery from inhibition differed greatly across NMDAR subtypes (Figure 12B; Figure 14D; Table 1), the presence of multiple NMDAR subtypes could alter interpretation of measurements obtained from neurons. Nevertheless, we see clear

concentration dependence of the time course of recovery from memantine inhibition across NMDAR subtypes, which is consistent with previous observations in neurons (Sobolevsky and Koshelev, 1998).

In addition, several of our experimental conditions may have facilitated observation of concentration-dependent recovery from memantine inhibition by permitting us to observe fast recovery from deep site inhibition by memantine. Concentration dependence of the time course of recovery from memantine inhibition can be detected only if recovery from deep site inhibition is much faster than recovery from SSI. The rapid component of recovery from inhibition was much faster than the slow component under our experimental conditions because of our use of: (a) solutions that promoted high NMDAR P_{open}, (b) a perfusion system that permitted rapid elimination of memantine from the extracellular solution, and (c) use of tsA201 cells, which are more compact than neurons, permitting nearly simultaneous solution exchange around the entire cell, and recording of currents that are not slowed by neurite cable properties. Our use of solutions that increased NMDAR P_{open} was important because recovery from memantine inhibition at the deep site can occur only when the channel is open; increasing P_{open} therefore accelerates recovery from memantine inhibition at the deep site. NMDAR P_{open} was increased by our use of a saturating concentration of the full agonist glutamate, rather than a low or intermediate concentration of the partial agonist NMDA or aspartate (Traynelis et al., 2010a) used in most other studies. To prevent NMDAR current rundown, thereby also maintaining a relatively high P_{open}, we included ATP in the intracellular solution (Tong and Jahr, 1994); ATP was not present in the intracellular solutions used in most other studies cited above. We also included 10 μM EDTA in our extracellular solution to chelate contaminating Zn^{2+}, which inhibits GluN1/2A receptors (Paoletti et al., 1997). Our fast perfusion system was capable of rapid solution exchange (see Methods), which should not be rate-

limiting for components with time constants slower than ~0.15 s. Probably resulting from our use of high P_{open} conditions and a relatively rapid perfusion system, our τ_{fast} values for recovery from memantine inhibition were ~5- to 20-fold faster than previously reported values (Bresink et al., 1996, Gilling et al., 2009, Gilling et al., 2007, Sobolevsky and Koshelev, 1998). Thus, we hypothesize that we observed especially strong concentration dependence of recovery from memantine inhibition because our conditions encouraged fast recovery from memantine inhibition at the deep site, which is the dominant binding site at low memantine concentrations. Nevertheless, our measured τ_{fast} values probably were limited by the speed of solution exchange, especially at higher drug concentrations (see Methods), a conclusion supported by the slightly faster τ's recorded using outside-out patches (Parsons et al., 2008a).

The identity and concentration of intracellular permeant cations affect the V_m dependence, microscopic binding rate, and potency, but not the microscopic unbinding rate, of NMDAR channel blockers including Mg^{2+} (Ruppersberg et al., 1994, Antonov and Johnson, 1999), memantine (Chen and Lipton, 1997, Parsons et al., 1999), and ketamine (MacDonald et al., 1991). Since recovery from inhibition depends upon the microscopic unbinding rate of the channel blocker and the NMDAR P_{open}, we do not expect our use of non-physiological intracellular Cs^+ strongly impacted measurements of recovery from inhibition by memantine or ketamine. However, it is possible that the identity of the intracellular cation affects the development or V_m dependence of SSI. It will be important in future studies to determine how physiological intracellular K^+, which speeds the microscopic binding rates of NMDAR channel blockers compared to Cs^+, affects SSI.

The time course of recovery from inhibition by memantine was adequately fit by double exponential functions, which we used to characterize phenomenologically the speed of recovery from inhibition. However, recovery from inhibition is expected to contain many kinetic

components, most of which cannot be resolved by exponential fits of whole-cell data. We determined that at least two separable processes were involved in recovery from memantine inhibition: recovery from deep site inhibition and recovery from SSI. Both processes should exhibit multiple kinetic components. The time course of the more rapid process, recovery from deep site inhibition, in principle depends on the kinetics of all channel gating transitions. However, because open channel blockers like memantine can unbind only when the channel is open, the P_{open} of blocked channels is of primary importance. The P_{open} of a blocked channel depends both on its intrinsic gating properties, and on any modifications of gating properties that result from channel occupation by the blocker. The NMDAR subtype dependence of P_{open} is probably the predominant determinant of the strong NMDAR subtype dependence of the time course of recovery from inhibition observed for both memantine and ketamine. Channel occupation by a blocker can result in either an increase or a decrease in the P_{open} of blocked channels compared to the P_{open} of unblocked channels. In the extreme case of a sequential (or foot-in-the-door) blocker, the blocker prevents channel closure (see, e.g. (Costa and Albuquerque, 1994, Vorobjev and Sharonova, 1994, Benveniste and Mayer, 1995, Sobolevsky, 1999, Sobolevsky et al., 1999, Antonov and Johnson, 1996, Paganelli and Popescu, 2015, Koshelev and Khodorov, 1995)). Memantine and ketamine, in contrast, are trapping channel blockers, which permit channel closure while blocking the channel. Channel occupation by trapping channel blockers nevertheless can affect channel gating (e.g. (Blanpied et al., 1997, Blanpied et al., 2005, Dilmore and Johnson, 1998, Glasgow et al., 2017, Sobolevskii and Khodorov, 2002, Sobolevsky, 1999, Sobolevsky et al., 1999)). Thus, the complex time course of recovery from inhibition at the deep site depends both on the intrinsic gating properties of the NMDAR subtype under study, and on the specific effects of a blocker on channel gating.

We identified recovery from SSI as the slower process involved in recovery from memantine inhibition based on multiple lines of evidence: (1) recovery from inhibition by memantine but not ketamine became slower at higher drug concentrations close to the memantine SSI IC_{50}, and memantine but not ketamine exhibits SSI; (2) the effect of Mg^{2+} on the time course of recovery from memantine inhibition and on memantine SSI exhibited the same NMDAR subtype dependence; (3) the slow component of recovery from memantine inhibition became more prominent at the higher memantine concentrations required to induce SSI; (4) the directly-measured $\tau_{recovery}$ SSI was nearly identical to the τ_{slow} of recovery from inhibition by 100 μM memantine for both GluN1/2A and GluN1/2C receptors. Because SSI involves transit of memantine from the second site to the deep site, recovery from SSI is also likely to exhibit a complex time course of recovery. Importantly, association of memantine with the second site does not require NMDAR activation (Figure 16). Thus, models of NMDAR inhibition by memantine in which memantine access to both of two sites requires channel activation (Sobolevsky and Koshelev, 1998, Sobolevsky, 1999) are inconsistent with the data presented here.

3.5.2 Mg^{2+} accelerates recovery from memantine and ketamine inhibition via multiple mechanisms

We found that extracellular Mg^{2+} accelerated recovery from memantine and ketamine inhibition, but with distinct NMDAR subtype dependence (Figure 14D; Figure 15D). Mg^{2+} accelerated recovery from ketamine inhibition only from GluN1/2B receptors, which also exhibit Mg^{2+}-induced potentiation via an increase in P_{open} (Paoletti et al., 1995). Therefore, Mg^{2+} potentiation alone may underlie Mg^{2+}-induced acceleration of recovery from ketamine inhibition

from GluN1/2B receptors. Mg^{2+} potentiation likely also partially underlies Mg^{2+}-induced acceleration of recovery from memantine inhibition of GluN1/2B receptors. However, because Mg^{2+} accelerated recovery from memantine inhibition of GluN1/2A as well as GluN1/2B receptors, we concluded that Mg^{2+} affects recovery from memantine and ketamine inhibition via distinct mechanisms. Our memantine SSI results (Figures 16-19) suggest that Mg^{2+} accelerates recovery from memantine inhibition because Mg^{2+} occupation of the deep site interferes with memantine transit from the second site to the deep site. As a result, the slow component of recovery from memantine inhibition, which reflects the time course of recovery from SSI, is reduced. Therefore, we propose that Mg^{2+} accelerates recovery from inhibition at two separate sites: (1) the site at which Mg^{2+} binds to GluN1/2B receptors to induce potentiation, and (2) the deep channel blocking site of GluN1/2A and GluN1/2B receptors.

Mg^{2+} recently was demonstrated to accelerate recovery from inhibition by MK-801, another NMDAR channel blocker, of cultured cortical neurons (McKay et al., 2013). Mg^{2+}-induced acceleration of recovery from MK-801 inhibition likely results in part from Mg^{2+} potentiation of neuronally expressed GluN1/2B receptors. It is unclear whether MK-801 also associates with the same second site as memantine, and can transit to the deep site. MK-801 can inhibit NMDARs from the intracellular solution (Rodríguez-Moreno and Paulsen, 2008, Berretta and Jones, 1996, Bouvier et al., 2015) as well as the extracellular solution, suggesting that, like memantine, MK-801 may be able to inhibit via multiple sites or routes. Unlike MK-801, intracellular memantine was found not to inhibit NMDARs (Parsons et al., 2008b). However, intracellular memantine was tested only at 30 μM, a concentration much lower than the intracellular MK-801 concentration typically used to inhibit NMDARs. The ability of Mg^{2+} to induce phenomenologically similar effects on the time course of recovery from inhibition by two

channel blockers suggests that multiple mechanisms of inhibition may be common among NMDAR channel blockers.

3.5.3 Mechanism of memantine second site inhibition

In previous studies, two experimental observations were ascribed to the ability of memantine to associate with two sites: (1) the time course of recovery from memantine inhibition depended on the concentration of memantine used to inhibit the NMDAR response; (2) exposure to memantine in the absence of agonist resulted in inhibition of a subsequent NMDAR response activated by agonist application shortly after removal of memantine (Blanpied et al., 1997, Chen and Lipton, 2005, Kotermanski et al., 2009, Sobolevsky and Koshelev, 1998). Our data support the hypothesis that memantine's ability to associate with two sites results in concentration dependence of recovery from memantine inhibition. The memantine IC_{50} is lower at the deep site than the second site, but recovery from memantine inhibition is faster from the deep site than the second site; increasing memantine concentration therefore increases association with the second site and slows recovery from inhibition. We found in addition that Mg^{2+} accelerates recovery from memantine inhibition and reduces memantine SSI in an NMDAR subtype-dependent manner. Both phenomena result from competition between Mg^{2+} and memantine, although surprisingly, not competition for association with the second site. Instead, competition between Mg^{2+} and memantine for binding to the deep site interferes with transit of memantine from the second site to the deep site. These phenomena can be explained by the hypothesis that memantine can associate with, but does not cause inhibition at, the second site; inhibition from the second site requires memantine transit to the deep site. Since memantine can associate with the second site of unactivated NMDARs, but deep site access requires channel opening, transit from the second site

to the deep site likely requires channel opening. If second site to deep site transit is slow enough, it may be possible to observe development of inhibition as memantine transit takes place. We propose that the initial phase of SSI development that was particularly clear with GluN1/2C receptors (e.g., Figure 16B and D, right; initial period of decreasing $I_{SSI}/I_{control}$) may represent the transit of memantine from the second site to the deep site.

Numerous NMDAR channel blocking antagonists other than memantine have been found to exhibit two distinct binding sites or modes, including: ketamine (Orser et al., 1997); some derivatives of adamantane (Antonov and Johnson, 1996); tetraethylammonium, MRZ 2/178, and 9-aminoacridine (Sobolevsky, 1999, Sobolevsky et al., 1999); amantadine and some derivatives of phencylcyclohexyl derivatives (Bolshakov et al., 2003); bupivacaine (Paganelli and Popescu, 2015). However, in each of these studies, the drug was found to inhibit NMDARs when occupying either of the two sites, suggesting mechanisms of action that differ from SSI by memantine.

Where might the second site be located? Our data are not inconsistent with the hypothesis that the second site is located near the external entrance to the NMDAR channel, as previously proposed (Blanpied et al., 1997, Chen and Lipton, 2005, Sobolevsky and Koshelev, 1998, Kotermanski et al., 2009). However, the paradoxical combination of high IC_{50} with very slow recovery from SSI suggests the second site may not be a traditional receptor binding site. An alternative possibility is that the second site represents a pool or reservoir of memantine that builds up during memantine application in the absence of agonists, and slowly depletes after memantine washout. Memantine SSI then would occur when memantine transits from the second site reservoir to the deep site. Due to memantine's lipophilicity (Chew et al., 2008, del Rio-Sancho et al., 2012, Zambrano et al., 2018), plausible locations of a memantine second site reservoir include the intracellular compartment or the membrane (Blanpied et al., 1997). As discussed above, there is

evidence that memantine does not inhibit from the intracellular compartment (Parsons et al., 2008b). However, the intracellular memantine concentration may reach much higher levels during the SSI protocol than the concentration previously tested. Determination of the location and the nature of the second site will require further investigation.

Full understanding of the complex effects of Mg^{2+} and of SSI on properties of memantine inhibition of NMDARs will require further investigation. For example, the therapeutic potential of targeting the second site remains to be determined. Although the memantine SSI IC_{50} is much higher than the estimated memantine concentration in the brain at therapeutic doses (0.5-1 μM (Parsons et al., 2007b)), SSI is an indirect measure of memantine association with a second site. Due to these necessarily indirect measurements, there may be yet undiscovered additional consequences of memantine association with a second site at lower concentrations. For example, there could be a rapid component of memantine dissociation from the second site that we did not observe because of the 1-s wash following memantine application in our SSI protocol. If this is the case, memantine may associate with the second site at concentrations lower than those used here. Thus, it will be important to further evaluate the implications of SSI. In addition to the influence of Mg^{2+} on SSI, physiological concentrations of Mg^{2+} impart selectivity of memantine or ketamine for GluN2C- and GluN2D-containing NMDARs that may be of high clinical significance (Khlestova et al., 2016, Povysheva and Johnson, 2016). Our demonstration that Mg^{2+} accelerates recovery of GluN1/2A and GluN1/2B receptors from memantine inhibition, and GluN1/2B receptors from ketamine inhibition, reveals that Mg^{2+} has NMDAR subtype-selective effects on drug kinetics as well as on IC_{50}. Insights into NMDAR inhibition by memantine and ketamine, in addition to advancing knowledge of two clinically useful drugs, may help elucidate broad mechanisms of NMDAR inhibition.

4.0 Inhibition of NMDA Receptors through a Membrane-to-Channel Path

4.1 Summary

N-methyl-D-aspartate receptors (NMDARs) are transmembrane proteins that are activated by the neurotransmitter glutamate and are found at most excitatory vertebrate synapses. NMDAR channel blockers, an antagonist class of broad pharmacological and clinical significance, inhibit by occluding the NMDAR ion channel. A vast literature demonstrates that NMDAR channel blockers, including MK-801, phencyclidine, ketamine, and the Alzheimer's disease drug memantine, act as open-channel blockers: they can bind and unbind only when the NMDAR channel is open. Here we reveal that numerous NMDAR open channel blockers can enter the open channel through two routes: the well-known path from extracellular solution to channel through the ion channel gate, and a previously undescribed path from plasma membrane to channel through a gated fenestration. We term inhibition via the latter path membrane-to-channel inhibition (MCI). MCI has previously been demonstrated for voltage-gated Na^+ and K^+ channels, and may be an inhibitory mechanism of very broad significance.

4.2 Introduction

N-methyl-D-aspartate receptors (NMDARs) are ionotropic glutamate receptors (iGluRs) present at most excitatory synapses in the mammalian brain. Among iGluRs, NMDARs exhibit unique features such as slow deactivation kinetics and high permeability to calcium (Traynelis et

al., 2010b, Paoletti et al., 2013, Glasgow et al., 2015). Calcium influx through NMDARs activates a multitude of intracellular signaling pathways that can give rise to synaptic plasticity, and ultimately contribute to learning and memory (e.g. (Li and Tsien, 2009)). On the other hand, aberrant activation of NMDARs can be pathological and is implicated in Alzheimer's disease, schizophrenia, and many other neurological and neuropsychiatric disorders (Lau and Tymianski, 2010, Zhou and Sheng, 2013). NMDARs are heterotetramers typically composed of two obligatory GluN1 and two GluN2(A-D) subunits and/or GluN3(A-B) subunits. NMDARs can assemble as diheteromers (e.g. GluN1/2A) or triheteromers (e.g. GluN1/2A/2B) (Traynelis et al., 2010b). Each subunit has three transmembrane helices (M1, M2, M4) and a pore-lining reentrant loop (M2) that lines the NMDAR channel. NMDAR antagonism has been extensively studied for therapeutic purposes, as well as to understand receptor structure and function. NMDAR open-channel blockers examined for therapeutic use include memantine, magnesium (Mg^{2+}), ketamine, MK-801, dextrorphan, and phencyclidine (PCP). These entities can access the pore through the permeation pathway and bind at the "deep site" located at the tips of the M2 regions (Kashiwagi et al., 2002, Chen and Lipton, 2005, Kotermanski et al., 2009, Glasgow et al., 2018). Memantine has been particularly successful among open-channel blockers: it is FDA-approved for the management of Alzheimer's disease and is being investigated for treatment of other pathological conditions (Yang et al., 2013).

Interestingly, inhibition by memantine has also been observed following exposure of NMDARs to memantine in the absence of agonist, producing "second site inhibition" (SSI) (Blanpied et al., 1997, Glasgow et al., 2018, Kotermanski et al., 2009, Sobolevsky et al., 1998, Chen and Lipton, 2005). Previous studies have suggested that memantine binds to a second site superficial to the pore that exhibits weak apparent V_m dependence and is accessible when

NMDARs are closed (Blanpied et al., 1997, Chen and Lipton, 2005, Glasgow et al., 2018, Kotermanski et al., 2009, Sobolevsky et al., 1998) (but see (Sobolevsky and Koshelev, 1998)). Glasgow et al. concluded that that an intact and unoccupied deep site is important for SSI, and found that during SSI, memantine occupancy of the second site is not sufficient for inhibition (Glasgow et al., 2018). This supports a mechanism for SSI that involves second site binding and SSI as two distinct processes. The authors hypothesized that memantine occupies the second site and then travels to the deep site, where it produces inhibition. This hypothesis suggests that SSI is a misnomer; the second site does not produce inhibition, but rather sequesters memantine that can relocate to the deep site.

Previous work has suggested that some NMDAR modulators may access binding sites on the NMDAR by first partitioning into the plasma membrane (Paganelli and Popescu, 2015, Song et al., 2018, Orser et al., 1997, Moring et al., 1994, Korinek et al., 2015). Drug access to the pore through the membrane is a well-established mechanism in voltage gated sodium channels (Na_vS) and is a common mechanism of local anesthetic action (Jorgensen et al., 2016, Gamal El-Din et al., 2018, Kaczmarski and Corry, 2014, Hille, 1977, Catterall and Swanson, 2015, Lirk et al., 2014, Boiteux et al., 2014b). In this work we first reveal that numerous NMDAR inhibitors in addition to memantine exhibit SSI, suggesting that SSI may be a broadly used mechanism. We then present electrophysiological and computational experiments to test the hypothesis that the plasma membrane is the second "site" involved in SSI. We conclude that drugs participating in SSI travel from the membrane to the deep site upon NMDAR activation through a membrane-facing fenestration. Based on the findings detailed here, we have renamed this phenomenon "membrane-to-channel inhibition" (MCI) and will refer to it as MCI throughout this work.

4.3 Methods

4.3.1 Cell culture and transfection

Experiments were performed on the tsA201 cell line (The European Collection of Authenticated Cell Cultures), a variant of the HEK 293 cell line. tsA201 cells were maintained as previously described in DMEM supplemented with 10% fetal bovine serum and 1% GlutaMAX (Thermo Fisher Scientific) (Glasgow and Johnson, 2014). 1×10^5 cells/dish were plated on 15 mm glass coverslips treated with poly D-lysine (0.1 mg/ml) and rat-tail collagen (0.1 mg/ml, BD Biosciences) in 35 mm petri dishes. 12–24 h after plating, cells were transiently co-transfected using FuGENE6 Transfection Reagent (Promega) with mammalian expression plasmids that contained cDNAs encoding enhanced green fluorescent protein (EGFP in pRK7) for identification of transfected cells, the rat GluN1-1a subunit (hereafter GluN1; GenBank X63255 in pcDNA3.1), and the rat GluN2A subunit (GenBank M91561 in pcDNA1). For some experiments cells were transfected with GluN1 and EGFP:pIRES:GluN2A (a generous gift from Dr. Kasper Hansen (Hansen, unpublished)), which was constructed by inserting EGFP in pIRES (Clontech) under transcriptional control of the CMV promoter, and rat GluN2A cDNA (GenBank D13211) after the IRES sequence. Site-directed mutagenesis was performed on cDNAs encoding GluN1 and GluN2A subunit genes in ampicillin resistance-encoding plasmids (pcDNA 3.1 or pcDNA1) using the Stratagene Quik-Change XL sited-directed mutagenesis kit. Mutagenized NMDAR subunit cDNAs from isolated colonies were sequenced from 100–200 bases upstream to 100–200 bases downstream of each mutation (University of Pittsburgh Genomics and Proteomics Core Laboratories). cDNA ratios used in transfection were 1:1:1 (EGFP, GluN1, and GluN2A) and 1:1 (GluN1 and EGFP:pIRES:GluN2A). Following transfection, the competitive NMDAR

antagonist **D,L**-2-amino-5-phosphonopentanoate (200 μM) was added to the media to prevent NMDAR-mediated cell death.

4.3.2 Solutions

The extracellular bath solution contained (in mM): 140 NaCl, 2.8 KCl, 1 $CaCl_2$, 10 HEPES, 0.1 glycine, 0.01 EDTA. Osmolality raised to 290 ± 10 mOsm with sucrose. Extracellular solution pH was balanced to 7.2 ± 0.05 or 9.0 ± 0.1 with NaOH and to 6.3 ± 0.05 with HCl as indicated. L-glutamate, memantine, D-APV, MK-801, PCP, dextrorphan, and RL-208 (Leiva et al., 2018) were added where indicated. Voltage clamp recordings were obtained from transfected tsA201 cells 12–24 h after transfection. Pipettes were pulled from borosilicate capillary tubing (Sutter Instruments) on a Sutter Instruments-Flaming Brown P-97 microelectrode puller and polished with a heated glass filament to a resistance of 2–5 MΩ. Whole-cell recordings were made from cells expressing eGFP identified by epifluorescence illumination on an inverted Zeiss Axiovert microscope. Cells were held at a V_m of −65 mV (corrected for a liquid junction potential of −6 mV) unless otherwise indicated. Whole-cell currents were amplified using an Axopatch 200B patch-clamp amplifier (Molecular Devices), low-pass filtered at 5 kHz and sampled with a Digidata 1440A at 10 or 20 kHz in pClamp10 (Molecular Devices). Series resistance was compensated 80–90% with the prediction and correction circuitry in all experiments. Solutions were delivered to cells using a previously described ten-barrel fast perfusion system (Glasgow et al., 2017).

4.3.3 Analysis

All data were analyzed with Clampfit 10.7 (Molecular Devices), Origin 16 or GraphPad Prism 7. The fractional response after MCI ($I_{MCI}/I_{Control}$) was measured by taking the ratio of I_{MCI} to the average of $I_{Control1}$ and $I_{Control2}$ with a point-by-point ratio of time-series $I_{MCI}/I_{Control}$, where $I_{Control} = ((I_{Control1} + I_{Control2})/2)$ (Iacobucci and Popescu, 2017b). Each current was aligned to the time of glutamate application. We measured the minimum $I_{MCI}/I_{Control}$ as the mean of $I_{MCI}/I_{Control}$ over a 30 ms window centered on the minimum ratio value. MCI measurements were excluded if $I_{Control2}$ did not recover to at least 80% of $I_{Control1}$. Cells with peak NMDAR currents > 2.5 nA were excluded from analysis.

4.3.4 Modeling and molecular dynamics simulations

A molecular dynamics (MD)-optimized model structure of the GluN1/2A NMDAR TMD in lipid bilayer and water with the ion channel closed was taken from our previous work (Mesbahi-Vasey et al., 2017). The full simulated system had 10159 water molecules, 108 DMPC membrane lipid molecules, and 534 protein residues, resulting in a total of 43850 atoms. All MD simulations were performed using AMBER (Case, 2018) package for molecular modeling with Amber FF12SB force-field for protein atoms (Hornak et al., 2006), TIP3P water, Lipid14 force field for lipid (Kukol, 2009) and GAFF force field parameters for memantine (developed using Antechamber module of AMBER). All simulations were performed with initial minimization of the systems using steepest descent algorithm, followed by constrained protein MD at room temperature maintained with Langevin thermostat (Berendsen et al., 1984), 1 atm pressure maintained with the Berendsen barostat and long range electrostatics accounted for with Particle

Mesh Ewald with cut off a 10A.Simulations were implemented in AMBER. The integration step was 1 fs. To develop an open channel model a set of 10 steered MD simulations was performed (<1 ns each) using harmonic constrains applied to the SYTANLAAF sequence region of all M3 helixes. The constrains were designed to gradually increased the distance between M3 helixes at the channel gate until the channel filled with water. The protocol was similar to the one used to produce an open AMPA model (Yelshanskaya et al., 2017). The program HOLE (Smart et al., 1996) was used to identify possible fenestrations. Memantine docking was performed using AutoDock Vina (Trott and Olson, 2010).

4.3.5 Statistics

Statistical tests were performed in GraphPad Prism 7. We used one-way ANOVA with Tukey's *post hoc* analysis and t-tests where indicated. All error bars indicate ± standard error of the mean (SEM). Current traces for presentation were refiltered offline in Clampfit 10.7 at 50 Hz.

4.4 Results

4.4.1 Numerous compounds participate in MCI

We first confirmed that memantine displayed MCI consistent with previous reports. MCI was measured using the following protocol: (a) 1 mM glutamate (Glu) was applied for 20 s, and control current before MCI ($I_{Control1}$) was measured (see below); (b) normal extracellular solution was applied for 10 s to allow full deactivation of receptors; (c) memantine in the absence of Glu

was applied for 30 s; (d) memantine was washed away by a 1 s application of normal extracellular solution; (e) 1 mM Glu was reapplied for 20-30 s and current during MCI (I_{MCI}) was measured; (f) normal extracellular solution was applied for 41 s; (g) 1 mM Glu was reapplied for 20 s and control current after MCI ($I_{Control2}$) was measured. The minimum fractional response after MCI ($I_{MCI}/I_{Control}$) was measured by taking the ratio of I_{MCI} to the average of $I_{Control1}$ and $I_{Control2}$ with a point-by-point ratio of $I_{MCI}/I_{Control}$, where $I_{Control} = ((I_{Control1} + I_{Control2})/2)$ (Iacobucci and Popescu, 2017b). The 30-s duration of memantine application was chosen based on evidence suggesting that memantine in the membrane reaches an equilibrium before 30 s of application. Kotermanski et al., 2009, demonstrated that the extent of MCI remains constant with memantine applications 30 s – 4 min. The duration of the wash after memantine application was also carefully chosen. Memantine unbinds from the membrane with a time constant of ~ 2 s (Kotermanski et al., 2009). Therefore, a 1-s wash allows visualization of significant MCI before much memantine leaves the membrane. We are confident that MCI results from occupancy of a second site rather than incomplete wash-off of drug from the cell for several reasons: (1) the 1 s wash is >30-fold longer than the time constant, τ of solution exchange (27 ms) (Glasgow et al., 2017); (2) the control MCI performed with D-APV, in which APV alone is applied and washed off to be sure APV is gone when glutamate is applied supports the idea that wash-off is complete (Glasgow et al., 2018) (3) ketamine does not show MCI at 500 μM (>500x its traditional IC_{50}) with a 0.4 s wash under the same conditions (Kotermanski et al., 2009). Therefore, ketamine serves as a negative control to confirm that full solution exchange occurs. We performed MCI experiments with 100 μM memantine at pH 7.2 and found that $I_{MCI}/I_{Control}$ values ($I_{MCI}/I_{Control} = 0.502 \pm 0.123$) were consistent with those reported in Glasgow et al. (2018). We then explored whether other NMDAR channel blockers exhibit MCI. We investigated several additional open-channel blockers: PCP,

dextrorphan, MK-801, and novel compound RL-208 (Leiva et al., 2018). Each drug displayed MCI (Figure 20), suggesting that MCI is a broadly applicable mechanism of NMDAR channel blocker action. It should be noted that the concentrations used in Figure 20 are many times the drugs' traditional (ion conduction pathway) IC_{50}s. However, the *ability* of numerous open channel blockers to produce MCI is entirely novel and suggests that our current understanding of NMDAR mechanisms of inhibition require expansion. We sought to first build upon the current understanding of memantine MCI to better understand the general MCI phenomenon.

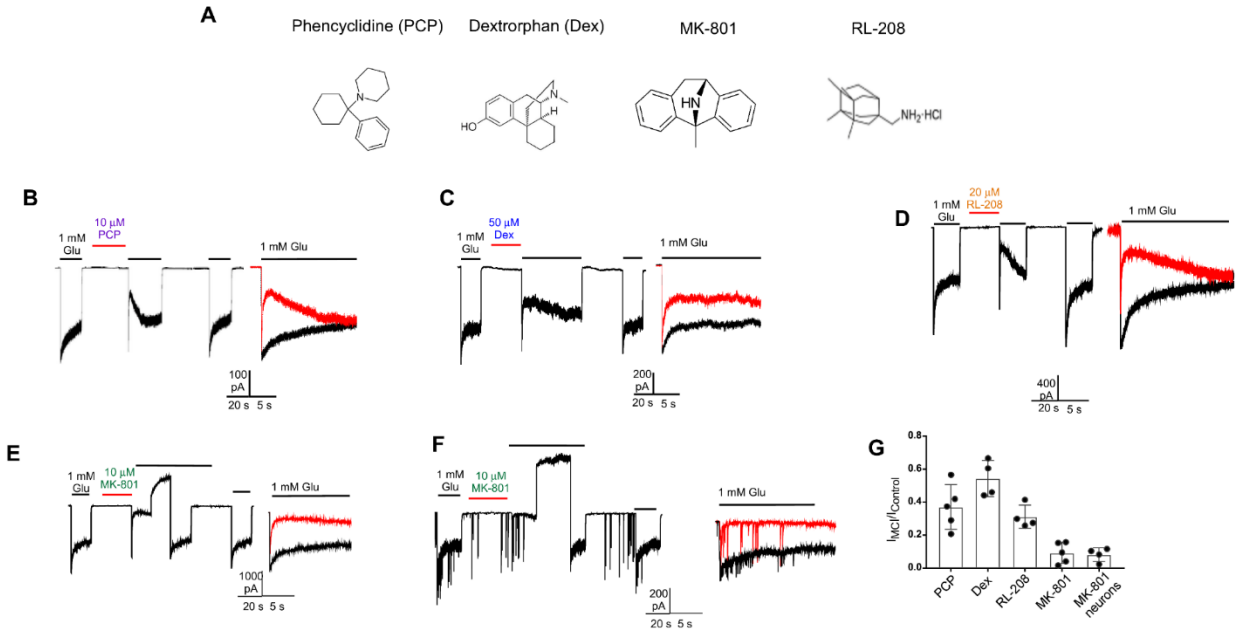

Figure 20 Multiple NMDAR inhibitors exhibit MCI

A, chemical structures of compounds examined electrophysiologically using the MCI protocol. B – D, MCI with 10 µM PCP (B), 50 µM Dextrorphan (Dex) (C), 20 µM RL-208 (D) in tsA201 cells. The MCI protocol in B-D consists of the following sequence of solution application: Control (5 s); Glu (20 s); Control (10 s); Drug (e.g. PCP) (30 s); Control (1 s); Glu (20-60 s); Control (41 s); Glu (20 s); Control (5 s). Modified MCI protocol with APV present during MK-801 application, as well as1 s before MK-801 application and 0.2 seconds after, in tsA201 cells (E) and neurons (F). G, Plot of $I_{MCI}/I_{Control}$ for the indicated compounds.

4.4.2 Memantine MCI depends on the pH during memantine application

Memantine is mostly charged at physiological pH due to protonation of its nitrogen (pKa = 10.3). Computational experiments suggest that charged memantine can reside in the membrane

(Chew et al., 2008). However, even at physiological pH, memantine is present in equilibrium between charged and uncharged forms. A parsimonious explanation for a voltage-independent second site that houses many different molecules (Figure 20), is that the second site is fairly nonspecific. One target of nonspecific molecular association is the plasma membrane. We postulated that, if the second site were the membrane, increasing the concentration of uncharged memantine (more hydrophobic form) would increase memantine partitioning into the membrane and increase MCI. We increased the concentration of uncharged memantine present during MCI by raising the pH of the memantine-containing solution. A similar approach has been used in the study of anesthetics, in which increases in drug solution pH were used to increase drug diffusion into the membrane (Perez-Isidoro et al., 2014, Chernoff and Strichartz, 1990). When memantine is applied at pH 9, cells experience a concentration of uncharged memantine ~50X higher than at pH 7.2 (with 100 μM total memantine, from 80 nM uncharged memantine at pH 7.2 to 5 μM uncharged memantine at pH 9, Figure 21A). We avoided raising pH above 9 due to the lack of receptor characterization at such a high pH (Traynelis and Cull-Candy, 1991, Vyklicky et al., 1990, Traynelis and Cull-Candy, 1990, Traynelis et al., 1995, Banke et al., 2005, Erreger and Traynelis, 2008, Kussius and Popescu, 2009). We found that memantine MCI produced by 100 μM memantine at pH 9 was significantly greater than MCI at pH 7.2 ($I_{MCI}/I_{Control}$: pH 7.2 = 0.48 ± 0.36; pH 9 = 0.12 ± 0.005, $p<0.001$, Figure 21C). However, we were concerned that increased pH could affect MCI through mechanisms apart from increasing the concentration of uncharged memantine. In particular, GluN1/2A receptors are over 50% inhibited by protons at pH 7.2, and proton inhibition is substantially lessened at pH 9 (Traynelis and Cull-Candy, 1990). To further explore the effect of memantine solution pH on MCI, we performed experiments in which the cell was exposed to pH 9 only during memantine application, and Glu and control solutions were

maintained at pH 7.2 ("pH 9 jump", Figure 21E). We also examined the effect of decreasing [uncharged memantine] in 100 μM memantine solution by performing the MCI protocol with memantine applied at pH 6.3 ("pH 6.3 jump"). To reduce responses from proton-activated currents during pH changes we performed pH jump experiments in the continuous presence of 20 μM amiloride (Waldmann et al., 1997). Similar to MCI experiments performed entirely at pH 9, the pH 9 jump experiments showed significantly increased MCI with 100 μM memantine relative to experiments at pH 7.2 ($I_{MCI}/I_{Control}$ pH 9 jump = 0.25 ± 0.017, p = 0.002). Next, we examined MCI with 100 μM at pH 6.3, where uncharged memantine is about 0.01% of the total memantine concentration in solution. We saw significantly reduced MCI produced by 100 μM memantine in the pH 6.3 jump protocol compared to int pH 7.2 ($I_{MCI}/I_{Control}$ pH 6.3 jump = 0.835 ± 0.327, p < 0.001). We then wanted to measure the IC_{50} of memantine MCI with memantine solution applied at different pH's using pH 7.2, pH 6.3 jump, and pH 9 jump protocols. We first performed pH 9 and 6.3 jump control experiments to examine whether amiloride and pH changes alone affected our measurement of $I_{MCI}/I_{Control}$. We found that average $I_{MCI}/I_{Control}$ for pH 9 jump control experiments was 0.906 ± .0541, suggesting that pH changes may slightly influence our measurement of MCI during the pH 9 jump protocol. We normalized all pH 9 jump $I_{MCI}/I_{Control}$ values to the average values of pH 9 jump control experiments. pH 6.3 jump control $I_{MCI}/I_{Control}$ as 0.931 ± 0.079. We then measured the IC_{50} of memantine MCI at pH 7.2 (Figure 21G,I; 80.7 ± 15.5 μM), and at pH 9 (Figure 21H,I; IC_{50}= 5.43 ± 0.75 μM, p < 0.0001). by applying various concentrations of memantine during MCI protocols. To obtain the pH 6.3 jump IC_{50} we fit the logistic equation to $I_{MCI}/I_{Control}$ values from pH 6.3 jump MCI experiments using 100 μM and 300 μM memantine. We chose not to examine higher [memantine] because of the possibility of nonspecific effects of memantine with concentrations >300 μM. The pH 6.3 jump MCI IC_{50} was

significantly different from the pH 7.2 MCI (877 ± 17 μM, $p < 0.0001$). Figure 22 shows that the memantine MCI IC_{50} decreased with increasing memantine solution pH. This suggests that [uncharged memantine] is correlated with $I_{MCI}/I_{Control}$, and further, that uncharged memantine mediates MCI.

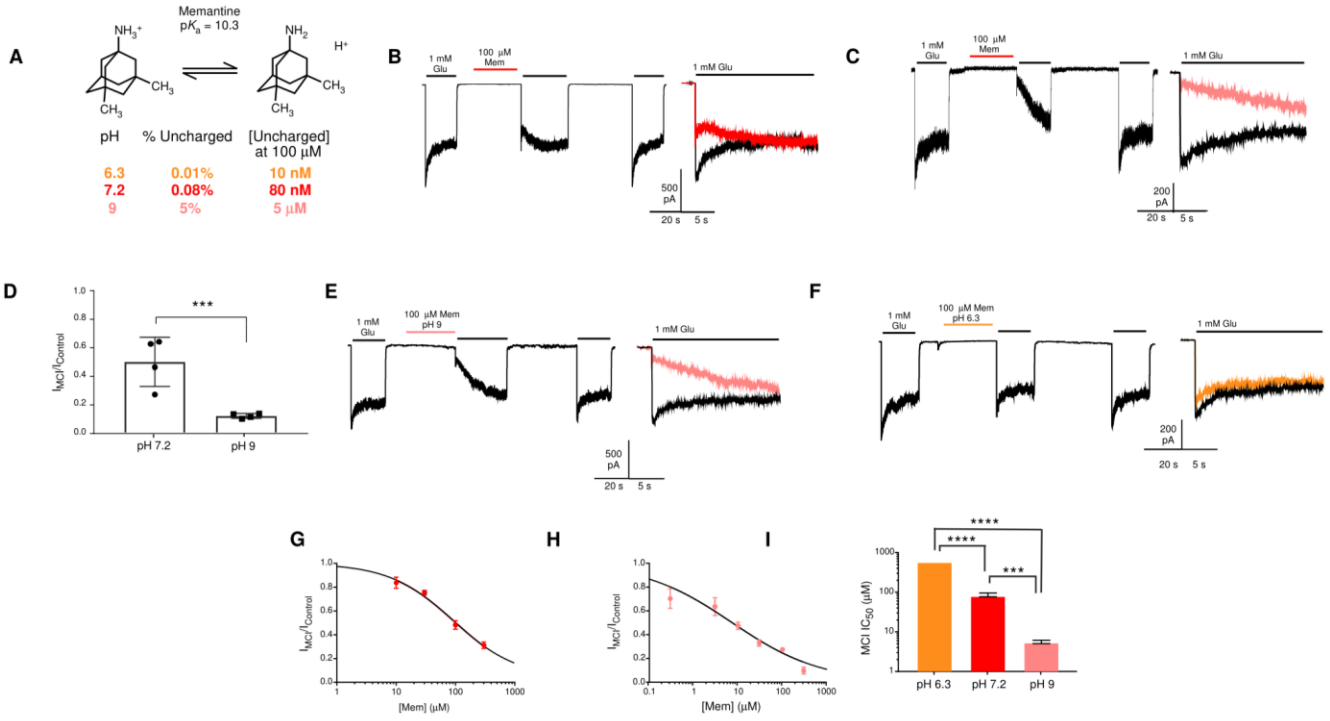

Figure 21 Memantine MCI is pH-dependent

A, Expected amount of charged and uncharged memantine at pH 6.3, 7.2, and 9. B – D, Data from MCI protocol performed at pH 7.2 (B) and 9 (D) with 100 μM memantine. E – F, Data from pH 9 jump protocol (E) and pH 6.3 jump protocol (F) with 100 μM memantine. Colored lines in B,C,E,F indicate the pH's used in the protocol. G – H, Plot of memantine MCI IC_{50} at pH 7.2 (G) and pH 9 jump (H). I, comparison of MCI IC_{50} at pH 6.3, 7.2, and 9. ****, P<0.00001

4.4.3 Memantine exhibits reservoir-like behavior

How many molecules can occupy the second site at once? Do drugs that participate in MCI bind to a specific site in the membrane region that holds one or two molecules? Many binding sites of well-known drugs are specific: they stabilize the binding of drug molecules through interactions with the drug's structure. However, nonspecific binding sites also exist. Many molecules interact nonspecifically with the membrane, for example. Often, large quantities of hydrophobic molecules can accumulate in membranes and reside there. We previously demonstrated that MCI is V_m-dependent: MCI is prominent at -65 mV but nearly abolished at 35 mV (Glasgow et al., 2018). Based on the V_m dependence of MCI, we devised an experiment to further probe the characteristics of the second site. We reasoned that including two 500 ms voltage jumps during recovery from MCI (during the Glu application immediately after removal of Mem) would causes memantine to quickly unbind from the deep site (Rammes et al., 2008). If the second site houses one or several molecules, increasing the rate of unbinding from the deep site would result in altered MCI time course of unbinding when compared to a typical MCI protocol if the second site housed just one or several molecules .We performed an MCI protocol with two 500 ms V_m jumps to 50 mV during recovery from MCI and measured $I_{MCI}/I_{Control}$ 100 ms after the second jump (Figure 22). We compared this measurement to $I_{MCI}/I_{Control}$ at the same timepoint in control MCI experiments performed entirely at -65 mV. We performed these experiments with memantine applied at pH 9 (in both control and V_m jump conditions), where MCI was more extensive, to allow clear observation of decreases in $I_{MCI}/I_{Control}$. $I_{MCI}/I_{Control}$ did not differ between V_m jump and control protocols (V_m jump = 0.38 ± 0.026; control = 0.43 ± 0.019, p = 0.14), indicating no significant alteration in the time course of recovery from MCI due to the two V_m jumps to 50 mV. The block quickly returns to near-control levels when V_m is returned to -65 mV. This observation suggests

that memantine can repeatedly bind to the deep site throughout recovery from MCI. We conclude that the second site can house a reservoir of memantine and is not a "traditional" binding site that binds one or several molecules (as assumed in (Kotermanski et al., 2009, Blanpied et al., 1997, Sobolevsky and Koshelev, 1998, Sobolevsky et al., 1998)). Further, it suggests that [memantine] at the second site is largely undisturbed by V_m changes, consistent with our previous observation (Glasgow et al., 2018). This is in contrast with *inhibition* resulting from the MCI protocol, which occurs at the deep site and is V_m-dependent. A parsimonious explanation for these data is that the second site represents a reservoir of memantine in the plasma membrane. There is extensive precedent hydrophobic and amphipathic molecules associating with the plasma membrane. For example, many local anesthetics act by first partitioning into the membrane (Boiteux et al., 2014b, Hille, 1977, Jorgensen et al., 2016).

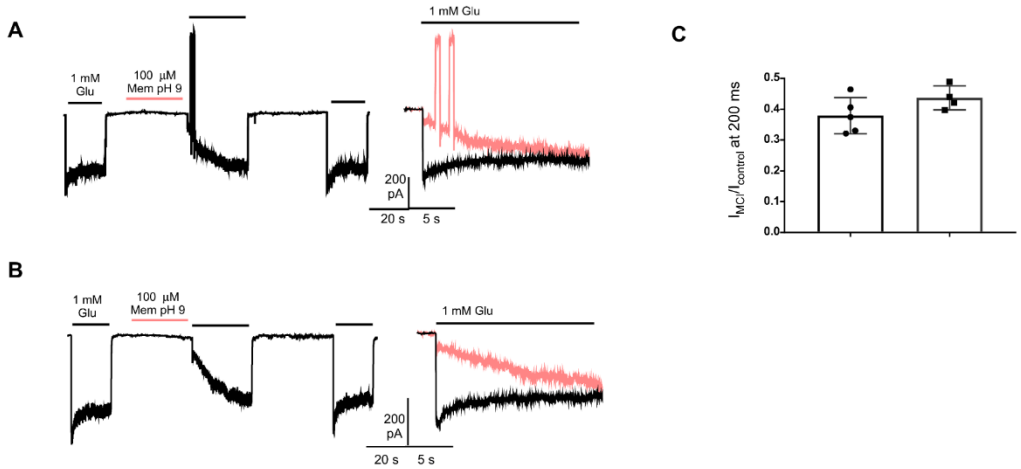

Figure 22 MCI exhibits reservoir-like behavior

A, Left, MCI arising from 100 μM memantine at pH 9 with two 500 ms V_m steps to 50 mV during recovery from MCI; Right, overlay of MCI trace highlighting the V_m steps to 50 mV. B, MCI with 100 μM memantine at pH 9 without Vm steps. C, $I_{MCI}/I_{Control}$ measured at the timepoint corresponding to 200 ms after the second V_m step back to -65 mV.

4.4.4 MK-801 MCI kinetics are concentration-dependent

Because drugs that participate in MCI are also NMDAR open-channel blockers, we hypothesized that access to the deep site in MCI is gated and occurs only in activated NMDARs. We wanted to develop an experiment to further test this hypothesis. As shown in Figure 20A-E, we observed a pronounced pre-inhibition peak immediately following agonist application with each drug tested. The presence of pre-inhibition peaks suggests that deep site binding via MCI occurs only in agonist-bound NMDARs. We further examined the pre-inhibition peaks apparent with memantine, PCP, dextrorphan, RL-208, and MK-801 MCI protocols and noted that the time course of MCI onset (τ_M) varied between channel blockers (e.g. 1 μM MK-801 = 995.5 ± 134.9 ms; 100 μM memantine = 85.1 ± 6.02 ms). Interestingly, GluN1/2C receptors show a more defined pre-inhibition peak and slower onset of memantine MCI than GluN1/2A receptors (Glasgow et al., 2018). This could reflect dependence of MCI onset kinetics on NMDAR open probability (P_{open}), again suggesting that blocker transit from membrane to the deep site requires NMDAR activation.

If MCI requires channel opening, we would predict that τ_M would vary with [drug] applied during MCI. This is also consistent with deep site inhibition through the MCI route occurring only in agonist-bound receptors. The pre-inhibition peak with memantine often was very small and τ_M was difficult to measure, possibly because τ_M is similar to the time course of NMDAR activation. Therefore, we performed MCI experiments with 1 μM and 10 μM MK-801 and examined whether

τ varied with MK-801 concentration. (Figure 23). At both concentrations we observed a defined pre-inhibition peak and a time-dependent increase in inhibition. Fitting a single exponential curve to the current decay immediately following the pre-inhibition peak of $I_{MCI}/I_{Control}$ allowed measurement of τ_M. τ was significantly different with 1 and 10 μM MK-801 (995.5 ± 134.9 ms and 312.0 ± 59.44 ms, respectively; p = 0.002). Concentration dependence of τ_M is consistent with the idea that MK-801 transits from the membrane to the deep site after channel opening, and that the membrane [MK-801] depends on the previous [MK-801] in solution. Concentration dependence of τ is inconsistent with the idea that MK-801 binds to a discrete "second site", since the rate of transit from a binding site should not depend on the previous [MK-801]. These results thus provide evidence against the second site binging one or several molecules and also suggests that MCI is state-dependent, with inhibition occurring only when NMDARs are active.

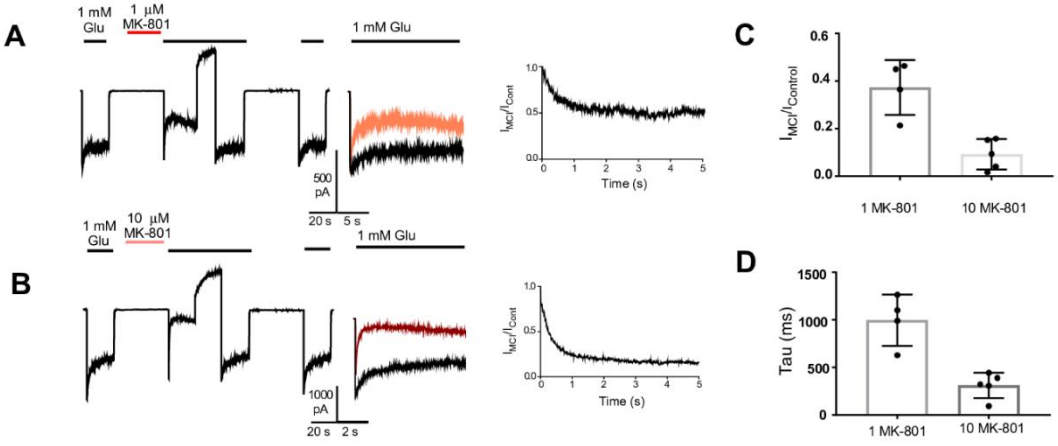

Figure 23 MK-801 MCI characteristics depend on [MK-801] applied during MCI

A,B, MCI protocol with 1 μM (A) and 10 μM (B) MK-801. In A and B, a V_m step to 30 mV was performed for ≤20 s during the second Glu application to facilitate rapid MK-801 unbinding from the deep site. C, $I_{MCI}/I_{Control}$ with 1 μM and 10 μM MK-801. D, τ of MCI onset with 1 μM and 10 μM MK-801.

4.4.5 Modeling NMDAR fenestrations

The above experiment evidence indicates that MCI requires transit of channel blockers from the membrane to the deep site after NMDARs are activated. Thus, there must be a path or fenestration in the NMDAR TMR through which channel blockers can pass only when NMDAR channels are in the open state. To find such a path, we first developed an open channel state of the NMDAR TMD using steered molecular dynamics (SMD) simulations. We started with a

previously developed closed NMDAR TMD structure that was equilibrated in water and DMPC lipid bilayer using MD simulations (Mesbahi-Vasey et al., 2017). To develop an open channel structure in lipid and water we used an SMD protocol previously used to model the AMPA receptor TMD in the open state (Yelshanskaya et al., 2017). The simulated open channel structure in water and lipid is shown in Figure 24A. Next, we identified all continuous paths from lipid to the ion channel in both closed and open TMD NMDAR structures using the pore predicting program HOLE (Smart et al., 1996). We found one lipid to ion channel path (fenestration) in GluN1/2A receptors that is unique to the open structure (Figure 24B). We further confirmed that memantine can traverse this open structure fenestration by performing multiple position molecular docking of the memantine molecule along this path (Figure 24C). Docking resulted in small negative energy values (-1.2 kcal/mol) indicating that memantine fits in the fenestration but does not bind with high affinity, consistent with a path rather than a binding site. Fenestration-lining residues are shown in Figure 24D.

We identified a methionine residue (GluN2A(M630)) that lines the fenestration and forms a constriction (Figure 24D-F). To examine how mutation of GluN2A(M630) may influence the constricted region, we performed in silico mutagenesis followed by molecular dynamics simulations. In silico, the GluN2A(M630A) and GluN2A(M630W) mutations influenced the radius of the fenestration near the GluN2A(630) position. Increasing residue size (GluN2A(M630W) mutation) decreased the radius of the fenestration, while decreasing residue size (GluN2A(M630A) mutation) increased the radius of the fenestration (Figure 24E-H). We hypothesize that increasing the radius of the fenestration may increase the rate of memantine transit from the membrane to the channel, while decreasing the fenestration radius may have an opposite effect.

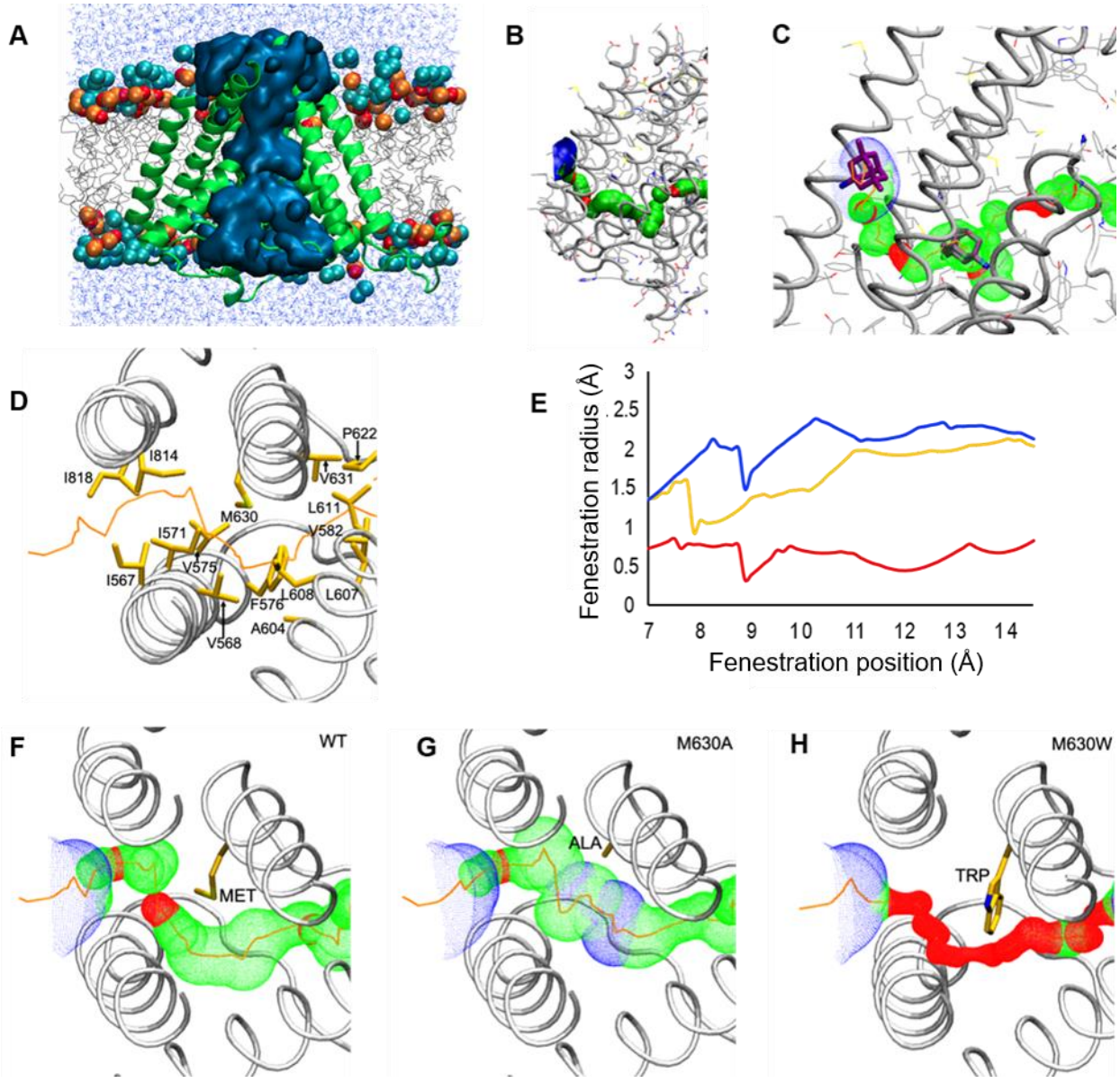

Figure 24 Simulations of NMDAR TMD reveal a state-dependent fenestration

A, Simulated open NMDAR TMD model in lipid bilayer and water. Protein is shown in green in cartoon representation; lipid tails are grey wireframe; lipid head groups are spheres (carbon in cyan, oxygen in red, phosphorus in orange); water channel is shown as a solid blue surface and bulk water in blue wireframe isosurface. B, Fenestration through the open GluN1/2A TMD between the lipid bilayer and the channel center identified using HOLE is shown as a solid

surface. The largest regions of the fenestration are shown in blue, intermediate regions are in green, and most constricted regions are in red. C, Memantine is shown docked at the entrance of the fenestration that leads from membrane to ion channel. D. Top view of the fenestration (B) shown as an orange line. Residues lining the pore are shown in yellow stick representation. E. Fenestration radius at different points along the fenestration ("fenestration position") is shown for WT GluN1/2A (yellow line), GluN1/2A(M630A) (blue) and GluN1/2A(M630W) (red line). F-H, The portion of the fenestration near position 630 of GluN2A, with the residue at position 630 identified and shown as stick models, is shown for WT GluN1/2A (F), GluN1/2A(M630A) (G), and GluN1/2A(M630W) (H) receptors.

4.4.6 Mutation of GluN2A(M630) specifically alters MCI

We performed site-directed mutagenesis to alter residues predicted to line the fenestration identified through molecular dynamics simulations (Figure 24). We compared at pH 7.2 MCI by 100 μM memantine of WT and mutant NMDARs. We found that mutation of the putative fenestration-lining methionine identified in our NMDAR TMD simulations, GluN2A(M630), specifically modulates MCI. We first increased the size of the residue by mutating GluN2A(M630) to tryptophan, which our simulations predicted would narrow the fenestration. Consistent with that prediction, GluN1/2A(M630W) receptors showed decreased memantine MCI ($I_{MCI}/I_{Control}$ = 0.717 ± 0.0225) relative to WT ($I_{MCI}/I_{Control}$ = 0.483 ± 0.362). We next examined MCI of GluN1/2A(M630A) receptors to test the prediction of our simulations that the mutation of GluN2A(M630) to a smaller alanine would increase the size of the fenestration.". Indeed, GluN1/2A(M630A) receptors showed increased MCI by 100 μM memantine ($I_{MCI}/I_{Control}$ = 0.254 ± 0.0113) relative to WT ($I_{MCI}/I_{Control}$ = 0.272 ±0.0138) (Figure 25). Given the importance of the

deep site in MCI, we examined whether changes in MCI could be explained by potential alterations in memantine affinity for the deep site. We measured the traditional IC_{50} for memantine inhibition of GluN1/2A(M630W) and GluN1/2A(M630A) receptors by coapplying memantine and glutamate to permit memantine access to the deep site from the extracellular solution. We found that the traditional memantine IC_{50}s of GluN1/2A(M630W) (1.489 ± 0.203 μM) and GluN1/2A(M630A) (1.524 ± 0.0696 μM) were not different from wildtype (1.709 ± 0.0638 μM, $p > 0.05$ by one-way ANOVA) (Figure 25). These results suggest that the membrane-to-channel path used by memantine during MCI is specifically altered in GluN1/2A(M630A) and GluN1/2A(M630W) receptors, strongly support the prediction of our simulations.

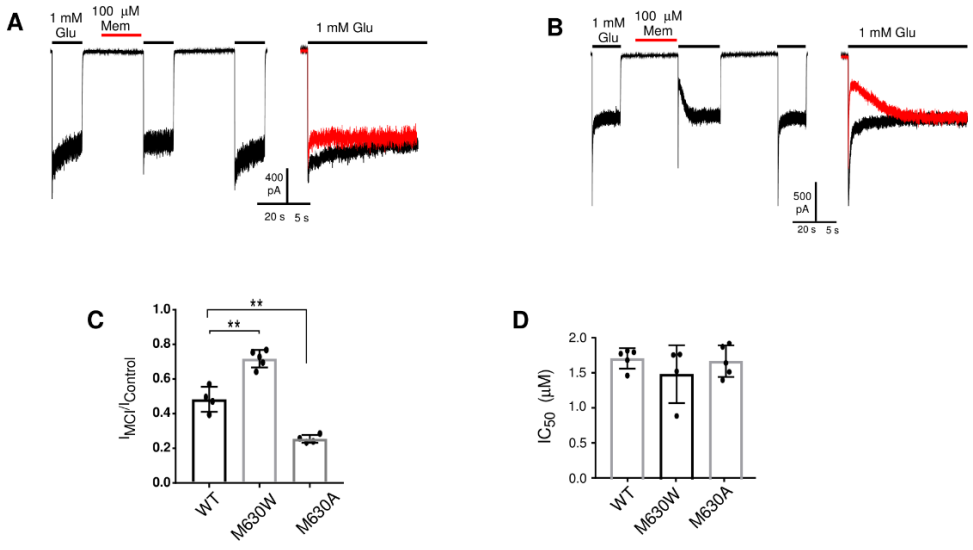

Figure 25 Fenestration-lining mutations alter MCI

A-D, The GluN2A(M630W) mutation reduced MCI (A, C), but did not affect traditional memantine IC_{50} (D). The GluN2A(M630A) mutation increased MCI (B,C) but had no effect on traditional memantine IC_{50} (D). These findings support the hypothesis that GluN2A(M630)

mutations specifically affects MCI by modifying the membrane to channel path. ***, $p < 0.0001$ by one-way ANOVA.

4.4.7 Mutation of additional fenestration lining residues

Based on the computational simulations of the fenestration, we examined MCI in receptors in which additional putative fenestration-lining residues were mutated to tryptophan. GluN1/2A(A570W), GluN1/2A(I571W), GluN1/2A(M630W)(A570W) and GluN1/2A(M630W)(I571W) (Figure 26). GluN1/2A(A570W) showed increased MCI compared to WT ($I_{MCI}/I_{Control}$ = 0.272 ± 0.0138), but showed reduced traditional memantine IC_{50} (0.933 ± 0.144 μM). Thus, the increased MCI seen in GluN1/2A(A570W) receptors could be caused by increased affinity of memantine at the deep site rather than a specific effect on the MCI pathway. GluN1/2A(M630W)(I571W) receptors showed no current. GluN1/N2A(M630W)(A570W) showed $I_{MCI}/I_{Control}$ similar to WT (0.559 ± 0.0790).

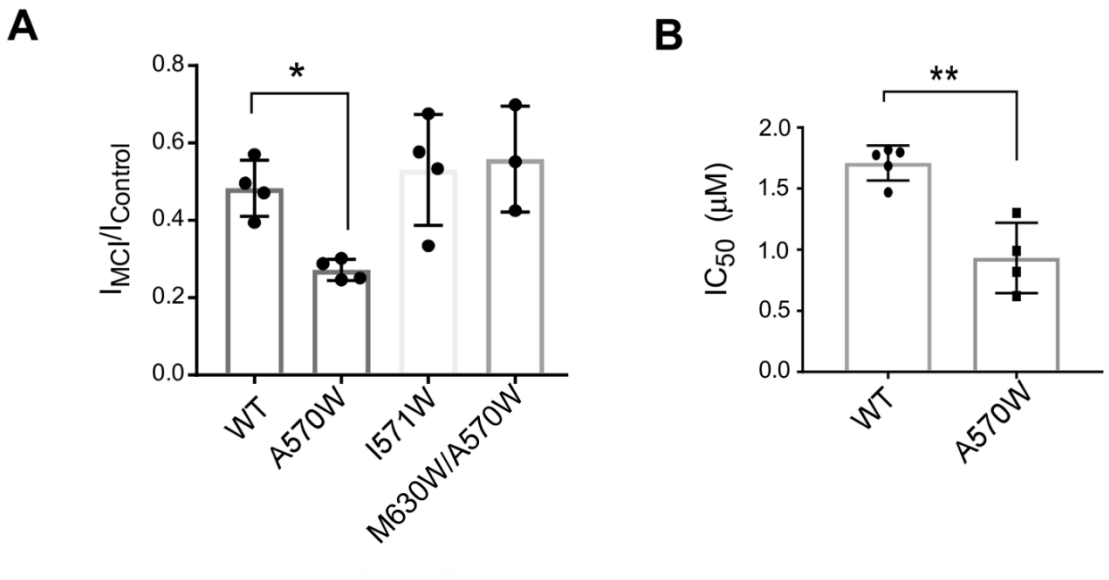

Figure 26 Mutation of additional fenestration-lining residues

A, Minimum $I_{MCI}/I_{Control}$ of NMDARs containing the indicated WT or mutated GluN2A in response to 100 μM MCI at pH 7.2. GluN1/2A(M630W)(I571W) receptors were also examined and showed no current in 3/3 cells. Only GluN1/2A(A570W) shows MCI that differed from WT. B, Traditional memantine IC_{50} of receptors containing WT GluN1/2A or GluN21/2A(A570W).

4.5 Discussion

We report here a systematic investigation of MCI, a little-explored route of NMDAR inhibition. MCI occurs when drugs first associate with the plasma membrane and then, after NMDAR activation, travel through a hydrophobic path to access the deep site. Using electrophysiological and computational methods we found that the plasma membrane is important for MCI and can house many molecules, unlike a traditional binding site. The logarithm of the partition coefficient of memantine (logP) is ~3.2 (Mealing et al., 1999), which indicates that the

uncharged form of memantine is >1000-fold more soluble in octanol than water. This suggests that uncharged memantine resides preferentially in the membrane, and is consistent with data indicating that the membrane is a reservoir of uncharged memantine.

Knowledge of receptor modulation through lipophilic pathways has existed for decades, and is well established in many ion channels, but has never been demonstrated for NMDARs. Hydrophobic fenestrations provide access by local anesthetics to their binding sites on VGSCs (Hille, 1977, Boiteux et al., 2014b, Catterall and Swanson, 2015, Lirk et al., 2014, Gamal El-Din et al., 2018). Interestingly, permanently charged local anesthetics seem unable to act through the hydrophobic pathway (Hille, 1977). Pore access through fenestrations also occurs in voltage gated potassium channels (Wrobel et al., 2016, Jorgensen et al., 2016) and may occur in voltage gated-calcium channels (Wu et al., 2018). Finally, several NMDAR modulators in addition to memantine have been proposed to travel through hydrophobic pathways, though the nature of these pathways remains unclear (Paganelli and Popescu, 2015, Korinek et al., 2015, Moring et al., 1994, Orser et al., 1997). Here, we present mechanistic and structural insight into the fenestration responsible for MCI.

In the present study, we found that MCI is exhibited by many channel blockers including memantine, PCP, dextrorphan, MK-801, and RL-208. However, it is possible that not all NMDAR channel blockers act through fenestrations: ketamine produces little-to-no MCI despite its high lipophilicity (Glasgow et al., 2018, Johnson et al., 2015, Kotermanski et al., 2009, Parsons et al., 2007a). Memantine transitions between the charged and uncharged forms with protonation and deprotonation of its amine group, and altering pH alters the ratio of charged to uncharged memantine. We examined whether we could alter MCI by changing the pH of the memantine-containing solution. Solution pH has been used to modulate drug protonation in work with VGSCs

and local anesthetics (Schwarz et al., 1977) (Chernoff and Strichartz, 1990). We observed changes in MCI correlated with the amount of uncharged memantine in solution. This supports the hypothesis that MCI requires entry of uncharged memantine into the membrane. However, it is important to note that changes of extracellular pH may influence NMDARs as well as [uncharged memantine]. pH modulates NMDAR responses and may also affect the structure of lipid membranes (Leung et al., 2013, Traynelis et al., 1995). We attempted to minimize the effects of pH change on NMDARs with our pH jump protocol by activating NMDARs only at pH 7.2, and by normalizing values of pH 9 jump MCI experiments to control pH 9 jump experiments. In the pH jump MCI protocols used, pH is returned to 7.2 1 s before glutamate application, providing ample time to reverse any effects of pH change on NMDARs or the membrane. However, we cannot exclude the possibility that pH change affects MCI by a mechanism separate from altering memantine accumulation. For example, it is possible that changes in amino acid charges due to changing pH can modulate memantine travel through the fenestration.

We took advantage of the V_m dependence of memantine MCI to examine whether the plasma membrane housed few or many memantine molecules during MCI. We expected that, if the second site binds just one or several memantine molecules, $I_{MCI}/I_{Control}$ after the second V_m jump would be different from $I_{MCI}/I_{Control}$ in control experiments because the memantine molecules producing MCI would be forced out of the deep site. We observed that $I_{MCI}/I_{Control}$ at 200 ms after the second V_m jump did not differ from control. The membrane seemed to continuously re-supply memantine for inhibition at the deep site, suggesting that the second site houses a reservoir of memantine. This observation is consistent with the hypothesis that the second site is the membrane.

Next, we explored the state-dependence of MCI. We found that MCI occurs only after agonist is applied and shows drug concentration dependence. We used two MK-801 concentrations

to determine whether the time course of MCI onset depends on the concentration of previously-applied drug. The time course of MCI onset with the [MK-801] applied during MCI. The dependence of the time course of MCI development on [MK-801] in solution suggests that drug transfer through the fenestration occurs only in open receptors (Figure 23).

Using structural molecular modeling of the NMDAR TMD, we identified a fenestration present only in the modeled open state of the NMDAR channel (Figure 24). We observed a constriction in the fenestration formed by residue M630 in the GluN2A subunit and found that mutation of GluN2A(M630) alters MCI (Figure 25). GluN1/2A(M630W) and GluN1/2A(M630A) receptors displayed alterations in MCI without changes in traditional memantine IC_{50}. It is possible that GluN2A(M630) mutations alter travel of memantine from the membrane to the deep site through a mechanism other than direct disruption of the fenestration. However, these data suggest that GluN2A(M630) lines the fenestration, and further support the conclusion that MCI and traditional deep site block occur through separate pathways. Molecular dynamics simulations of in silico mutations at GluN2A(M630) support electrophysiological data (Figure 24). We then mutated additional residues predicted to line the fenestration (Figure 26). We found that only mutation of GluN2A(M630) alters MCI without changing traditional memantine IC_{50}. A recent paper by Song et al., 2018, suggested that the closed NMDAR contains tunnels through which lipids or small molecules may be able to access the receptor. It is unlikely that fenestrations in closed NMDARs allow transit of channel blockers, which can access the deep site only when the NMDAR is open. Figure 27 illustrates the two methods of NMDAR block by memantine, which are likely relevant to other NMDAR open channel blockers.

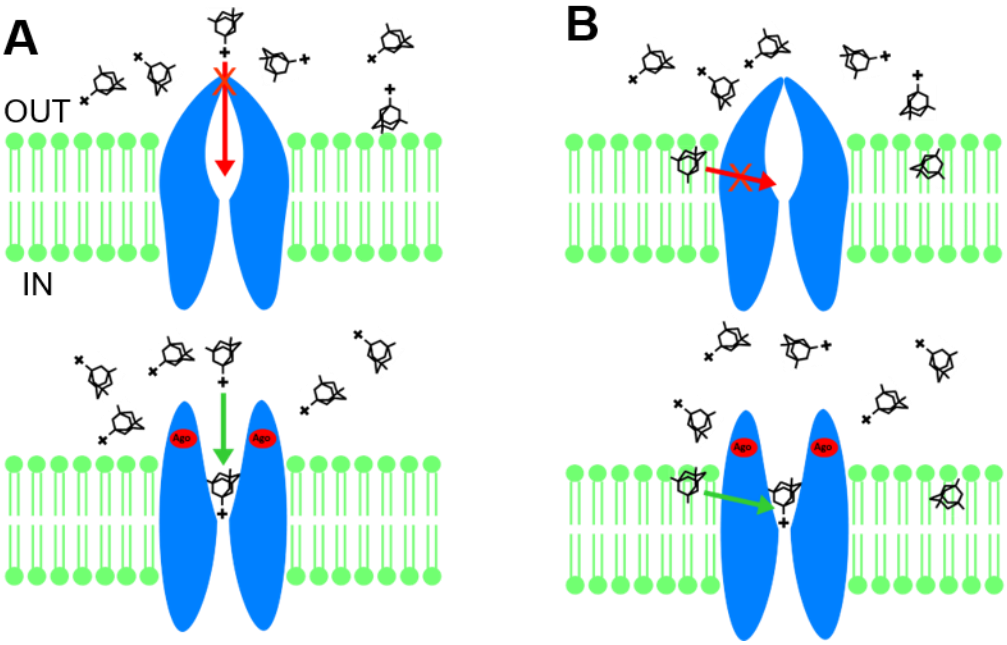

Figure 27 Schematic of the two routes of memantine access to its NMDAR channel blocking site

A, Traditional route. Charged memantine can access the deep site only when agonists (Ago) bind and the channel opens. B, Newly discovered route. Uncharged memantine enters the membrane and can access its blocking site through gated fenestrations only when agonists bind and the channel opens.

5.0 General Discussion

The work presented in this dissertation focuses largely on the characteristics of the NMDAR TMD and its many critical roles in receptor function. With my coauthors and collaborators, I explored the roles of a conserved tryptophan residue in the GluN1, GluN2A, and GluN2B M2 regions (Chapter 2). We revealed that the roles of the conserved tryptophan are subtype-dependent. The GluN1(W608C) mutation dramatically slowed deactivation in GluN1(W608C)/2A receptors and was found to interact with the nearby GluN2A(S632) position to influence deactivation kinetics (Figure 9). GluN2B(W607C)-containing receptors show enhanced voltage-independent potentiation by Mg^{2+} (Figure 11). Even at saturating concentrations, Mg^{2+} inhibited GluN2B(W607C)-containing receptors only ~50%, suggesting that significant Mg^{2+} permeation occurs through GluN2B(W607C)-containing receptors (Figure 11). In GluN1/2A receptors, the GluN2A(W606C) mutation did not affect Mg^{2+} IC_{50}, while mutation of a residue predicted to be nearby, GluN1(M634), increased Mg^{2+} IC_{50} (Figure 10) The GluN1(M634) and GluN2A(W606) sites interact functionally, though it is unclear whether the residues are physically proximal. The results of Chapter 2 suggest that intersubunit interactions in the TMD are critical for both gating and Mg^{2+} block of NMDARs, and that the role of the conserved M2 tryptophan varies in GluN1, GluN2A, and GluN2B subunits.

Chapter 3 began with an investigation of the effects of Mg^{2+} on recovery from inhibition by memantine and ketamine of GluN1/2A, GluN1/2B, GluN1/2C, and GluN1/2D receptors. We found that the time course of recovery from memantine and ketamine inhibition depended on the concentration of blocker applied (prior to recovery from block) and on the NMDAR subtype studied (Figures 12-15). In GluN1/2A and GluN1/2B receptors, Mg^{2+} caused substantial

acceleration of memantine unbinding. We then explored the possibility that the concentration-dependence of memantine unbinding was due to binding of memantine at a second site distinct from binding at the deep site (Figures 16-19). We termed this "second site inhibition" (SSI), meant to refer to a mechanism distinct from diffusion of extracellular memantine into the pore and binding at the deep site. We found that the time course of recovery from SSI in GluN1/2A and GluN1/2C receptors was strikingly similar to the slow time constant of recovery from memantine inhibition (Figure 16). We also found that Mg^{2+} disrupted SSI of GluN1/2A but not GluN1/2C receptors, paralleling the effects of Mg^{2+} on the slow time constant of memantine recovery from inhibition in GluN1/2A and GluN1/2C receptors (Figure 17). These data suggest that the slow component of recovery from memantine inhibition is due to SSI. Experiments suggested that Mg^{2+} does not compete with memantine for occupancy of the second site, but rather inhibits GluN1/2A SSI by occupying the deep site. Thus, we proposed that, although memantine occupancy of a second site is necessary for SSI, memantine occupancy of the second site is not in itself inhibitory. This hypothesis implies that SSI is a misnomer, for inhibition does not occur at the second site. Instead, our data suggested that memantine gives rise to SSI by associating with a non-inhibitory second site (distinct from the deep site) and transitioning to the deep site upon receptor activation. Memantine occupancy of the second site was found to be largely voltage-independent, while SSI was V_m-dependent (Figure 19). Accordingly, disruption of the highly V_m-dependent deep site with the GluN1(N616R) mutation in GluN1/2A and GluN1/2C receptors abolished SSI (Figure 18).

In Chapter 4 we reveal that memantine SSI arises through memantine association with the membrane and transit through a fenestration to reach the NMDAR pore. We renamed SSI membrane-to-channel inhibition (MCI) to more accurately describe the inhibitory mechanism. Two experiments led to us to initially hypothesize that the plasma membrane is the second site of

memantine association. Manipulation of the pH of the memantine solution applied during MCI suggested that the uncharged form of memantine mediates MCI (Figure 21). Additionally, we observed reservoir-like behavior of the second site consistent with memantine accumulation in the membrane (Figure 22). Using molecular dynamics simulations of an open NMDAR TMD model we identified a fenestration that leads from the plasma membrane to the NMDAR pore (Figure 24). Mutation of a residue predicted to line the fenestration, GluN2A(M630), to alanine (GluN2A(M630A)) caused increased MCI, while the GluN2A(M630W) mutation resulted in decreased MCI (Figure 25). Importantly, changes in MCI in GluN1/2A(M630A) and GluN1/2A(M630W) receptors were not accompanied by changes in memantine affinity for the deep site measured using an open-channel block protocol. Molecular dynamics simulations of GluN1/2A(M630A) receptors showed increased fenestration size near the GluN2A(M630) position compared to WT GluN1/2A receptors, while GluN1/2A(M630W) receptors showed decreased fenestration size near the GluN2A(M630) position (Figure 24). Compared to WT GluN1/2A receptors, GluN1/2A(M630A) and GluN1/2A(M630W) receptors also had increased and decreased fenestration diameter, respectively, at the intersection of the fenestration and the ion channel.

In addition to the discovery that memantine can travel from the membrane to the NMDAR deep site through a fenestration, we showed that open channel blockers besides memantine display MCI. PCP, MK-801, dextrorphan, and RL-208 caused NMDAR inhibition in response to the MCI protocol (Figure 20). Therefore, PCP, MK-801, dextrorphan and RL-208 may travel from the membrane to the pore through the same fenestration proposed to be involved in memantine MCI. Ion channel inhibition by transit of drugs from membrane to channel via fenestrations has been

demonstrated for voltage-gated Na^+ and K^+ channels and may also be an inhibitory mechanism of broad significance in NMDARs.

5.1 The Role of a Conserved Tryptophan in the TMD

The conserved tryptophan in the M2 region of the TMD was previously explored by several groups. Williams et al. found that the GluN1(W608L) mutation did not affect Mg^{2+} block in GluN1(W608L)/2B receptors (Williams et al., 1998, Kashiwagi et al., 1997), although GluN1(W608) interacts with the GluN2A S/L site to influence Mg^{2+} IC_{50} (Siegler Retchless et al., 2012). GluN1(W608L)/2B receptors showed decreased potentiation by spermine and decreased proton inhibition (Kashiwagi et al., 1997). The homologous mutation in GluN2B (GluN2B(W607L)) increased spermine potentiation without affecting proton inhibition. Modulation of spermine potentiation by GluN1(W608) and GluN2B(W607) mutations in GluN1/2B receptors is intriguing because spermine potentiation stems from spermine binding in the NTD, far from the M2 region (Mony et al., 2011). Potentiation of GluN2B-containing receptors by Mg^{2+} and spermine are thought to be mechanistically similar (Paoletti et al., 1995, Mony et al., 2011). Therefore, our observation that GluN2B(W607C)-containing receptors show increased potentiation by Mg^{2+} is consistent with the increased spermine potentiation seen in GluN2B(W607L)-containing receptors (Kashiwagi et al., 1997). The consistent influence of a GluN2B M2 residue on an NTD-mediated form of NMDAR potentiation underscores the importance of long-range allosteric effects in NMDARs.

Consistent with the results of Chapter 2, previous publications demonstrate that the conserved M2 tryptophan regulates NMDAR permeation and block in a subunit-specific manner.

GluN1/2B(W607L) and GluN1/2A(W606L) receptors showed increased permeability to the polyamine derivative N^1-dansyl-spermine and to Mg^{2+}, while GluN1(W608L)/2B receptors displayed N^1-dansyl-spermine and Mg^{2+} permeability similar to WT GluN1/2B receptors (Kashiwagi et al., 1997, Williams et al., 1998). GluN1/2A(W606L) receptors showed Mg^{2+} permeability similar to GluN1/2B(W607L) receptors. Interestingly, GluN1/2B(W607L) receptors showed drastically increased Mg^{2+} IC_{50} in GluN1/2A(W606L) receptors at -70 mV was only slightly altered (Williams et al., 1998). This suggests that V_m-dependent Mg^{2+} block and permeation may be regulated differently in GluN1/2A and GluN1/2B receptors.

The conserved M2 tryptophan is also involved in NMDAR gating. GluN1(W608C)/2A receptors show drastically slowed deactivation kinetics, suggesting that GluN1(W608) is an important determinant of receptor gating. Buck et al., showed that mutation of a tryptophan three residues C-terminal to GluN1(W608) (GluN1(W611)) alters receptor P_{open} (Buck et al., 2000). Like GluN1(W608), GluN1(W611) faces the GluN2 M3 region in the neighboring subunit. Together, these data suggest that the conformation of the GluN1 M2 – GluN2 M3 interface changes during receptor gating. Additionally, the observation that GluN1(W608L)/2B receptors show reduced proton sensitivity and spermine potentiation suggest that GluN1(W608) is important for regulation of gating (Kashiwagi et al., 1997).

5.2 Importance of the Deep Site in MCI

A conclusion of chapter 3 is that memantine MCI occurs through occupancy of a non-inhibitory site and subsequent translocation to the deep site. An important finding used to support this argument is the observation that Mg^{2+} inhibited MCI when applied throughout the MCI

protocol, but not when applied just during memantine application ("modified Mg^{2+} protocol," Figure 17). Similar experiments by Sobolevsky et al. examined the influence of Mg^{2+} present only during memantine application on NMDAR inhibition in an MCI-like protocol (Sobolevsky et al., 1998). In contrast to our results, Sobolevsky et al. found that co-application of Mg^{2+} and memantine during an MCI protocol greatly reduced inhibition (Sobolevsky et al., 1998). However, Sobolevsky et al. observed a dramatic decrease in NMDAR inhibition by an MCI-like protocol with inclusion of APV during memantine application, suggesting that significant open channel block occurred during memantine application in their MCI-like protocols. APV was not present during co-application of memantine and Mg^{2+}, which likely allowed Mg^{2+} binding to the deep site.

Mg^{2+} was found to increase the speed of memantine unbinding from GluN1/2A receptors (Figure 14) and subsequent experiments in Chapters 3 and 4 suggested that Mg^{2+} eliminates the slow component of memantine unblock by interfering with memantine MCI. The speed of MK-801 unbinding from NMDARs also increases in the presence of Mg^{2+}, though increased MK-801 unbinding may be caused by Mg^{2+} prevention of subsequent re-binding of MK-801 (McKay et al., 2013).

Our data suggest that MCI requires an intact and unoccupied deep site. MCI was abolished in GluN1(N616R)/2A receptors, which show dramatically decreased sensitivity to open channel block by memantine. Kotermanski et al. examined MCI in GluN1(N616Q) mutants and found that MCI was unchanged (Kotermanski et al., 2009). However, the GluN1(N616Q) mutation reduces memantine IC_{50} only 2-6 fold (Chen and Lipton, 2005, Kotermanski and Johnson, 2009), while the GluN1(N616R) mutation reduces memantine IC_{50} >40-fold (Kashiwagi et al., 2002, Chen and Lipton, 2005). At concentrations used to test MCI in Kotermanski et al. (100 and 500 μM

memantine), a several-fold decrease in memantine potency at the deep site would likely not alter MCI.

5.3 Memantine MCI Relative to MCI of Other Compounds

Does MCI potency depend only on traditional channel block potency and pKa? The open-channel block IC_{50} of MK-801 is 15 nM, that of PCP is 0.82 μM, and that of dextrorphan is 1.3 μM, and that of memantine is 4.4 at pH 7.6 (Dravid et al., 2007). Based on Figure 20 we can conclude that 10 μM MK-801 produced ~90% MCI, 10 μM PCP produced ~60% MCI, 50 μM dextrorphan produced ~45% MCI. From examination of Figure 21G we determine that 100 μM memantine produced ~45% MCI and estimate that ~1 mM memantine is necessary to produce ~90% MCI. Using these values we can conclude that the approximate MCI IC_{50} is 23X greater than the open channel block IC_{50} for memantine, 12X greater for PCP and 38X greater for dextrorphan. Therefore, PCP MCI is slightly more potent than memantine and dextrorphan MCI, relative to the open channel block IC_{50} of each drug. To compare the relative MCI potency of MK-801 and memantine, we can compare the drug concentration that produces ~90% MCI with the open channel block IC_{50}. The concentration of MK-801 that produces 90% MCI is 667X greater than the open channel block IC_{50} for MK-801. The concentration of memantine that produces 90% MCI is 227X greater than open channel block IC_{50}.227 for memantine. Therefore, memantine MCI is more potent than MK-801 MCI, relative to each drug's open channel block potency.

Do the expected MCI potencies (PCP < memantine < dextrorphan < MK-801) correlate with the amount of uncharged drug in solution? The pKas of drugs dictate the fraction of uncharged drug in solution in a pH-dependent way. The pKas of MK-801 (8.5), PCP (8.5) and dextrorphan

(9.2) are all more acidic than that of memantine (10.3) (Dravid et al., 2007). This means that, at physiological pH, each of these compounds contains a greater proportion of uncharged molecules in solution than does memantine. The ranking of drug pKa (memantine > dextrorphan > PCP = MK-801) does not correlate with the ranking of drug MCI potency relative to open channel block potency. This suggests that MCI potency depends on something in addition to open channel block potency and pKa.

5.4 Comparison of MCI with Fenestration-Dependent Modulation of Other Channels

Numerous channels have been proposed to allow pore access through fenestrations. Perhaps the most well-known example is voltage gated sodium (Na_V) channels. A hydrophobic route of access to the Na_V channel pore was proposed to be important for the action of local anesthetics on Na_V channels over 40 years ago (Hille, 1977). Na_V channels have closed, open, and inactivated states. While an obvious mechanism of drug access to the pore is through open-channel entry, some uncharged drugs can access the closed channel through fenestrations (Hille, 1977, Payandeh et al., 2012, Payandeh et al., 2011, Montini et al., 2018, Gamal El-Din et al., 2018). This allows for "tonic block," or block of resting Na_V channels. Resting block seems to occur only with uncharged drugs: charged molecules are unable to produce tonic block of resting channels (Strichartz, 1973, Payandeh et al., 2012, Payandeh et al., 2011). NMDAR and Na_V channel fenestrations may be similar in that only uncharged molecules can travel through them.

Crystal structures of prokaryotic voltage gated sodium channels from *Arcobacter butzleri* (NavAb) and *Magnetococcus marinus* (NavM) have allowed visualization of lateral fenestrations leading from the membrane to the Na_V pore (Payandeh et al., 2011, Payandeh et al., 2012, Lenaeus

et al., 2017, Sula et al., 2017). Prokaryotic sodium channels are thought to be good models for human (Sula et al., 2017) and other eukaryotic Na_Vs (Bagneris et al., 2014). Comparisons of prokaryotic Na_V channel structures in the closed, open and inactivated states suggest that fenestrations change shape with the activation state of the channel, which may give rise to state-dependent fenestration access (Montini et al., 2018, Payandeh et al., 2012). Mutation of a phenylalanine residue (NavAb(F203)) to alanine or tryptophan resulted in bidirectional modulation of fenestration size in molecular modeling simulations (Gamal El-Din et al., 2018). The NavAb(F203A) mutation increased fenestration size, along with tonic block of NavAb by local anesthetics, while the NavAb(F203W) mutation decreased fenestration size and tonic block. These results suggest that a change in a single residue can alter the passage of molecules through an NavAb channel fenestration. The results from Gamal El-Din et al. (2018) also remarkably parallel the increased memantine MCI and broadened fenestration we observed in GluN1/2A(M630A) receptors, and decreased MCI and narrowed fenestration we observed in GluN1/2A(M630W) receptors (Figures 24,25).

In Na_V channels, the size and lipophilicity of drugs influence fenestration-dependent block. Drug lipophilicity is correlated with degree of tonic block (Li et al., 1999). Size also restricts molecular passage through fenestrations in NavAbs, which tolerate a maximum molecular width the width of a benzene ring (Boiteux et al., 2014a, Kaczmarski and Corry, 2014, Buyan et al., 2018). Interestingly, ketamine does not display significant MCI (Kotermanski et al., 2009) despite being more lipophilic than other molecules that participate in MCI (Mealing et al., 1999). One possibility is that ketamine participates in MCI, but leaves the membrane too quickly for us to observe using our MCI protocol. The MCI protocol used includes a 1-s wash following removal of channel blocking drug, which requires that drugs remain in the membrane for >1 second to

allow observation of MCI. Most of the molecules shown to display MCI are substantially larger than a benzene ring. Therefore, NMDAR fenestrations are likely larger or more flexible than NavAb fenestrations. We have not systematically determined the maximal dimensions of molecules able to participate in MCI but doing so may yield important insight into the NMDAR fenestration.

Computational studies based on crystal structures suggest that potassium channels also have fenestrations. Molecular dynamics simulations showed that the voltage-gated channel Kv1.2, the G protein-gated inward rectifying channel GIRK2 (Kir3.2), and the human two-pore domain TWIK-1 (K2P1.1) have lateral fenestrations (Jorgensen et al., 2016). Molecular dynamics simulations suggest that fenestrations in Kv1.2 and Kir3.2 are unable to pass molecules larger than water. However, the TWIK-1 channel fenestrations were larger and allowed entry of lipids. The crystal structure of the TREK-2 channel (K2P10.2) showed norfluoxetine bound within a fenestration, suggesting that fenestrations may include important drug binding sites in addition to allowing drug passage (Dong et al., 2015). Fenestrations are state-dependent in TREK-2, apparent in the "down state" and absent in the "up state" (Dong et al., 2015). Like TREK-2 channels, NMDARs seem to show state-dependent membrane-to-channel access allowing a complete path from the membrane to the pore only in the activated state.

Most clinically useful local anesthetic molecules pass from the extracellular region into the membrane phase and/or intracellular space to reach their binding sites. Unlike in NMDARs, open channel blockers of Na_Vs enter the pore from the intracellular solution. Uncharged molecules typically enter the membrane phase more readily than charged molecules, and Na_V channels can be inhibited by uncharged molecules binding in the pore region. However, Na_V channel inhibition by the charged form of a local anesthetic molecule is often more potent than inhibition by the same

molecule in the uncharged form (Buyan et al., 2018). Many local anesthetics contain a protonatable amine group and have pKa ~7, suggesting that a near-equal proportion of molecules exist in both charged and uncharged states near physiological pH. This allows the uncharged form of molecules to pass through the membrane, take on a proton within the cytoplasm, and exhibit high-affinity block of Na_V channels (Buyan et al., 2018). To explain the V_m dependence of inhibition in MCI, we hypothesized that uncharged memantine accepts a proton after travelling through the fenestration and entering the open NMDAR pore. Protonation of uncharged memantine is likely mediated by H_3O^+ molecules in the pore region. It is unclear how the rate of protonation may affect MCI by memantine and other molecules. The time course of MCI may depend not only on memantine transit through the fenestration but also on protonation.

5.5 MCI and Block from the Intracellular Solution

Numerous studies use intracellular MK-801 to inhibit NMDARs on the MK-801 filled cell (e.g. (Bender et al., 2006, Brasier and Feldman, 2008, Corlew et al., 2007)). Intracellular MK-801 has been hypothesized to reach the deep site through either direct diffusion into the pore from the intracellular space or through diffusion into the extracellular space followed by typical open-channel block. Diffusion from the intracellular space to the deep site is unlikely because MK-801 is too large (~ 7.2 Å) (Chang and Kuo, 2008) to access the deep site from the intracellular solution (Amin et al., 2018, Villarroel et al., 1995, Kuner et al., 1996, Wollmuth et al., 1996). Evidence suggests that intracellular MK-801 does not block NMDARs on the filled cell by first diffusing into the extracellular space (Lavzin et al., 2012). It is tempting to speculate that block by intracellular MK-801 occurs through entry into the membrane and transit to the deep site through

NMDAR fenestrations. Interestingly, a very high concentration of intracellular MK-801 is required to achieve block of NMDARs. Similarly, intracellular memantine does not block NMDARs at up to 30 μM (Parsons et al., 2008b), though our unpublished data suggest that significant block by intracellular memantine occurs at concentrations of 1 mM and larger. If block by intracellular memantine and MK-801 occurs through the fenestration responsible for MCI, it is unclear why much larger concentrations of drug are needed to produce block from the intracellular space than from the extracellular space. A potential explanation for this is that drug entry into the membrane from the intracellular space is much slower than entry from the extracellular space. Differing lipid content between the inner and outer leaflets, or the existence of a barrier between the intracellular solution and the membrane inner leaflet, could be responsible for slowing entry into membrane from the intracellular space. Additional studies into differences in MCI when drug is applied to the intracellular versus extracellular spaces are required to better understand MCI.

5.6 Physiological Role of MCI

Is MCI a therapeutically relevant mechanism? Memantine is typically administered orally and absorbed in the gastrointestinal tract (Jarvis and Figgitt, 2003). Concentrations of memantine found in cerebrospinal fluid (CSF) of patients taking oral memantine are typically sub-micromolar (Kornhuber and Quack, 1995). At physiological pH, these concentrations would not be expected to result in significant MCI with the experimental setup and protocols used in Chapter 4. However, memantine has a fairly long half-life (60 – 100 hours) (Jarvis and Figgitt, 2003). Assuming that 1 μM memantine is present in the blood, ~ 0.1% of that, or 1 nM, is expected to be uncharged. Because uncharged memantine has a high partition coefficient (logP = 3.2 (Mealing et al., 1999)),

>99% of uncharged memantine will reside in the membrane rather than in aqueous solution after reaching equilibrium. Despite the observation that cells exposed to memantine for 30 s – 4 m show similar MCI, it is possible that 4 min is not enough to reach equilibrium. Over hours of continued exposure to memantine, membranes in vivo may accumulate a higher concentration of memantine than in our experiments. Additionally, physiological conditions are much different from conditions in whole-cell patch-clamp recordings. For example, in our recordings cells are internally perfused, whereas neurons in vivo contain a complex intracellular milieu that could influence MCI.

Another important factor in considering the physiological relevance of MCI is the presence of ~ 1 mM Mg^{2+} extracellularly. Continuous Mg^{2+} presence occludes MCI in GluN1/2A receptors in the experimental setup we used (Figure 17). However, this may not be the case under natural conditions. In neurons, action potentials cause brief removal of resting Mg^{2+} block. With memantine present in the membrane and NMDARs open, MCI may allow for memantine to occupy the deep site before Mg^{2+} block recurs. Thus, some NMDARs that would normally be blocked by Mg^{2+} would instead be blocked by memantine. Therefore, a drug that participates in MCI may compete more effectively with Mg^{2+} than a drug that exhibits only open channel block.

Additionally, while the physiological role for memantine MCI is unknown, MCI may be a therapeutically relevant mechanism of NMDAR inhibition by compounds we have not yet examined. As discussed, PCP shows a greater MCI potency relative to open channel block IC_{50} than other compounds tested. Study of additional compounds may reveal molecules with even greater relative propensity to participate in MCI. These drugs may prove to be therapeutically useful due, in part, to their MCI mechanism.

Finally, drugs that participate in MCI may have unique therapeutically relevant characteristics in addition to their involvement in MCI. For example, the long-lived biological

availability of memantine may cause memantine accumulation in intracellular compartments ("acid trapping"). This has been shown to regulate the lipid composition of the plasma membrane (Honegger et al., 1993). Further, some molecules subject to acid trapping can become packaged into synaptic vesicles and may be released at axon terminals (Tucker et al., 2015).

5.7 Future Directions

5.7.1 The conserved tryptophan in the TMD M2 region

We demonstrated that GluN2B(W607C)-containing receptors show increased potentiation by Mg^{2+} and assumed that this was due to potentiation of receptors through an NTD and exon 5-dependent mechanism. However, it is worthwhile to examine whether GluN2B(W607C)-containing receptors show enhanced Mg^{2+} potentiation when combined with exon 5-lacking GluN1 subunits. If indeed the GluN2B(W607C) mutation dramatically influences NTD-dependent properties, it would be interesting to explore the mechanisms linking changes in this residue to the NTD.

The experiments that indicated crosslinking between GluN1(W608C) and GluN2A(S632C) were not quantitative and gave minimal insight into the frequency of residue crosslinking. Although Western blots showed greater relative diheteromer signal in the GluN1(W608C)/2A(S632C) lane compared to the WT GluN1/2A lane, and mass spectrometry experiments confirmed that crosslinking between GluN1(W608C) and GluN2A(S632C) occurs, it is unclear how much of the diheteromer band is due to crosslinking between the introduced cysteines. Therefore, to gather data about the frequency of this crosslink, Western blots of cysteine

single mutants (GluN1(W608C)/2A and GluN1/2A(S632C)) should also be performed. If the diheteromer signal apparent in WT GluN1/2A receptors arises from disulfide crosslinking of intracellular proteins at endogenous cysteines, receptors containing mutations at endogenous cysteines may show stronger relative diheteromer signal stronger than WT GluN1/2A receptors. If the diheteromer band in the GluN1(W608C)/2A(S632C) lane includes substantial protein due to crosslinking between these two residues, we would expect that the GluN1(W608C)/2A(S632C) lane would show a significantly larger diheteromer to GluN1 monomer ratio than the sum of the diheteromer to monomer ratios in GluN1(W608C)/2A, GluN1/2A(S632C) receptors.

The work in Chapter 2 began with the observation that the tryptophan residue at position GluN1(W608) is conserved not only within NMDAR GluN2 subunits, but also within other structurally and evolutionarily related channels. We discovered that mutation of the conserved M2 tryptophan in the GluN1 and GluN2B subunits drastically affects NMDAR gating and block by Mg^{2+}. Investigating the effects of mutating the conserved tryptophan in related channels may yield further insight into the structural and functional importance of maintaining a tryptophan residue at this location.

5.7.2 MCI

Direct exploration of the relationship between membrane accumulation of molecules and MCI could link molecule reservoirs in the membrane to NMDAR inhibition. We attempted to visualize changes in membrane fluidity associated with application of high memantine concentrations to provide further evidence that the membrane provides a reservoir of memantine in MCI. Unfortunately, due to technical difficulties, these experiments did not yield interpretable results. However, imaging memantine accumulation in the membrane, along with analyzing the

time course of memantine accumulation, may strengthen the hypothesis that the membrane serves as a drug reservoir in MCI. Additionally, although our experiments suggest that the uncharged form of memantine mediates MCI, it is unclear whether charged memantine also plays a role in MCI. To explore whether charged memantine contributes to MCI our collaborator Dr. Santiago Vazquez synthesized for us a permanently charged version of memantine (trimethylmemantine). Trimethylmemantine is structurally identical to memantine apart from the addition of three methyl groups at the protonatable amine in memantine. Examining whether trimethylmemantine exhibits pH-dependent MCI may lend insight into whether charged memantine is involved in MCI.

A more complete characterization of MCI dependence on NMDAR subtype and drug characteristics may reveal important information about pore-accessible fenestrations in NMDARs. Further experiments should be carried out with the drugs shown to participate in MCI, and MCI by additional molecules should be examined. We have shown that the GluN2A(M630) residue influences memantine MCI. Examining MCI by MK-801, PCP, dextrorphan and RL-208 in GluN1/2A(M630A) and GluN1/2A(M630W) receptors is a potential next step in exploring whether these drugs interact with the proposed fenestration in a manner similar to memantine. The subtype-dependence of the MCI pathway also warrants further exploration. Whether GluN1/2B and GluN1/2D receptors exhibit memantine MCI has not been directly tested. Additionally, it is unclear whether all receptor subtypes tolerate MCI by the same molecules. Examination of an alignment of the GluN2A-D subunit TMDs provides a logical starting point for exploring the structural causes of potential subtype-dependent differences in MCI (Figure 28). Finally, based on our hypothesis that MCI involves drug accumulation in the membrane and subsequent transit to the pore, MCI is likely to vary with agonist concentration and membrane composition. A detailed characterization of MCI will improve and expand our understanding of NMDAR inhibition.

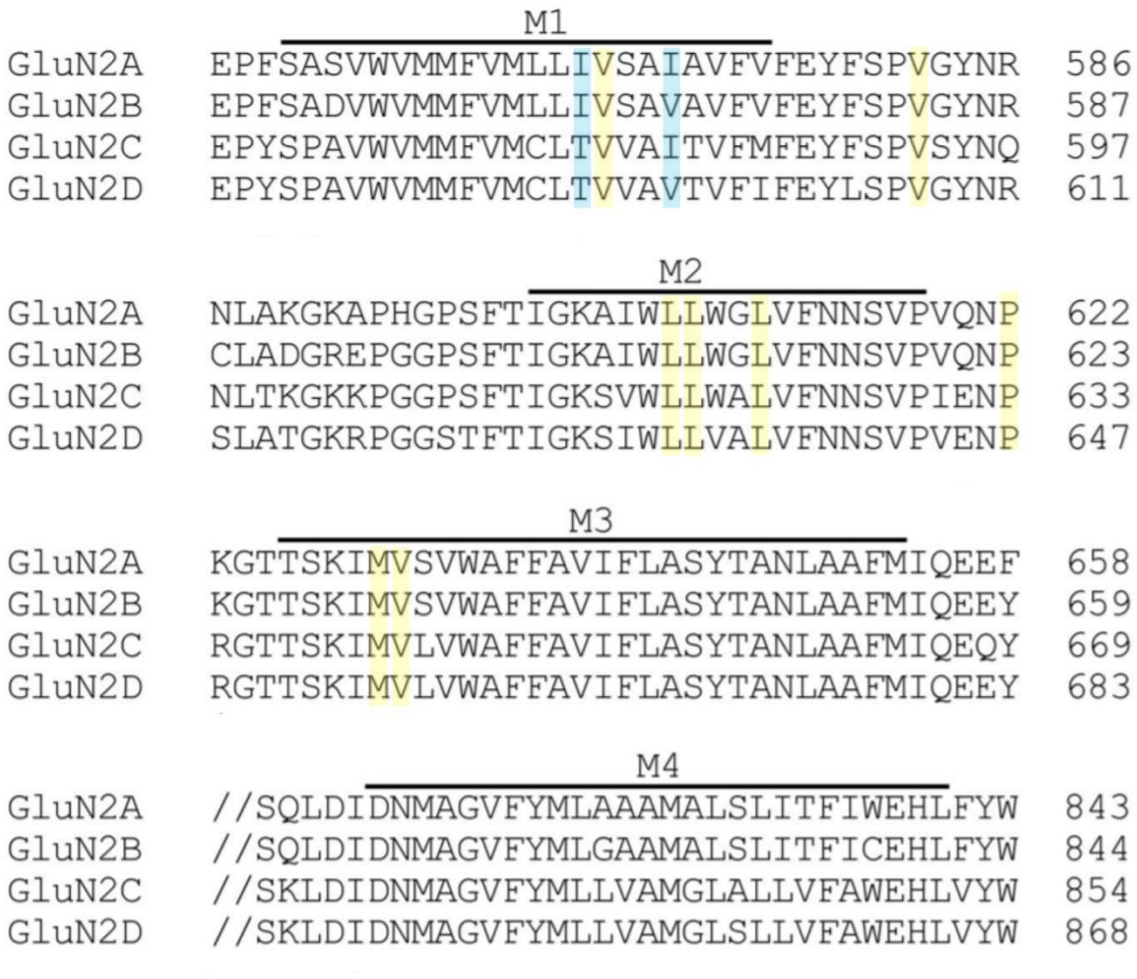

Figure 28 Sequence alignment of GluN2 TMDs

Sequence alignment of the TMDs of the *rattus norvegicus* GluN2A-D subunits. Residues highlighted in yellow indicate positions predicted to line the GluN1/2A fenestration that are conserved between subunits. Residues highlighted in blue indicate positions predicted to line the GluN1/2A fenestration that are not fully conserved between subunits. Residues highlighted in blue may give rise to subtype-specific changes in MCI. Figure adapted from Siegler Retchless et al., 2012.

Bibliography

2019. Highlights of Prescribing Information: Spravato. *In:* FDA (ed.).

ABDALLAH, C. G., AVERILL, L. A. & KRYSTAL, J. H. 2015. Ketamine as a promising prototype for a new generation of rapid-acting antidepressants. *Ann N Y Acad Sci*.

ADAMUSOVA, E., CAIS, O., VYKLICKY, V., KUDOVA, E., CHODOUNSKA, H., HORAK, M. & VYKLICKY, L., JR. 2013. Pregnenolone sulfate activates NMDA receptor channels. *Physiol Res,* 62**,** 731-6.

ADDIS, L., VIRDEE, J. K., VIDLER, L. R., COLLIER, D. A., PAL, D. K. & URSU, D. 2017. Epilepsy-associated GRIN2A mutations reduce NMDA receptor trafficking and agonist potency - molecular profiling and functional rescue. *Sci Rep,* 7**,** 66.

AL-HALLAQ, R. A., CONRADS, T. P., VEENSTRA, T. D. & WENTHOLD, R. J. 2007. NMDA Di-Heteromeric Receptor Populations and Associated Proteins in Rat Hippocampus. *Journal of Neuroscience,* 27**,** 8334-8343.

AMIN, J. B., LENG, X., GOCHMAN, A., ZHOU, H. X. & WOLLMUTH, L. P. 2018. A conserved glycine harboring disease-associated mutations permits NMDA receptor slow deactivation and high Ca(2+) permeability. *Nat Commun,* 9**,** 3748.

AMIN, J. B., SALUSSOLIA, C. L., CHAN, K., REGAN, M. C., DAI, J., ZHOU, H. X., FURUKAWA, H., BOWEN, M. E. & WOLLMUTH, L. P. 2017. Divergent roles of a peripheral transmembrane segment in AMPA and NMDA receptors. *J Gen Physiol,* 149**,** 661-680.

ANFINSEN, C. B. & HABER, E. 1961. Studies on the reduction and re-formation of protein disulfide bonds. *J Biol Chem,* 236**,** 1361-3.

ANTONOV, S. M. & JOHNSON, J. W. 1996. Voltage-dependent interaction of open-channel blocking molecules with gating of NMDA receptors in rat cortical neurons. *J Physiol,* 493 (Pt 2)**,** 425-45.

ANTONOV, S. M. & JOHNSON, J. W. 1999. Permeant ion regulation of N-methyl-D-aspartate receptor channel block by Mg(2+). *Proc Natl Acad Sci U S A,* 96**,** 14571-6.

ARANEDA, R. C., LAN, J. Y., ZHENG, X., ZUKIN, R. S. & BENNETT, M. V. 1999. Spermine and arcaine block and permeate N-methyl-D-aspartate receptor channels. *Biophys J,* 76**,** 2899-911.

ASCHER, P. & NOWAK, L. 1988. The role of divalent cations in the N-methyl-D-aspartate responses of mouse central neurones in culture. *J Physiol,* 399**,** 247-66.

ASSOCIATION, A. S. 2018. Alzheimer's Association Report: 2018 Alzheimer's disease facts and figures. *Alzheimer's and Dementia,* 14**,** 367-429.

ATES-ALAGOZ, Z. & ADEJARE, A. 2013. NMDA Receptor Antagonists for Treatment of Depression. *Pharmaceuticals (Basel),* 6**,** 480-99.

BAGNERIS, C., DECAEN, P. G., NAYLOR, C. E., PRYDE, D. C., NOBELI, I., CLAPHAM, D. E. & WALLACE, B. A. 2014. Prokaryotic NavMs channel as a structural and functional model for eukaryotic sodium channel antagonism. *Proc Natl Acad Sci U S A,* 111**,** 8428-33.

BALU, D. T. 2016. The NMDA Receptor and Schizophrenia: From Pathophysiology to Treatment. *Adv Pharmacol,* 76**,** 351-82.

BANKE, T. G., DRAVID, S. M. & TRAYNELIS, S. F. 2005. Protons trap NR1/NR2B NMDA receptors in a nonconducting state. *J Neurosci,* 25**,** 42-51.

BECK, C., WOLLMUTH, L. P., SEEBURG, P. H., SAKMANN, B. & KUNER, T. 1999. NMDAR channel segments forming the extracellular vestibule inferred from the accessibility of substituted cysteines. *Neuron,* 22**,** 559-70.

BENDER, V. A., BENDER, K. J., BRASIER, D. J. & FELDMAN, D. E. 2006. Two coincidence detectors for spike timing-dependent plasticity in somatosensory cortex. *J Neurosci,* 26**,** 4166-77.

BENVENISTE, M. & MAYER, M. L. 1991. Kinetic analysis of antagonist action at N-methyl-D-aspartic acid receptors. Two binding sites each for glutamate and glycine. *Biophys J,* 59**,** 560-73.

BENVENISTE, M. & MAYER, M. L. 1993. Multiple effects of spermine on N-methyl-D-aspartic acid receptor responses of rat cultured hippocampal neurones. *J Physiol,* 464**,** 131-63.

BENVENISTE, M. & MAYER, M. L. 1995. Trapping of glutamate and glycine during open channel block of rat hippocampal neuron NMDA receptors by 9-aminoacridine. *J Physiol,* 483 (Pt 2)**,** 367-84.

BERENDSEN, H. J. C., POSTMA, J. P. M., VAN GUNSTEREN, W. F., DINOLA, A. & HAAK, J. R. 1984. Molecular dynamics with coupling to an external bath. *The Journal of Chemical Physics,* 81**,** 3684-3690.

BERRETTA, N. & JONES, R. S. 1996. Tonic facilitation of glutamate release by presynaptic N-methyl-D-aspartate autoreceptors in the entorhinal cortex. *Neuroscience,* 75**,** 339-44.

BLANPIED, T. A., BOECKMAN, F. A., AIZENMAN, E. & JOHNSON, J. W. 1997. Trapping channel block of NMDA-activated responses by amantadine and memantine. *J Neurophysiol,* 77**,** 309-23.

BLANPIED, T. A., CLARKE, R. J. & JOHNSON, J. W. 2005. Amantadine inhibits NMDA receptors by accelerating channel closure during channel block. *J Neurosci,* 25**,** 3312-22.

BOITEUX, C., VOROBYOV, I. & ALLEN, T. W. 2014a. Ion conduction and conformational flexibility of a bacterial voltage-gated sodium channel. *Proc Natl Acad Sci U S A,* 111**,** 3454-9.

BOITEUX, C., VOROBYOV, I., FRENCH, R. J., FRENCH, C., YAROV-YAROVOY, V. & ALLEN, T. W. 2014b. Local anesthetic and antiepileptic drug access and binding to a bacterial voltage-gated sodium channel. *Proc Natl Acad Sci U S A,* 111**,** 13057-62.

BOLSHAKOV, K. V., GMIRO, V. E., TIKHONOV, D. B. & MAGAZANIK, L. G. 2003. Determinants of trapping block of N-methyl-d-aspartate receptor channels. *J Neurochem,* 87**,** 56-65.

BOROVSKA, J., VYKLICKY, V., STASTNA, E., KAPRAS, V., SLAVIKOVA, B., HORAK, M., CHODOUNSKA, H. & VYKLICKY, L., JR. 2012. Access of inhibitory neurosteroids to the NMDA receptor. *Br J Pharmacol,* 166**,** 1069-83.

BOUVIER, G., BIDORET, C., CASADO, M. & PAOLETTI, P. 2015. Presynaptic NMDA receptors: Roles and rules. *Neuroscience,* 311**,** 322-40.

BOWIE, D. & MAYER, M. L. 1995. Inward rectification of both AMPA and kainate subtype glutamate receptors generated by polyamine-mediated ion channel block. *Neuron,* 15**,** 453-62.

BRASIER, D. J. & FELDMAN, D. E. 2008. Synapse-specific expression of functional presynaptic NMDA receptors in rat somatosensory cortex. *J Neurosci,* 28**,** 2199-211.

BRESINK, I., BENKE, T. A., COLLETT, V. J., SEAL, A. J., PARSONS, C. G., HENLEY, J. M. & COLLINGRIDGE, G. L. 1996. Effects of memantine on recombinant rat NMDA receptors expressed in HEK 293 cells. *Br J Pharmacol,* 119**,** 195-204.

BUCK, D. P., HOWITT, S. M. & CLEMENTS, J. D. 2000. NMDA channel gating is influenced by a tryptophan residue in the M2 domain but calcium permeation is not altered. *Biophys J,* 79**,** 2454-62.

BURNASHEV, N., MONYER, H., SEEBURG, P. H. & SAKMANN, B. 1992a. Divalent ion permeability of AMPA receptor channels is dominated by the edited form of a single subunit. *Neuron,* 8**,** 189-98.

BURNASHEV, N., SCHOEPFER, R., MONYER, H., RUPPERSBERG, J. P., GUNTHER, W., SEEBURG, P. H. & SAKMANN, B. 1992b. Control by asparagine residues of calcium permeability and magnesium blockade in the NMDA receptor. *Science,* 257**,** 1415-9.

BURNASHEV, N. & SZEPETOWSKI, P. 2015. NMDA receptor subunit mutations in neurodevelopmental disorders. *Curr Opin Pharmacol,* 20**,** 73-82.

BURNASHEV, N., ZHOU, Z., NEHER, E. & SAKMANN, B. 1995. Fractional calcium currents through recombinant GluR channels of the NMDA, AMPA and kainate receptor subtypes. *J Physiol,* 485 (Pt 2)**,** 403-18.

BUYAN, A., SUN, D. & CORRY, B. 2018. Protonation state of inhibitors determines interaction sites within voltage-gated sodium channels. *Proc Natl Acad Sci U S A,* 115**,** E3135-E3144.

CALON, F., MORISSETTE, M., GHRIBI, O., GOULET, M., GRONDIN, R., BLANCHET, P. J., BEDARD, P. J. & DI PAOLO, T. 2002. Alteration of glutamate receptors in the striatum of dyskinetic 1-methyl-4-phenyl-1,2,3,6-tetrahydropyridine-treated monkeys following dopamine agonist treatment. *Prog Neuropsychopharmacol Biol Psychiatry,* 26**,** 127-38.

CASE, D. A. B.-S., I.Y. BROZELL, S.R. CERUTTI, D.S., CHEATHAM, T.E. CRUZEIRO, V.W.D. 2018. AMBER. University of California, San Francisco.

CATTERALL, W. A. & SWANSON, T. M. 2015. Structural Basis for Pharmacology of Voltage-Gated Sodium and Calcium Channels. *Mol Pharmacol,* 88**,** 141-50.

CHANG, H. R. & KUO, C. C. 2008. The activation gate and gating mechanism of the NMDA receptor. *J Neurosci,* 28**,** 1546-56.

CHEN, H. S. & LIPTON, S. A. 1997. Mechanism of memantine block of NMDA-activated channels in rat retinal ganglion cells: uncompetitive antagonism. *J Physiol,* 499 (Pt 1)**,** 27-46.

CHEN, H. S. & LIPTON, S. A. 2005. Pharmacological implications of two distinct mechanisms of interaction of memantine with N-methyl-D-aspartate-gated channels. *J Pharmacol Exp Ther,* 314**,** 961-71.

CHEN, N., LUO, T. & RAYMOND, L. A. 1999. Subtype-dependence of NMDA receptor channel open probability. *J Neurosci,* 19**,** 6844-54.

CHEN, W., SHIEH, C., SWANGER, S. A., TANKOVIC, A., AU, M., MCGUIRE, M., TAGLIATI, M., GRAHAM, J. M., MADAN-KHETARPAL, S., TRAYNELIS, S. F., YUAN, H. & PIERSON, T. M. 2017. GRIN1 mutation associated with intellectual disability alters NMDA receptor trafficking and function. *J Hum Genet,* 62**,** 589-597.

CHEN, Z. W., BRACAMONTES, J. R., BUDELIER, M. M., GERMANN, A. L., SHIN, D. J., KATHIRESAN, K., QIAN, M. X., MANION, B., CHENG, W. W. L., REICHERT, D. E., AKK, G., COVEY, D. F. & EVERS, A. S. 2019. Multiple functional neurosteroid binding sites on GABAA receptors. *PLoS Biol,* 17**,** e3000157.

CHERNOFF, D. M. & STRICHARTZ, G. R. 1990. Kinetics of local anesthetic inhibition of neuronal sodium currents. pH and hydrophobicity dependence. *Biophys J,* 58**,** 69-81.

CHEW, C. F., GUY, A. & BIGGIN, P. C. 2008. Distribution and dynamics of adamantanes in a lipid bilayer. *Biophys J,* 95**,** 5627-36.

CHOI, Y. B. & LIPTON, S. A. 1999. Identification and mechanism of action of two histidine residues underlying high-affinity Zn2+ inhibition of the NMDA receptor. *Neuron,* 23**,** 171-80.

CHOPRA, D. A., MONAGHAN, D. T. & DRAVID, S. M. 2015. Bidirectional Effect of Pregnenolone Sulfate on GluN1/GluN2A N-Methyl-D-Aspartate Receptor Gating Depending on Extracellular Calcium and Intracellular Milieu. *Mol Pharmacol,* 88**,** 650-9.

CHRISTINE, C. W. & CHOI, D. W. 1990. Effect of zinc on NMDA receptor-mediated channel currents in cortical neurons. *J Neurosci,* 10**,** 108-16.

CLARK, D. F., GO, E. P., TOUMI, M. L. & DESAIRE, H. 2011. Collision induced dissociation products of disulfide-bonded peptides: ions result from the cleavage of more than one bond. *J Am Soc Mass Spectrom,* 22**,** 492-8.

CLARKE, R. J., GLASGOW, N. G. & JOHNSON, J. W. 2013. Mechanistic and structural determinants of NMDA receptor voltage-dependent gating and slow Mg2+ unblock. *J Neurosci,* 33**,** 4140-50.

CLARKE, R. J. & JOHNSON, J. W. 2008. Voltage-dependent gating of NR1/2B NMDA receptors. *J Physiol,* 586**,** 5727-41.

CORLEW, R., WANG, Y., GHERMAZIEN, H., ERISIR, A. & PHILPOT, B. D. 2007. Developmental switch in the contribution of presynaptic and postsynaptic NMDA receptors to long-term depression. *J Neurosci,* 27**,** 9835-45.

COSTA, A. C. & ALBUQUERQUE, E. X. 1994. Dynamics of the actions of tetrahydro-9-aminoacridine and 9-aminoacridine on glutamatergic currents: concentration-jump studies in cultured rat hippocampal neurons. *J Pharmacol Exp Ther,* 268**,** 503-14.

DAU, A., GLADDING, C. M., SEPERS, M. D. & RAYMOND, L. A. 2014. Chronic blockade of extrasynaptic NMDA receptors ameliorates synaptic dysfunction and pro-death signaling in Huntington disease transgenic mice. *Neurobiol Dis,* 62**,** 533-42.

DAVIES, J., FRANCIS, A. A., JONES, A. W. & WATKINS, J. C. 1981. 2-Amino-5-phosphonovalerate (2APV), a potent and selective antagonist of amino acid-induced and synaptic excitation. *Neurosci Lett,* 21**,** 77-81.

DEL RIO-SANCHO, S., SERNA-JIMENEZ, C. E., CALATAYUD-PASCUAL, M. A., BALAGUER-FERNANDEZ, C., FEMENIA-FONT, A., MERINO, V. & LOPEZ-CASTELLANO, A. 2012. Transdermal absorption of memantin--effect of chemical enhancers, iontophoresis, and role of enhancer lipophilicity. *Eur J Pharm Biopharm,* 82**,** 164-70.

DILMORE, J. G. & JOHNSON, J. W. 1998. Open channel block and alteration of N-methyl-D-aspartic acid receptor gating by an analog of phencyclidine. *Biophys J,* 75**,** 1801-16.

DINGLEDINE, R., BORGES, K., BOWIE, D. & TRAYNELIS, S. F. 1999. The glutamate receptor ion channels. *Pharmacol Rev,* 51**,** 7-61.

DOMINGUES, A., ALMEIDA, S., DA CRUZ E SILVA, E. F., OLIVEIRA, C. R. & REGO, A. C. 2007. Toxicity of beta-amyloid in HEK293 cells expressing NR1/NR2A or NR1/NR2B N-methyl-D-aspartate receptor subunits. *Neurochem Int,* 50**,** 872-80.

DONG, Y. Y., PIKE, A. C., MACKENZIE, A., MCCLENAGHAN, C., ARYAL, P., DONG, L., QUIGLEY, A., GRIEBEN, M., GOUBIN, S., MUKHOPADHYAY, S., RUDA, G. F., CLAUSEN, M. V., CAO, L., BRENNAN, P. E., BURGESS-BROWN, N. A., SANSOM, M. S., TUCKER, S. J. & CARPENTER, E. P. 2015. K2P channel gating mechanisms revealed by structures of TREK-2 and a complex with Prozac. *Science,* 347**,** 1256-9.

DRAVID, S. M., ERREGER, K., YUAN, H., NICHOLSON, K., LE, P., LYUBOSLAVSKY, P., ALMONTE, A., MURRAY, E., MOSELY, C., BARBER, J., FRENCH, A., BALSTER, R., MURRAY, T. F. & TRAYNELIS, S. F. 2007. Subunit-specific mechanisms and proton sensitivity of NMDA receptor channel block. *J Physiol,* 581**,** 107-28.

DRAVID, S. M., PRAKASH, A. & TRAYNELIS, S. F. 2008a. Activation of recombinant NR1/NR2C NMDA receptors. *The Journal of Physiology,* 586**,** 4425-4439.

DRAVID, S. M., PRAKASH, A. & TRAYNELIS, S. F. 2008b. Activation of recombinant NR1/NR2C NMDA receptors. *J Physiol,* 586**,** 4425-39.

DUMAN, R. S. 2018. Ketamine and rapid-acting antidepressants: a new era in the battle against depression and suicide. *F1000Res,* 7.

DURRMEYER, X., VUTSKITS, L., ANAND, K. J. & RIMENSBERGER, P. C. 2010. Use of analgesic and sedative drugs in the NICU: integrating clinical trials and laboratory data. *Pediatr Res,* 67**,** 117-27.

EGEBJERG, J. & HEINEMANN, S. F. 1993. Ca2+ permeability of unedited and edited versions of the kainate selective glutamate receptor GluR6. *Proc Natl Acad Sci U S A,* 90**,** 755-9.

EMRE, M., TSOLAKI, M., BONUCCELLI, U., DESTEE, A., TOLOSA, E., KUTZELNIGG, A., CEBALLOS-BAUMANN, A., ZDRAVKOVIC, S., BLADSTROM, A., JONES, R. & STUDY, I. 2010. Memantine for patients with Parkinson's disease dementia or dementia with Lewy bodies: a randomised, double-blind, placebo-controlled trial. *Lancet Neurol,* 9**,** 969-77.

ERREGER, K., DRAVID, S. M., BANKE, T. G., WYLLIE, D. J. & TRAYNELIS, S. F. 2005. Subunit-specific gating controls rat NR1/NR2A and NR1/NR2B NMDA channel kinetics and synaptic signalling profiles. *J Physiol,* 563**,** 345-58.

ERREGER, K. & TRAYNELIS, S. F. 2008. Zinc inhibition of rat NR1/NR2A N-methyl-D-aspartate receptors. *J Physiol,* 586**,** 763-78.

EWALD, R. C. & CLINE, H. T. 2009. NMDA Receptors and Brain Development. *In:* VAN DONGEN, A. M. (ed.) *Biology of the NMDA Receptor.* Boca Raton (FL).

FEDELE, L., NEWCOMBE, J., TOPF, M., GIBB, A., HARVEY, R. J. & SMART, T. G. 2018. Disease-associated missense mutations in GluN2B subunit alter NMDA receptor ligand binding and ion channel properties. *Nat Commun,* 9**,** 957.

FERREIRA, I. L., BAJOUCO, L. M., MOTA, S. I., AUBERSON, Y. P., OLIVEIRA, C. R. & REGO, A. C. 2012. Amyloid beta peptide 1-42 disturbs intracellular calcium homeostasis through activation of GluN2B-containing N-methyl-d-aspartate receptors in cortical cultures. *Cell Calcium,* 51**,** 95-106.

FOSTER, A. C. & WONG, E. H. 1987. The novel anticonvulsant MK-801 binds to the activated state of the N-methyl-D-aspartate receptor in rat brain. *Br J Pharmacol,* 91**,** 403-9.

FRANKIEWICZ, T., POTIER, B., BASHIR, Z. I., COLLINGRIDGE, G. L. & PARSONS, C. G. 1996. Effects of memantine and MK-801 on NMDA-induced currents in cultured neurones and on synaptic transmission and LTP in area CA1 of rat hippocampal slices. *Br J Pharmacol,* 117**,** 689-97.

GALLAGHER, M. J., HUANG, H., PRITCHETT, D. B. & LYNCH, D. R. 1996. Interactions between ifenprodil and the NR2B subunit of the N-methyl-D-aspartate receptor. *J Biol Chem,* 271**,** 9603-11.

GAMAL EL-DIN, T. M., LENAEUS, M. J., ZHENG, N. & CATTERALL, W. A. 2018. Fenestrations control resting-state block of a voltage-gated sodium channel. *Proc Natl Acad Sci U S A,* 115**,** 13111-13116.

GAO, K., TANKOVIC, A., ZHANG, Y., KUSUMOTO, H., ZHANG, J., CHEN, W., XIANGWEI, W., SHAULSKY, G. H., HU, C., TRAYNELIS, S. F., YUAN, H. & JIANG, Y. 2017. A de novo loss-of-function GRIN2A mutation associated with childhood focal epilepsy and acquired epileptic aphasia. *PLoS One,* 12**,** e0170818.

GIDEONS, E. S., KAVALALI, E. T. & MONTEGGIA, L. M. 2014. Mechanisms underlying differential effectiveness of memantine and ketamine in rapid antidepressant responses. *Proc Natl Acad Sci U S A,* 111**,** 8649-54.

GIELEN, M., LE GOFF, A., STROEBEL, D., JOHNSON, J. W., NEYTON, J. & PAOLETTI, P. 2008. Structural rearrangements of NR1/NR2A NMDA receptors during allosteric inhibition. *Neuron,* 57**,** 80-93.

GIELEN, M., SIEGLER RETCHLESS, B., MONY, L., JOHNSON, J. W. & PAOLETTI, P. 2009. Mechanism of differential control of NMDA receptor activity by NR2 subunits. *Nature,* 459**,** 703-7.

GILLING, K. E., JATZKE, C., HECHENBERGER, M. & PARSONS, C. G. 2009. Potency, voltage-dependency, agonist concentration-dependency, blocking kinetics and partial untrapping of the uncompetitive N-methyl-D-aspartate (NMDA) channel blocker

memantine at human NMDA (GluN1/GluN2A) receptors. *Neuropharmacology,* 56**,** 866-75.

GILLING, K. E., JATZKE, C. & PARSONS, C. G. 2007. Agonist concentration dependency of blocking kinetics but not equilibrium block of N-methyl-D-aspartate receptors by memantine. *Neuropharmacology,* 53**,** 415-20.

GLADSTONE, D. J., BLACK, S. E., HAKIM, A. M., HEART & STROKE FOUNDATION OF ONTARIO CENTRE OF EXCELLENCE IN STROKE, R. 2002. Toward wisdom from failure: lessons from neuroprotective stroke trials and new therapeutic directions. *Stroke,* 33**,** 2123-36.

GLASGOW, N. G. & JOHNSON, J. W. 2014. Whole-cell patch-clamp analysis of recombinant NMDA receptor pharmacology using brief glutamate applications. *Methods Mol Biol,* 1183**,** 23-41.

GLASGOW, N. G., POVYSHEVA, N. V., AZOFEIFA, A. M. & JOHNSON, J. W. 2017. Memantine and Ketamine Differentially Alter NMDA Receptor Desensitization. *J Neurosci,* 37**,** 9686-9704.

GLASGOW, N. G., SIEGLER RETCHLESS, B. & JOHNSON, J. W. 2015. Molecular bases of NMDA receptor subtype-dependent properties. *J Physiol,* 593**,** 83-95.

GLASGOW, N. G., WILCOX, M. R. & JOHNSON, J. W. 2018. Effects of Mg(2+) on recovery of NMDA receptors from inhibition by memantine and ketamine reveal properties of a second site. *Neuropharmacology,* 137**,** 344-358.

GORMAN, J. J., WALLIS, T. P. & PITT, J. J. 2002. Protein disulfide bond determination by mass spectrometry. *Mass Spectrom Rev,* 21**,** 183-216.

HACKOS, D. H. & HANSON, J. E. 2017. Diverse modes of NMDA receptor positive allosteric modulation: Mechanisms and consequences. *Neuropharmacology,* 112**,** 34-45.

HALL, R. W. & SHBAROU, R. M. 2009. Drugs of choice for sedation and analgesia in the neonatal ICU. *Clin Perinatol,* 36**,** 215-26, vii.

HALLETT, P. J. & STANDAERT, D. G. 2004. Rationale for and use of NMDA receptor antagonists in Parkinson's disease. *Pharmacol Ther,* 102**,** 155-74.

HANSEN, K. B., OGDEN, K. K., YUAN, H. & TRAYNELIS, S. F. 2014. Distinct functional and pharmacological properties of Triheteromeric GluN1/GluN2A/GluN2B NMDA receptors. *Neuron,* 81**,** 1084-1096.

HANSEN, K. B., YI, F., PERSZYK, R. E., FURUKAWA, H., WOLLMUTH, L. P., GIBB, A. J. & TRAYNELIS, S. F. 2018. Structure, function, and allosteric modulation of NMDA receptors. *J Gen Physiol,* 150**,** 1081-1105.

HARDINGHAM, G. E. & BADING, H. 2010. Synaptic versus extrasynaptic NMDA receptor signalling: implications for neurodegenerative disorders. *Nat Rev Neurosci,* 11**,** 682-96.

HARRISON, P. J. & WEINBERGER, D. R. 2005. Schizophrenia genes, gene expression, and neuropathology: on the matter of their convergence. *Mol Psychiatry,* 10**,** 40-68; image 5.

HESSELINK, M. B., DE BOER, A. G., BREIMER, D. D. & DANYSZ, W. 1999. Dopamine release in the prefrontal cortex in response to memantine following sub-chronic NMDA receptor blockade with memantine: a microdialysis study in rats. *J Neural Transm,* 106**,** 803-18.

HILLE, B. 1977. Local anesthetics: hydrophilic and hydrophobic pathways for the drug-receptor reaction. *J Gen Physiol,* 69**,** 497-515.

HONEGGER, U. E., QUACK, G. & WIESMANN, U. N. 1993. Evidence for lysosomotropism of memantine in cultured human cells: cellular kinetics and effects of memantine on phospholipid content and composition, membrane fluidity and beta-adrenergic transmission. *Pharmacol Toxicol,* 73**,** 202-8.

HORAK, M., VLCEK, K., CHODOUNSKA, H. & VYKLICKY, L., JR. 2006. Subtype-dependence of N-methyl-D-aspartate receptor modulation by pregnenolone sulfate. *Neuroscience,* 137**,** 93-102.

HORNAK, V., ABEL, R., OKUR, A., STROCKBINE, B., ROITBERG, A. & SIMMERLING, C. 2006. Comparison of multiple Amber force fields and development of improved protein backbone parameters. *Proteins,* 65**,** 712-25.

HUETTNER, J. E. & BEAN, B. P. 1988. Block of N-methyl-D-aspartate-activated current by the anticonvulsant MK-801: selective binding to open channels. *Proc Natl Acad Sci U S A,* 85**,** 1307-11.

IACOBUCCI, G. J. & POPESCU, G. K. 2017a. NMDA receptors: linking physiological output to biophysical operation. *Nat Rev Neurosci,* 18**,** 236-249.

IACOBUCCI, G. J. & POPESCU, G. K. 2017b. Resident Calmodulin Primes NMDA Receptors for Ca(2+)-Dependent Inactivation. *Biophys J,* 113**,** 2236-2248.

ISAEV, D., IVANCHICK, G., KHMYZ, V., ISAEVA, E., SAVRASOVA, A., KRISHTAL, O., HOLMES, G. L. & MAXIMYUK, O. 2012. Surface charge impact in low-magnesium model of seizure in rat hippocampus. *J Neurophysiol,* 107**,** 417-23.

JANG, M. K., MIERKE, D. F., RUSSEK, S. J. & FARB, D. H. 2004. A steroid modulatory domain on NR2B controls N-methyl-D-aspartate receptor proton sensitivity. *Proc Natl Acad Sci U S A,* 101**,** 8198-203.

JARVIS, B. & FIGGITT, D. P. 2003. Memantine. *Drugs Aging,* 20**,** 465-76; discussion 477-8.

JAVITT, D. C. & ZUKIN, S. R. 1991. Recent advances in the phencyclidine model of schizophrenia. *Am J Psychiatry,* 148**,** 1301-8.

JOHNSON, J. W., GLASGOW, N. G. & POVYSHEVA, N. V. 2015. Recent insights into the mode of action of memantine and ketamine. *Curr Opin Pharmacol,* 20**,** 54-63.

JONES, K. S., VANDONGEN, H. M. & VANDONGEN, A. M. 2002. The NMDA receptor M3 segment is a conserved transduction element coupling ligand binding to channel opening. *J Neurosci,* 22**,** 2044-53.

JORGENSEN, C., DARRE, L., OAKES, V., TORELLA, R., PRYDE, D. & DOMENE, C. 2016. Lateral Fenestrations in K(+)-Channels Explored Using Molecular Dynamics Simulations. *Mol Pharm,* 13**,** 2263-73.

KACZMARSKI, J. A. & CORRY, B. 2014. Investigating the size and dynamics of voltage-gated sodium channel fenestrations. *Channels (Austin),* 8**,** 264-77.

KAFI, H., SALAMZADEH, J., BELADIMOGHADAM, N., SISTANIZAD, M. & KOUCHEK, M. 2014. Study of the neuroprotective effects of memantine in patients with mild to moderate ischemic stroke. *Iran J Pharm Res,* 13**,** 591-8.

KARAKAS, E. & FURUKAWA, H. 2014. Crystal structure of a heterotetrameric NMDA receptor ion channel. *Science,* 344**,** 992-7.

KARAKAS, E., SIMOROWSKI, N. & FURUKAWA, H. 2009. Structure of the zinc-bound amino-terminal domain of the NMDA receptor NR2B subunit. *EMBO J,* 28**,** 3910-20.

KARAKAS, E., SIMOROWSKI, N. & FURUKAWA, H. 2011. Subunit arrangement and phenylethanolamine binding in GluN1/GluN2B NMDA receptors. *Nature,* 475**,** 249-53.

KASHIWAGI, K., MASUKO, T., NGUYEN, C. D., KUNO, T., TANAKA, I., IGARASHI, K. & WILLIAMS, K. 2002. Channel blockers acting at N-methyl-D-aspartate receptors: differential effects of mutations in the vestibule and ion channel pore. *Mol Pharmacol,* 61**,** 533-45.

KASHIWAGI, K., PAHK, A. J., MASUKO, T., IGARASHI, K. & WILLIAMS, K. 1997. Block and modulation of N-methyl-D-aspartate receptors by polyamines and protons: role of amino acid residues in the transmembrane and pore-forming regions of NR1 and NR2 subunits. *Mol Pharmacol,* 52**,** 701-13.

KATZ, B. A. & KOSSIAKOFF, A. 1986. The crystallographically determined structures of atypical strained disulfides engineered into subtilisin. *J Biol Chem,* 261**,** 15480-5.

KAYSER, M. S. & DALMAU, J. 2011. Anti-NMDA Receptor Encephalitis in Psychiatry. *Curr Psychiatry Rev,* 7**,** 189-193.

KEGELES, L. S., SHUNGU, D. C., ANJILVEL, S., CHAN, S., ELLIS, S. P., XANTHOPOULOS, E., MALASPINA, D., GORMAN, J. M., MANN, J. J., LARUELLE, M. & KAUFMANN,

C. A. 2000. Hippocampal pathology in schizophrenia: magnetic resonance imaging and spectroscopy studies. *Psychiatry Res,* 98**,** 163-75.

KEMP, J. A., FOSTER, A. C., LEESON, P. D., PRIESTLEY, T., TRIDGETT, R., IVERSEN, L. L. & WOODRUFF, G. N. 1988. 7-Chlorokynurenic acid is a selective antagonist at the glycine modulatory site of the N-methyl-D-aspartate receptor complex. *Proc Natl Acad Sci U S A,* 85**,** 6547-50.

KHLESTOVA, E., JOHNSON, J. W., KRYSTAL, J. H. & LISMAN, J. 2016. The Role of GluN2C-Containing NMDA Receptors in Ketamine's Psychotogenic Action and in Schizophrenia Models. *J Neurosci,* 36**,** 11151-11157.

KIROV, G., POCKLINGTON, A. J., HOLMANS, P., IVANOV, D., IKEDA, M., RUDERFER, D., MORAN, J., CHAMBERT, K., TONCHEVA, D., GEORGIEVA, L., GROZEVA, D., FJODOROVA, M., WOLLERTON, R., REES, E., NIKOLOV, I., VAN DE LAGEMAAT, L. N., BAYES, A., FERNANDEZ, E., OLASON, P. I., BOTTCHER, Y., KOMIYAMA, N. H., COLLINS, M. O., CHOUDHARY, J., STEFANSSON, K., STEFANSSON, H., GRANT, S. G., PURCELL, S., SKLAR, P., O'DONOVAN, M. C. & OWEN, M. J. 2012. De novo CNV analysis implicates specific abnormalities of postsynaptic signalling complexes in the pathogenesis of schizophrenia. *Mol Psychiatry,* 17**,** 142-53.

KISS, J. P., SZASZ, B. K., FODOR, L., MIKE, A., LENKEY, N., KURKO, D., NAGY, J. & VIZI, E. S. 2012. GluN2B-containing NMDA receptors as possible targets for the neuroprotective and antidepressant effects of fluoxetine. *Neurochem Int,* 60**,** 170-6.

KORINEK, M., VYKLICKY, V., BOROVSKA, J., LICHNEROVA, K., KANIAKOVA, M., KRAUSOVA, B., KRUSEK, J., BALIK, A., SMEJKALOVA, T., HORAK, M. & VYKLICKY, L. 2015. Cholesterol modulates open probability and desensitization of NMDA receptors. *J Physiol,* 593**,** 2279-93.

KORNHUBER, J. & QUACK, G. 1995. Cerebrospinal fluid and serum concentrations of the N-methyl-D-aspartate (NMDA) receptor antagonist memantine in man. *Neurosci Lett,* 195**,** 137-9.

KOSHELEV, S. G. & KHODOROV, B. I. 1995. Blockade of open NMDA channel by tetrabutylammmonium, 9-aminoacridine and tacrine prevents channels closing and desensitization. *Membr. and Cell Biol.,* 9**,** 93-109.

KOTERMANSKI, S. E. & JOHNSON, J. W. 2009. Mg2+ imparts NMDA receptor subtype selectivity to the Alzheimer's drug memantine. *J Neurosci,* 29**,** 2774-9.

KOTERMANSKI, S. E., JOHNSON, J. W. & THIELS, E. 2013. Comparison of behavioral effects of the NMDA receptor channel blockers memantine and ketamine in rats. *Pharmacol Biochem Behav,* 109**,** 67-76.

KOTERMANSKI, S. E., WOOD, J. T. & JOHNSON, J. W. 2009. Memantine binding to a superficial site on NMDA receptors contributes to partial trapping. *J Physiol,* 587**,** 4589-604.

KRYSTAL, J. H., D'SOUZA, D. C., MATHALON, D., PERRY, E., BELGER, A. & HOFFMAN, R. 2003. NMDA receptor antagonist effects, cortical glutamatergic function, and schizophrenia: toward a paradigm shift in medication development. *Psychopharmacology (Berl),* 169**,** 215-33.

KRYSTAL, J. H., KARPER, L. P., SEIBYL, J. P., FREEMAN, G. K., DELANEY, R., BREMNER, J. D., HENINGER, G. R., BOWERS, M. B., JR. & CHARNEY, D. S. 1994. Subanesthetic effects of the noncompetitive NMDA antagonist, ketamine, in humans. Psychotomimetic, perceptual, cognitive, and neuroendocrine responses. *Arch Gen Psychiatry,* 51**,** 199-214.

KUKOL, A. 2009. Lipid Models for United-Atom Molecular Dynamics Simulations of Proteins. *J Chem Theory Comput,* 5**,** 615-26.

KUNER, T. & SCHOEPFER, R. 1996. Multiple structural elements determine subunit specificity of Mg2+ block in NMDA receptor channels. *J Neurosci,* 16**,** 3549-58.

KUNER, T., WOLLMUTH, L. P., KARLIN, A., SEEBURG, P. H. & SAKMANN, B. 1996. Structure of the NMDA receptor channel M2 segment inferred from the accessibility of substituted cysteines. *Neuron,* 17**,** 343-52.

KUSSIUS, C. L., KAUR, N. & POPESCU, G. K. 2009. Pregnanolone sulfate promotes desensitization of activated NMDA receptors. *J Neurosci,* 29**,** 6819-27.

KUSSIUS, C. L. & POPESCU, G. K. 2009. Kinetic basis of partial agonism at NMDA receptors. *Nat Neurosci,* 12**,** 1114-20.

LAU, A. & TYMIANSKI, M. 2010. Glutamate receptors, neurotoxicity and neurodegeneration. *Pflugers Arch,* 460**,** 525-42.

LAVZIN, M., RAPOPORT, S., POLSKY, A., GARION, L. & SCHILLER, J. 2012. Nonlinear dendritic processing determines angular tuning of barrel cortex neurons in vivo. *Nature,* 490**,** 397-401.

LEE, C. H. & GOUAUX, E. 2011. Amino terminal domains of the NMDA receptor are organized as local heterodimers. *PLoS One,* 6**,** e19180.

LEE, C. H., LU, W., MICHEL, J. C., GOEHRING, A., DU, J., SONG, X. & GOUAUX, E. 2014. NMDA receptor structures reveal subunit arrangement and pore architecture. *Nature,* 511**,** 191-7.

LEE, H. K. 2006. AMPA Receptor Phosphorylation in Synaptic Plasticity: Insights from Knockin Mice. *In:* KITTLER, J. T. & MOSS, S. J. (eds.) *The Dynamic Synapse: Molecular Methods in Ionotropic Receptor Biology.* Boca Raton (FL).

LEGENDRE, P. & WESTBROOK, G. L. 1990. The inhibition of single N-methyl-D-aspartate-activated channels by zinc ions on cultured rat neurones. *J Physiol,* 429**,** 429-49.

LEIVA, R., PHILLIPS, M. B., TURCU, A. L., GRATACOS-BATLLE, E., LEON-GARCIA, L., SUREDA, F. X., SOTO, D., JOHNSON, J. W. & VAZQUEZ, S. 2018. Pharmacological and Electrophysiological Characterization of Novel NMDA Receptor Antagonists. *ACS Chem Neurosci,* 9**,** 2722-2730.

LENAEUS, M. J., GAMAL EL-DIN, T. M., ING, C., RAMANADANE, K., POMES, R., ZHENG, N. & CATTERALL, W. A. 2017. Structures of closed and open states of a voltage-gated sodium channel. *Proc Natl Acad Sci U S A,* 114**,** E3051-E3060.

LERMA, J. 1992. Spermine regulates N-methyl-D-aspartate receptor desensitization. *Neuron,* 8**,** 343-52.

LERMA, J., ZUKIN, R. S. & BENNETT, M. V. 1991. Interaction of Mg^{2+} and phencyclidine in use-dependent block of NMDA channels. *Neurosci Lett,* 123**,** 187-91.

LESTER, R. A., CLEMENTS, J. D., WESTBROOK, G. L. & JAHR, C. E. 1990. Channel kinetics determine the time course of NMDA receptor-mediated synaptic currents. *Nature,* 346**,** 565-7.

LEUNG, C. Y., PALMER, L. C., KEWALRAMANI, S., QIAO, B., STUPP, S. I., OLVERA DE LA CRUZ, M. & BEDZYK, M. J. 2013. Crystalline polymorphism induced by charge regulation in ionic membranes. *Proc Natl Acad Sci U S A,* 110**,** 16309-14.

LI, F. & TSIEN, J. Z. 2009. Memory and the NMDA receptors. *N Engl J Med,* 361**,** 302-3.

LI, H. L., GALUE, A., MEADOWS, L. & RAGSDALE, D. S. 1999. A molecular basis for the different local anesthetic affinities of resting versus open and inactivated states of the sodium channel. *Mol Pharmacol,* 55**,** 134-41.

LI, V. & WANG, Y. T. 2016. Molecular mechanisms of NMDA receptor-mediated excitotoxicity: implications for neuroprotective therapeutics for stroke. *Neural Regen Res,* 11**,** 1752-1753.

LINSENBARDT, A. J., TAYLOR, A., EMNETT, C. M., DOHERTY, J. J., KRISHNAN, K., COVEY, D. F., PAUL, S. M., ZORUMSKI, C. F. & MENNERICK, S. 2014. Different oxysterols have opposing actions at N-methyl-D-aspartate receptors. *Neuropharmacology,* 85**,** 232-42.

LIPTON, S. A. 2006. Paradigm shift in neuroprotection by NMDA receptor blockade: memantine and beyond. *Nat Rev Drug Discov,* 5**,** 160-70.

LIRK, P., PICARDI, S. & HOLLMANN, M. W. 2014. Local anaesthetics: 10 essentials. *Eur J Anaesthesiol,* 31**,** 575-85.

LIU, J., CHANG, L., SONG, Y., LI, H. & WU, Y. 2019. The Role of NMDA Receptors in Alzheimer's Disease. *Front Neurosci,* 13**,** 43.

LODGE, D., WATKINS, J. C., BORTOLOTTO, Z. A., JANE, D. E. & VOLIANSKIS, A. 2019. The 1980s: D-AP5, LTP and a Decade of NMDA Receptor Discoveries. *Neurochem Res,* 44**,** 516-530.

LORD, B., WINTMOLDERS, C., LANGLOIS, X., NGUYEN, L., LOVENBERG, T. & BONAVENTURE, P. 2013. Comparison of the ex vivo receptor occupancy profile of ketamine to several NMDA receptor antagonists in mouse hippocampus. *Eur J Pharmacol,* 715**,** 21-5.

LU, C. W., LIN, T. Y. & WANG, S. J. 2010. Memantine depresses glutamate release through inhibition of voltage-dependent Ca2+ entry and protein kinase C in rat cerebral cortex nerve terminals: an NMDA receptor-independent mechanism. *Neurochemistry international,* 57**,** 168-76.

LUO, J., WANG, Y., YASUDA, R. P., DUNAH, A. W. & WOLFE, B. B. 1997. The majority of N-methyl-D-aspartate receptor complexes in adult rat cerebral cortex contain at least three different subunits (NR1/NR2A/NR2B). *Mol Pharmacol,* 51**,** 79-86.

LUSCHER, C. & MALENKA, R. C. 2012. NMDA receptor-dependent long-term potentiation and long-term depression (LTP/LTD). *Cold Spring Harb Perspect Biol,* 4.

MACDONALD, J. F., BARTLETT, M. C., MODY, I., PAHAPILL, P., REYNOLDS, J. N., SALTER, M. W., SCHNEIDERMAN, J. H. & PENNEFATHER, P. S. 1991. Actions of ketamine, phencyclidine and MK-801 on NMDA receptor currents in cultured mouse hippocampal neurones. *J Physiol,* 432**,** 483-508.

MAJ, J., ROGOZ, Z., SKUZA, G. & KOLODZIEJCZYK, K. 1994. Some central effects of kynurenic acid, 7-chlorokynurenic acid and 5,7- dichloro-kynurenic acid, glycine site antagonists. *Pol J Pharmacol,* 46**,** 115-24.

MAJ, J., ROGOZ, Z., SKUZA, G. & SOWINSKA, H. 1992. The effect of antidepressant drugs on the locomotor hyperactivity induced by MK-801, a non-competitive NMDA receptor antagonist. *Neuropharmacology,* 31**,** 685-91.

MALAYEV, A., GIBBS, T. T. & FARB, D. H. 2002. Inhibition of the NMDA response by pregnenolone sulphate reveals subtype selective modulation of NMDA receptors by sulphated steroids. *Br J Pharmacol,* 135**,** 901-9.

MASKELL, P. D., SPEDER, P., NEWBERRY, N. R. & BERMUDEZ, I. 2003. Inhibition of human alpha 7 nicotinic acetylcholine receptors by open channel blockers of N-methyl-D-aspartate receptors. *British Journal of Pharmacology,* 140**,** 1313-9.

MAYER, M. L. & VYKLICKY, L., JR. 1989. The action of zinc on synaptic transmission and neuronal excitability in cultures of mouse hippocampus. *J Physiol,* 415**,** 351-65.

MAYER, M. L., WESTBROOK, G. L. & GUTHRIE, P. B. 1984. Voltage-dependent block by Mg2+ of NMDA responses in spinal cord neurones. *Nature,* 309**,** 261-3.

MCGURK, J. F., BENNETT, M. V. & ZUKIN, R. S. 1990. Polyamines potentiate responses of N-methyl-D-aspartate receptors expressed in xenopus oocytes. *Proc Natl Acad Sci U S A,* 87**,** 9971-4.

MCKAY, S., BENGTSON, C. P., BADING, H., WYLLIE, D. J. & HARDINGHAM, G. E. 2013. Recovery of NMDA receptor currents from MK-801 blockade is accelerated by Mg2+ and memantine under conditions of agonist exposure. *Neuropharmacology,* 74**,** 119-25.

MCMENIMEN, K. A., DOUGHERTY, D. A., LESTER, H. A. & PETERSSON, E. J. 2006. Probing the Mg2+ blockade site of an N-methyl-D-aspartate (NMDA) receptor with unnatural amino acid mutagenesis. *ACS Chem Biol,* 1**,** 227-34.

MCNAMARA, D. & DINGLEDINE, R. 1990. Dual effect of glycine on NMDA-induced neurotoxicity in rat cortical cultures. *J Neurosci,* 10**,** 3970-6.

MEALING, G. A., LANTHORN, T. H., MURRAY, C. L., SMALL, D. L. & MORLEY, P. 1999. Differences in degree of trapping of low-affinity uncompetitive N-methyl-D-aspartic acid receptor antagonists with similar kinetics of block. *J Pharmacol Exp Ther,* 288**,** 204-10.

MESBAHI-VASEY, S., VERAS, L., YONKUNAS, M., JOHNSON, J. W. & KURNIKOVA, M. G. 2017. All atom NMDA receptor transmembrane domain model development and simulations in lipid bilayers and water. *PLoS One,* 12**,** e0177686.

MONTINI, G., BOOKER, J., SULA, A. & WALLACE, B. A. 2018. Comparisons of voltage-gated sodium channel structures with open and closed gates and implications for state-dependent drug design. *Biochem Soc Trans,* 46**,** 1567-1575.

MONY, L., ZHU, S., CARVALHO, S. & PAOLETTI, P. 2011. Molecular basis of positive allosteric modulation of GluN2B NMDA receptors by polyamines. *EMBO J,* 30**,** 3134-46.

MONYER, H., BURNASHEV, N., LAURIE, D. J., SAKMANN, B. & SEEBURG, P. H. 1994. Developmental and regional expression in the rat brain and functional properties of four NMDA receptors. *Neuron,* 12**,** 529-40.

MONYER, H., SPRENGEL, R., SCHOEPFER, R., HERB, A., HIGUCHI, M., LOMELI, H., BURNASHEV, N., SAKMANN, B. & SEEBURG, P. H. 1992. Heteromeric NMDA receptors: molecular and functional distinction of subtypes. *Science,* 256**,** 1217-21.

MORAN, P., STOKES, J., MARR, J., BOCK, G., DESBONNET, L., WADDINGTON, J. & O'TUATHAIGH, C. 2016. Gene x Environment Interactions in Schizophrenia: Evidence from Genetic Mouse Models. *Neural Plast,* 2016**,** 2173748.

MORI, H., MASAKI, H., YAMAKURA, T. & MISHINA, M. 1992. Identification by mutagenesis of a Mg(2+)-block site of the NMDA receptor channel. *Nature,* 358**,** 673-5.

MORING, J., NIEGO, L. A., GANLEY, L. M., TRUMBORE, M. W. & HERBETTE, L. G. 1994. Interaction of the NMDA receptor noncompetitive antagonist MK-801 with model and native membranes. *Biophys J,* 67**,** 2376-86.

MORRIS, B. J., COCHRAN, S. M. & PRATT, J. A. 2005. PCP: from pharmacology to modelling schizophrenia. *Curr Opin Pharmacol,* 5**,** 101-6.

MOTT, D. D., DOHERTY, J. J., ZHANG, S., WASHBURN, M. S., FENDLEY, M. J., LYUBOSLAVSKY, P., TRAYNELIS, S. F. & DINGLEDINE, R. 1998. Phenylethanolamines inhibit NMDA receptors by enhancing proton inhibition. *Nat Neurosci,* 1**,** 659-67.

MUIR, K. W. 2006. Glutamate-based therapeutic approaches: clinical trials with NMDA antagonists. *Curr Opin Pharmacol,* 6**,** 53-60.

NASH, J. E. & BROTCHIE, J. M. 2002. Characterisation of striatal NMDA receptors involved in the generation of parkinsonian symptoms: intrastriatal microinjection studies in the 6-OHDA-lesioned rat. *Mov Disord,* 17**,** 455-66.

NICOLL, R. A. 2017. A Brief History of Long-Term Potentiation. *Neuron,* 93**,** 281-290.

NIKOLAEV, M. V., MAGAZANIK, L. G. & TIKHONOV, D. B. 2012. Influence of external magnesium ions on the NMDA receptor channel block by different types of organic cations. *Neuropharmacology,* 62**,** 2078-85.

NOWAK, L., BREGESTOVSKI, P., ASCHER, P., HERBET, A. & PROCHIANTZ, A. 1984. Magnesium gates glutamate-activated channels in mouse central neurones. *Nature,* 307**,** 462-5.

OH, J. D., RUSSELL, D. S., VAUGHAN, C. L. & CHASE, T. N. 1998. Enhanced tyrosine phosphorylation of striatal NMDA receptor subunits: effect of dopaminergic denervation and L-DOPA administration. *Brain Res,* 813**,** 150-9.

OKAMOTO, S., POULADI, M. A., TALANTOVA, M., YAO, D., XIA, P., EHRNHOEFER, D. E., ZAIDI, R., CLEMENTE, A., KAUL, M., GRAHAM, R. K., ZHANG, D., VINCENT CHEN, H. S., TONG, G., HAYDEN, M. R. & LIPTON, S. A. 2009. Balance between synaptic versus extrasynaptic NMDA receptor activity influences inclusions and neurotoxicity of mutant huntingtin. *Nat Med,* 15**,** 1407-13.

ORSER, B. A., PENNEFATHER, P. S. & MACDONALD, J. F. 1997. Multiple mechanisms of ketamine blockade of N-methyl-D-aspartate receptors. *Anesthesiology,* 86**,** 903-17.

OTTON, H. J., LAWSON MCLEAN, A., PANNOZZO, M. A., DAVIES, C. H. & WYLLIE, D. J. 2011. Quantification of the Mg2+-induced potency shift of amantadine and memantine voltage-dependent block in human recombinant GluN1/GluN2A NMDARs. *Neuropharmacology,* 60**,** 388-96.

PAGANELLI, M. A., KUSSIUS, C. L. & POPESCU, G. K. 2013. Role of cross-cleft contacts in NMDA receptor gating. *PLoS One,* 8**,** e80953.

PAGANELLI, M. A. & POPESCU, G. K. 2015. Actions of bupivacaine, a widely used local anesthetic, on NMDA receptor responses. *J Neurosci,* 35**,** 831-42.

PAHK, A. J. & WILLIAMS, K. 1997. Influence of extracellular pH on inhibition by ifenprodil at N-methyl-D-aspartate receptors in Xenopus oocytes. *Neurosci Lett,* 225**,** 29-32.

PANG, X. & ZHOU, H. X. 2017. Structural modeling for the open state of an NMDA receptor. *J Struct Biol,* 200**,** 369-375.

PAOLETTI, P., ASCHER, P. & NEYTON, J. 1997. High-affinity zinc inhibition of NMDA NR1-NR2A receptors. *J Neurosci,* 17**,** 5711-25.

PAOLETTI, P., BELLONE, C. & ZHOU, Q. 2013. NMDA receptor subunit diversity: impact on receptor properties, synaptic plasticity and disease. *Nat Rev Neurosci,* 14**,** 383-400.

PAOLETTI, P. & NEYTON, J. 2007. NMDA receptor subunits: function and pharmacology. *Curr Opin Pharmacol,* 7**,** 39-47.

PAOLETTI, P., NEYTON, J. & ASCHER, P. 1995. Glycine-independent and subunit-specific potentiation of NMDA responses by extracellular Mg2+. *Neuron,* 15**,** 1109-20.

PARSONS, C. G., DANYSZ, W., BARTMANN, A., SPIELMANNS, P., FRANKIEWICZ, T., HESSELINK, M., EILBACHER, B. & QUACK, G. 1999. Amino-alkyl-cyclohexanes are novel uncompetitive NMDA receptor antagonists with strong voltage-dependency and fast blocking kinetics: in vitro and in vivo characterization. *Neuropharmacology,* 38**,** 85-108.

PARSONS, C. G., GILLING, K. E. & JATZKE, C. 2008a. Blocking kinetics of memantine on NR1a/2A receptors recorded in inside-out and outside-out patches from Xenopus oocytes. *J Neural Transm (Vienna),* 115**,** 1367-73.

PARSONS, C. G., GILLING, K. E. & JATZKE, C. 2008b. Memantine does not show intracellular block of the NMDA receptor channel. *Eur J Pharmacol,* 587**,** 99-103.

PARSONS, C. G., GRUNER, R., ROZENTAL, J., MILLAR, J. & LODGE, D. 1993. Patch clamp studies on the kinetics and selectivity of N-methyl-D-aspartate receptor antagonism by memantine (1-amino-3,5-dimethyladamantan). *Neuropharmacology,* 32**,** 1337-50.

PARSONS, C. G., PANCHENKO, V. A., PINCHENKO, V. O., TSYNDRENKO, A. Y. & KRISHTAL, O. A. 1996. Comparative patch-clamp studies with freshly dissociated rat hippocampal and striatal neurons on the NMDA receptor antagonistic effects of amantadine and memantine. *Eur J Neurosci,* 8**,** 446-54.

PARSONS, C. G., QUACK, G., BRESINK, I., BARAN, L., PRZEGALINSKI, E., KOSTOWSKI, W., KRZASCIK, P., HARTMANN, S. & DANYSZ, W. 1995. Comparison of the potency, kinetics and voltage-dependency of a series of uncompetitive NMDA receptor antagonists in vitro with anticonvulsive and motor impairment activity in vivo. *Neuropharmacology,* 34**,** 1239-58.

PARSONS, C. G., STOFFLER, A. & DANYSZ, W. 2007a. Memantine: a NMDA receptor antagonist that improves memory by restoration of homeostasis in the glutamatergic

system--too little activation is bad, too much is even worse. *Neuropharmacology,* 53**,** 699-723.

PARSONS, C. G., STÖFFLER, A. & DANYSZ, W. 2007b. Memantine: a NMDA receptor antagonist that improves memory by restoration of homeostasis in the glutamatergic system - too little activation is bad, too much is even worse. *Neuropharmacology,* 53**,** 699-723.

PARSONS, M. P. & RAYMOND, L. A. 2014. Extrasynaptic NMDA receptor involvement in central nervous system disorders. *Neuron,* 82**,** 279-93.

PAUL, I. A., TRULLAS, R., SKOLNICK, P. & NOWAK, G. 1992. Down-regulation of cortical beta-adrenoceptors by chronic treatment with functional NMDA antagonists. *Psychopharmacology (Berl),* 106**,** 285-7.

PAYANDEH, J., GAMAL EL-DIN, T. M., SCHEUER, T., ZHENG, N. & CATTERALL, W. A. 2012. Crystal structure of a voltage-gated sodium channel in two potentially inactivated states. *Nature,* 486**,** 135-9.

PAYANDEH, J., SCHEUER, T., ZHENG, N. & CATTERALL, W. A. 2011. The crystal structure of a voltage-gated sodium channel. *Nature,* 475**,** 353-8.

PECHMANN, S., WILLMUND, F. & FRYDMAN, J. 2013. The ribosome as a hub for protein quality control. *Mol Cell,* 49**,** 411-21.

PEOPLES, R. W., WHITE, G., LOVINGER, D. M. & WEIGHT, F. F. 1997. Ethanol inhibition of N-methyl-D-aspartate-activated current in mouse hippocampal neurones: whole-cell patch-clamp analysis. *Br J Pharmacol,* 122**,** 1035-42.

PEREZ-ISIDORO, R., SIERRA-VALDEZ, F. J. & RUIZ-SUAREZ, J. C. 2014. Anesthetic diffusion through lipid membranes depends on the protonation rate. *Sci Rep,* 4**,** 7534.

PERSSON, J. 2013. Ketamine in pain management. *CNS neuroscience & therapeutics,* 19**,** 396-402.

PHILLIPS, R. J. S. 1960. "Lurcher," a new gene in linkage group XI of the house mouse. *J. Genet.,* 57**,** 35-42.

POVYSHEVA, N. V. & JOHNSON, J. W. 2016. Effects of memantine on the excitation-inhibition balance in prefrontal cortex. *Neurobiol Dis,* 96**,** 75-83.

QIAN, A., BULLER, A. L. & JOHNSON, J. W. 2005. NR2 subunit-dependence of NMDA receptor channel block by external Mg2+. *J Physiol,* 562**,** 319-31.

RADANT, A. D., BOWDLE, T. A., COWLEY, D. S., KHARASCH, E. D. & ROY-BYRNE, P. P. 1998. Does ketamine-mediated N-methyl-D-aspartate receptor antagonism cause schizophrenia-like oculomotor abnormalities? *Neuropsychopharmacology,* 19**,** 434-44.

RAMMES, G., DANYSZ, W. & PARSONS, C. G. 2008. Pharmacodynamics of memantine: an update. *Curr Neuropharmacol,* 6**,** 55-78.

REN, H., ZHAO, Y., DWYER, D. S. & PEOPLES, R. W. 2012. Interactions among positions in the third and fourth membrane-associated domains at the intersubunit interface of the N-methyl-D-aspartate receptor forming sites of alcohol action. *J Biol Chem,* 287**,** 27302-12.

REYNOLDS, I. J. & MILLER, R. J. 1988. [3H]MK801 binding to the N-methyl-D-aspartate receptor reveals drug interactions with the zinc and magnesium binding sites. *J Pharmacol Exp Ther,* 247**,** 1025-31.

RIOU, M., STROEBEL, D., EDWARDSON, J. M. & PAOLETTI, P. 2012. An alternating GluN1-2-1-2 subunit arrangement in mature NMDA receptors. *PLoS One,* 7**,** e35134.

ROBINSON, D. M. & KEATING, G. M. 2006. Memantine: a review of its use in Alzheimer's disease. *Drugs,* 66**,** 1515-34.

ROCK, D. M. & MACDONALD, R. L. 1992. Spermine and related polyamines produce a voltage-dependent reduction of N-methyl-D-aspartate receptor single-channel conductance. *Mol Pharmacol,* 42**,** 157-64.

RODRÍGUEZ-MORENO, A. & PAULSEN, O. 2008. Spike timing–dependent long-term depression requires presynaptic NMDA receptors. *Nature Neuroscience,* 11**,** 744-745.

ROMERO-HERNANDEZ, A., SIMOROWSKI, N., KARAKAS, E. & FURUKAWA, H. 2016. Molecular Basis for Subtype Specificity and High-Affinity Zinc Inhibition in the GluN1-GluN2A NMDA Receptor Amino-Terminal Domain. *Neuron,* 92**,** 1324-1336.

RUDOLF, G. D., CRONIN, C. A., LANDWEHRMEYER, G. B., STANDAERT, D. G., PENNEY, J. B., JR. & YOUNG, A. B. 1996. Expression of N-methyl-D-aspartate glutamate receptor subunits in the prefrontal cortex of the rat. *Neuroscience,* 73**,** 417-27.

RUPPERSBERG, J. P., V. KITZING, E. & SCHOEPFER, R. 1994. The mechanism of magnesium block of NMDA receptors. *Sem. Neurosci.,* 6**,** 87-96.

SACKTOR, T. C. 2008. PKMzeta, LTP maintenance, and the dynamic molecular biology of memory storage. *Prog Brain Res,* 169**,** 27-40.

SCHNEGGENBURGER, R. 1996. Simultaneous measurement of Ca2+ influx and reversal potentials in recombinant N-methyl-D-aspartate receptor channels. *Biophys J,* 70**,** 2165-74.

SCHWARTZ, J., MURROUGH, J. W. & IOSIFESCU, D. V. 2016. Ketamine for treatment-resistant depression: recent developments and clinical applications. *Evid Based Ment Health,* 19**,** 35-8.

SCHWARZ, W., PALADE, P. T. & HILLE, B. 1977. Local anesthetics. Effect of pH on use-dependent block of sodium channels in frog muscle. *Biophys J,* 20**,** 343-68.

SHEN, W., MENNERICK, S., COVEY, D. F. & ZORUMSKI, C. F. 2000. Pregnenolone sulfate modulates inhibitory synaptic transmission by enhancing GABA(A) receptor desensitization. *J Neurosci,* 20**,** 3571-9.

SIBAROV, D. A., POGUZHELSKAYA, E. E. & ANTONOV, S. M. 2018. Downregulation of calcium-dependent NMDA receptor desensitization by sodium-calcium exchangers: a role of membrane cholesterol. *BMC Neurosci,* 19**,** 73.

SIEGLER RETCHLESS, B., GAO, W. & JOHNSON, J. W. 2012. A single GluN2 subunit residue controls NMDA receptor channel properties via intersubunit interaction. *Nat Neurosci,* 15**,** 406-13, S1-2.

SMART, O. S., NEDUVELIL, J. G., WANG, X., WALLACE, B. A. & SANSOM, M. S. 1996. HOLE: a program for the analysis of the pore dimensions of ion channel structural models. *J Mol Graph,* 14**,** 354-60, 376.

SNYDER, M. A. & GAO, W. J. 2013. NMDA hypofunction as a convergence point for progression and symptoms of schizophrenia. *Front Cell Neurosci,* 7**,** 31.

SOBOLEVSKII, A. I. & KHODOROV, B. I. 2002. Blocker studies of the functional architecture of the NMDA receptor channel. *Neurosci Behav Physiol,* 32**,** 157-71.

SOBOLEVSKY, A. & KOSHELEV, S. 1998. Two blocking sites of amino-adamantane derivatives in open N-methyl-D-aspartate channels. *Biophys J,* 74**,** 1305-19.

SOBOLEVSKY, A. I. 1999. Two-component blocking kinetics of open NMDA channels by organic cations. *Biochim Biophys Acta,* 1416**,** 69-91.

SOBOLEVSKY, A. I. 2000. Quantitative analysis of tetrapentylammonium-induced blockade of open N-methyl-D-aspartate channels. *Biophys J,* 79**,** 1324-35.

SOBOLEVSKY, A. I., KOSHELEV, S. G. & KHODOROV, B. I. 1998. Interaction of memantine and amantadine with agonist-unbound NMDA-receptor channels in acutely isolated rat hippocampal neurons. *J Physiol,* 512 (Pt 1)**,** 47-60.

SOBOLEVSKY, A. I., KOSHELEV, S. G. & KHODOROV, B. I. 1999. Probing of NMDA channels with fast blockers. *J Neurosci,* 19**,** 10611-26.

SOBOLEVSKY, A. I., PRODROMOU, M. L., YELSHANSKY, M. V. & WOLLMUTH, L. P. 2007. Subunit-specific contribution of pore-forming domains to NMDA receptor channel structure and gating. *J Gen Physiol,* 129**,** 509-25.

SONG, X., JENSEN, M. O., JOGINI, V., STEIN, R. A., LEE, C. H., MCHAOURAB, H. S., SHAW, D. E. & GOUAUX, E. 2018. Mechanism of NMDA receptor channel block by MK-801 and memantine. *Nature,* 556**,** 515-519.

STANDAERT, D. G., LANDWEHRMEYER, G. B., KERNER, J. A., PENNEY, J. B., JR. & YOUNG, A. B. 1996. Expression of NMDAR2D glutamate receptor subunit mRNA in

neurochemically identified interneurons in the rat neostriatum, neocortex and hippocampus. *Brain Res Mol Brain Res,* 42**,** 89-102.

STERN, P., BEHE, P., SCHOEPFER, R. & COLQUHOUN, D. 1992. Single-channel conductances of NMDA receptors expressed from cloned cDNAs: comparison with native receptors. *Proc Biol Sci,* 250**,** 271-7.

STERN, P., CIK, M., COLQUHOUN, D. & STEPHENSON, F. A. 1994. Single channel properties of cloned NMDA receptors in a human cell line: comparison with results from Xenopus oocytes. *J Physiol,* 476**,** 391-7.

STRICHARTZ, G. R. 1973. The inhibition of sodium currents in myelinated nerve by quaternary derivatives of lidocaine. *J Gen Physiol,* 62**,** 37-57.

STROEBEL, D., CARVALHO, S., GRAND, T., ZHU, S. & PAOLETTI, P. 2014. Controlling NMDA receptor subunit composition using ectopic retention signals. *J Neurosci,* 34**,** 16630-6.

STROEBEL, D., CASADO, M. & PAOLETTI, P. 2018. Triheteromeric NMDA receptors: from structure to synaptic physiology. *Curr Opin Physiol,* 2**,** 1-12.

SULA, A., BOOKER, J., NG, L. C., NAYLOR, C. E., DECAEN, P. G. & WALLACE, B. A. 2017. The complete structure of an activated open sodium channel. *Nat Commun,* 8**,** 14205.

SUN, W., WONG, J. M., GRAY, J. A. & CARTER, B. C. 2018. Incomplete block of NMDA receptors by intracellular MK-801. *Neuropharmacology,* 143**,** 122-129.

SWANSON, G. T., FELDMEYER, D., KANEDA, M. & CULL-CANDY, S. G. 1996. Effect of RNA editing and subunit co-assembly single-channel properties of recombinant kainate receptors. *J Physiol,* 492 (Pt 1)**,** 129-42.

SWANSON, G. T., KAMBOJ, S. K. & CULL-CANDY, S. G. 1997. Single-channel properties of recombinant AMPA receptors depend on RNA editing, splice variation, and subunit composition. *J Neurosci,* 17**,** 58-69.

SZEGEDI, V., JUHASZ, G., PARSONS, C. G. & BUDAI, D. 2010. In vivo evidence for functional NMDA receptor blockade by memantine in rat hippocampal neurons. *J Neural Transm (Vienna),* 117**,** 1189-94.

TAJIMA, N., KARAKAS, E., GRANT, T., SIMOROWSKI, N., DIAZ-AVALOS, R., GRIGORIEFF, N. & FURUKAWA, H. 2016. Activation of NMDA receptors and the mechanism of inhibition by ifenprodil. *Nature,* 534**,** 63-8.

TALUKDER, I. & WOLLMUTH, L. P. 2011. Local constraints in either the GluN1 or GluN2 subunit equally impair NMDA receptor pore opening. *J Gen Physiol,* 138**,** 179-94.

TEXIDO, L., MARTIN-SATUE, M., ALBERDI, E., SOLSONA, C. & MATUTE, C. 2011. Amyloid beta peptide oligomers directly activate NMDA receptors. *Cell Calcium,* 49**,** 184-90.

THOMAS, S. J. & GROSSBERG, G. T. 2009. Memantine: a review of studies into its safety and efficacy in treating Alzheimer's disease and other dementias. *Clin Interv Aging,* 4**,** 367-77.

TIKHONOV, D. B. 2007. Ion channels of glutamate receptors: structural modeling. *Mol Membr Biol,* 24**,** 135-47.

TIKHONOV, D. B., BRUHOVA, I. & ZHOROV, B. S. 2006. Atomic determinants of state-dependent block of sodium channels by charged local anesthetics and benzocaine. *FEBS Lett,* 580**,** 6027-32.

TOFT, A. K., LUNDBYE, C. J. & BANKE, T. G. 2016. Dysregulated NMDA-Receptor Signaling Inhibits Long-Term Depression in a Mouse Model of Fragile X Syndrome. *J Neurosci,* 36**,** 9817-27.

TONG, G. & JAHR, C. E. 1994. Regulation of glycine-insensitive desensitization of the NMDA receptor in outside-out patches. *J Neurophysiol,* 72**,** 754-61.

TOVAR, K. R. & WESTBROOK, G. L. 2012. Amino-terminal ligands prolong NMDA Receptor-mediated EPSCs. *J Neurosci,* 32**,** 8065-73.

TRAYNELIS, S. F. & CULL-CANDY, S. G. 1990. Proton inhibition of N-methyl-D-aspartate receptors in cerebellar neurons. *Nature,* 345**,** 347-50.

TRAYNELIS, S. F. & CULL-CANDY, S. G. 1991. Pharmacological properties and H+ sensitivity of excitatory amino acid receptor channels in rat cerebellar granule neurones. *J Physiol,* 433**,** 727-63.

TRAYNELIS, S. F., HARTLEY, M. & HEINEMANN, S. F. 1995. Control of proton sensitivity of the NMDA receptor by RNA splicing and polyamines. *Science,* 268**,** 873-6.

TRAYNELIS, S. F. & WAHL, P. 1997. Control of rat GluR6 glutamate receptor open probability by protein kinase A and calcineurin. *J Physiol,* 503 (Pt 3)**,** 513-31.

TRAYNELIS, S. F., WOLLMUTH, L. P., MCBAIN, C. J., MENNITI, F. S., VANCE, K. M., OGDEN, K. K., HANSEN, K. B., YUAN, H., MYERS, S. J. & DINGLEDINE, R. 2010a. Glutamate receptor ion channels: structure, regulation, and function. *Pharmacological reviews,* 62**,** 405-96.

TRAYNELIS, S. F., WOLLMUTH, L. P., MCBAIN, C. J., MENNITI, F. S., VANCE, K. M., OGDEN, K. K., HANSEN, K. B., YUAN, H., MYERS, S. J. & DINGLEDINE, R. 2010b. Glutamate receptor ion channels: structure, regulation, and function. *Pharmacol Rev,* 62**,** 405-96.

TROTT, O. & OLSON, A. J. 2010. Software News and Update AutoDock Vina: Improving the Speed and Accuracy of Docking with a New Scoring Function, Efficient Optimization, and Multithreading. *Journal of Computational Chemistry,* 31**,** 455-461.

TRULLAS, R. & SKOLNICK, P. 1990. Functional antagonists at the NMDA receptor complex exhibit antidepressant actions. *Eur J Pharmacol,* 185**,** 1-10.

TUCKER, K. R., BLOCK, E. R. & LEVITAN, E. S. 2015. Action potentials and amphetamine release antipsychotic drug from dopamine neuron synaptic VMAT vesicles. *Proc Natl Acad Sci U S A,* 112**,** E4485-94.

VICINI, S., WANG, J. F., LI, J. H., ZHU, W. J., WANG, Y. H., LUO, J. H., WOLFE, B. B. & GRAYSON, D. R. 1998. Functional and pharmacological differences between recombinant N-methyl-D-aspartate receptors. *J Neurophysiol,* 79**,** 555-66.

VILLARROEL, A., BURNASHEV, N. & SAKMANN, B. 1995. Dimensions of the narrow portion of a recombinant NMDA receptor channel. *Biophys J,* 68**,** 866-75.

VOROBJEV, V. S. & SHARONOVA, I. N. 1994. Tetrahydroaminoacridine blocks and prolongs NMDA receptor-mediated responses in a voltage-dependent manner. *Eur J Pharmacol,* 253**,** 1-8.

VYKLICKY, L., JR., VLACHOVA, V. & KRUSEK, J. 1990. The effect of external pH changes on responses to excitatory amino acids in mouse hippocampal neurones. *J Physiol,* 430**,** 497-517.

VYKLICKY, V., KRAUSOVA, B., CERNY, J., BALIK, A., ZAPOTOCKY, M., NOVOTNY, M., LICHNEROVA, K., SMEJKALOVA, T., KANIAKOVA, M., KORINEK, M., PETROVIC, M., KACER, P., HORAK, M., CHODOUNSKA, H. & VYKLICKY, L. 2015. Block of NMDA receptor channels by endogenous neurosteroids: implications for the agonist induced conformational states of the channel vestibule. *Sci Rep,* 5**,** 10935.

VYKLICKY, V., KRAUSOVA, B., CERNY, J., LADISLAV, M., SMEJKALOVA, T., KYSILOV, B., KORINEK, M., DANACIKOVA, S., HORAK, M., CHODOUNSKA, H., KUDOVA, E. & VYKLICKY, L. 2018. Surface Expression, Function, and Pharmacology of Disease-Associated Mutations in the Membrane Domain of the Human GluN2B Subunit. *Front Mol Neurosci,* 11**,** 110.

WALDMANN, R., CHAMPIGNY, G., BASSILANA, F., HEURTEAUX, C. & LAZDUNSKI, M. 1997. A proton-gated cation channel involved in acid-sensing. *Nature,* 386**,** 173-7.

WANG, L. Y. & MACDONALD, J. F. 1995. Modulation by magnesium of the affinity of NMDA receptors for glycine in murine hippocampal neurones. *J Physiol,* 486 (Pt 1)**,** 83-95.

WANG, M. 2011. Neurosteroids and GABA-A Receptor Function. *Front Endocrinol (Lausanne),* 2**,** 44.

WANG, R. & REDDY, P. H. 2017. Role of Glutamate and NMDA Receptors in Alzheimer's Disease. *J Alzheimers Dis,* 57**,** 1041-1048.

WANG, S. & KALTASHOV, I. A. 2015. Identification of reduction-susceptible disulfide bonds in transferrin by differential alkylation using O(16)/O(18) labeled iodoacetic acid. *J Am Soc Mass Spectrom,* 26**,** 800-7.

WANG, Z. C., ZHAO, J. & LI, S. 2013. Dysregulation of synaptic and extrasynaptic N-methyl-D-aspartate receptors induced by amyloid-beta. *Neurosci Bull,* 29**,** 752-60.

WATANABE, J., BECK, C., KUNER, T., PREMKUMAR, L. S. & WOLLMUTH, L. P. 2002. DRPEER: a motif in the extracellular vestibule conferring high Ca2+ flux rates in NMDA receptor channels. *J Neurosci,* 22**,** 10209-16.

WILLIAMS, K. 1993. Ifenprodil discriminates subtypes of the N-methyl-D-aspartate receptor: selectivity and mechanisms at recombinant heteromeric receptors. *Mol Pharmacol,* 44**,** 851-9.

WILLIAMS, K., PAHK, A. J., KASHIWAGI, K., MASUKO, T., NGUYEN, N. D. & IGARASHI, K. 1998. The selectivity filter of the N-methyl-D-aspartate receptor: a tryptophan residue controls block and permeation of Mg2+. *Mol Pharmacol,* 53**,** 933-41.

WITT, A., MACDONALD, N. & KIRKPATRICK, P. 2004. Memantine hydrochloride. *Nat Rev Drug Discov,* 3**,** 109-10.

WOLLMUTH, L. P., KUNER, T. & SAKMANN, B. 1998. Adjacent asparagines in the NR2-subunit of the NMDA receptor channel control the voltage-dependent block by extracellular Mg2+. *J Physiol,* 506 (Pt 1)**,** 13-32.

WOLLMUTH, L. P., KUNER, T., SEEBURG, P. H. & SAKMANN, B. 1996. Differential contribution of the NR1- and NR2A-subunits to the selectivity filter of recombinant NMDA receptor channels. *J Physiol,* 491 (Pt 3)**,** 779-97.

WONG, E. H., KEMP, J. A., PRIESTLEY, T., KNIGHT, A. R., WOODRUFF, G. N. & IVERSEN, L. L. 1986. The anticonvulsant MK-801 is a potent N-methyl-D-aspartate antagonist. *Proc Natl Acad Sci U S A,* 83**,** 7104-8.

WRIGHT, J. M., PEOPLES, R. W. & WEIGHT, F. F. 1996. Single-channel and whole-cell analysis of ethanol inhibition of NMDA-activated currents in cultured mouse cortical and hippocampal neurons. *Brain Res,* 738**,** 249-56.

WRIGHTON, D. C., BAKER, E. J., CHEN, P. E. & WYLLIE, D. J. 2008. Mg2+ and memantine block of rat recombinant NMDA receptors containing chimeric NR2A/2D subunits expressed in Xenopus laevis oocytes. *J Physiol,* 586**,** 211-25.

WROBEL, E., ROTHENBERG, I., KRISP, C., HUNDT, F., FRAENZEL, B., ECKEY, K., LINDERS, J. T., GALLACHER, D. J., TOWART, R., POTT, L., PUSCH, M., YANG, T., RODEN, D. M., KURATA, H. T., SCHULZE-BAHR, E., STRUTZ-SEEBOHM, N.,

WOLTERS, D. & SEEBOHM, G. 2016. KCNE1 induces fenestration in the Kv7.1/KCNE1 channel complex that allows for highly specific pharmacological targeting. *Nat Commun,* 7**,** 12795.

WU, M., WHITE, H. V., BOEHM, B. A., MERINEY, C. J., KERRIGAN, K., FRASSO, M., LIANG, M., GOTWAY, E. M., WILCOX, M. R., JOHNSON, J. W., WIPF, P. & MERINEY, S. D. 2018. New Cav2 calcium channel gating modifiers with agonist activity and therapeutic potential to treat neuromuscular disease. *Neuropharmacology,* 131**,** 176-189.

WU, Q. J. & TYMIANSKI, M. 2018. Targeting NMDA receptors in stroke: new hope in neuroprotection. *Mol Brain,* 11**,** 15.

WYLLIE, D. J., BEHE, P. & COLQUHOUN, D. 1998. Single-channel activations and concentration jumps: comparison of recombinant NR1a/NR2A and NR1a/NR2D NMDA receptors. *J Physiol,* 510 (Pt 1)**,** 1-18.

WYLLIE, D. J., BEHE, P., NASSAR, M., SCHOEPFER, R. & COLQUHOUN, D. 1996. Single-channel currents from recombinant NMDA NR1a/NR2D receptors expressed in Xenopus oocytes. *Proc Biol Sci,* 263**,** 1079-86.

WYLLIE, D. J., LIVESEY, M. R. & HARDINGHAM, G. E. 2013. Influence of GluN2 subunit identity on NMDA receptor function. *Neuropharmacology,* 74**,** 4-17.

XU, M., SMOTHERS, C. T. & WOODWARD, J. J. 2015. Cysteine substitution of transmembrane domain amino acids alters the ethanol inhibition of GluN1/GluN2A N-methyl-D-aspartate receptors. *J Pharmacol Exp Ther,* 353**,** 91-101.

YAMAKURA, T., MORI, H., MASAKI, H., SHIMOJI, K. & MISHINA, M. 1993. Different sensitivities of NMDA receptor channel subtypes to non-competitive antagonists. *Neuroreport,* 4**,** 687-90.

YAMASAKI, M., OKADA, R., TAKASAKI, C., TOKI, S., FUKAYA, M., NATSUME, R., SAKIMURA, K., MISHINA, M., SHIRAKAWA, T. & WATANABE, M. 2014. Opposing role of NMDA receptor GluN2B and GluN2D in somatosensory development and maturation. *J Neurosci,* 34**,** 11534-48.

YANG, Z., ZHOU, X. & ZHANG, Q. 2013. Effectiveness and safety of memantine treatment for Alzheimer's disease. *J Alzheimers Dis,* 36**,** 445-58.

YELSHANSKAYA, M. V., MESBAHI-VASEY, S., KURNIKOVA, M. G. & SOBOLEVSKY, A. I. 2017. Role of the Ion Channel Extracellular Collar in AMPA Receptor Gating. *Sci Rep,* 7**,** 1050.

YI, F., ZACHARIASSEN, L. G., DORSETT, K. N. & HANSEN, K. B. 2018. Properties of Triheteromeric N-Methyl-d-Aspartate Receptors Containing Two Distinct GluN1 Isoforms. *Mol Pharmacol,* 93**,** 453-467.

YUAN, H., ERREGER, K., DRAVID, S. M. & TRAYNELIS, S. F. 2005. Conserved structural and functional control of N-methyl-D-aspartate receptor gating by transmembrane domain M3. *J Biol Chem,* 280**,** 29708-16.

YUAN, H., HANSEN, K. B., VANCE, K. M., OGDEN, K. K. & TRAYNELIS, S. F. 2009. Control of NMDA receptor function by the NR2 subunit amino-terminal domain. *J Neurosci,* 29**,** 12045-58.

YUAN, H., HANSEN, K. B., ZHANG, J., PIERSON, T. M., MARKELLO, T. C., FAJARDO, K. V., HOLLOMAN, C. M., GOLAS, G., ADAMS, D. R., BOERKOEL, C. F., GAHL, W. A. & TRAYNELIS, S. F. 2014. Functional analysis of a de novo GRIN2A missense mutation associated with early-onset epileptic encephalopathy. *Nat Commun,* 5**,** 3251.

ZAMBRANO, P., SUWALSKY, M., JEMIOLA-RZEMINSKA, M. & STRZALKA, K. 2018. Studies on the interaction of NMDA receptor antagonist memantine with cell membranes: A mini-review. *Chem Biol Interact,* 283**,** 47-50.

ZANOS, P., MOADDEL, R., MORRIS, P. J., GEORGIOU, P., FISCHELL, J., ELMER, G. I., ALKONDON, M., YUAN, P., PRIBUT, H. J., SINGH, N. S., DOSSOU, K. S., FANG, Y., HUANG, X. P., MAYO, C. L., WAINER, I. W., ALBUQUERQUE, E. X., THOMPSON, S. M., THOMAS, C. J., ZARATE, C. A., JR. & GOULD, T. D. 2016. NMDAR inhibition-independent antidepressant actions of ketamine metabolites. *Nature,* 533**,** 481-6.

ZAREI, M. M. & DANI, J. A. 1994. Ionic permeability characteristics of the N-methyl-D-aspartate receptor channel. *J Gen Physiol,* 103**,** 231-48.

ZHANG, J. B., CHANG, S., XU, P., MIAO, M., WU, H., ZHANG, Y., ZHANG, T., WANG, H., ZHANG, J., XIE, C., SONG, N., LUO, C., ZHANG, X. & ZHU, S. 2018. Structural Basis of the Proton Sensitivity of Human GluN1-GluN2A NMDA Receptors. *Cell Rep,* 25**,** 3582-3590 e4.

ZHANG, Y., LI, P., FENG, J. & WU, M. 2016. Dysfunction of NMDA receptors in Alzheimer's disease. *Neurol Sci,* 37**,** 1039-47.

ZHAO, Y., REN, H. & PEOPLES, R. W. 2016. Intersubunit interactions at putative sites of ethanol action in the M3 and M4 domains of the NMDA receptor GluN1 and GluN2B subunits. *Br J Pharmacol,* 173**,** 1950-65.

ZHAO, Y., SIVAJI, S., CHIANG, M. C., ALI, H., ZUKOWSKI, M., ALI, S., KENNEDY, B., SKLYAR, A., CHENG, A., GUO, Z., REED, A. K., KODALI, R., BOROWSKI, J., FROST, G., BEUKEMA, P. & WILLS, Z. P. 2017. Amyloid Beta Peptides Block New Synapse Assembly by Nogo Receptor-Mediated Inhibition of T-Type Calcium Channels. *Neuron,* 96**,** 355-372 e6.

ZHENG, F., ERREGER, K., LOW, C. M., BANKE, T., LEE, C. J., CONN, P. J. & TRAYNELIS, S. F. 2001. Allosteric interaction between the amino terminal domain and the ligand binding domain of NR2A. *Nat Neurosci,* 4**,** 894-901.

ZHOU, H. X. 2017. Gating Motions and Stationary Gating Properties of Ionotropic Glutamate Receptors: Computation Meets Electrophysiology. *Acc Chem Res,* 50**,** 814-822.

ZHOU, Q. & SHENG, M. 2013. NMDA receptors in nervous system diseases. *Neuropharmacology,* 74**,** 69-75.

ZHU, S., STEIN, R. A., YOSHIOKA, C., LEE, C. H., GOEHRING, A., MCHAOURAB, H. S. & GOUAUX, E. 2016. Mechanism of NMDA Receptor Inhibition and Activation. *Cell,* 165**,** 704-14.

ZUO, J., DE JAGER, P. L., TAKAHASHI, K. A., JIANG, W., LINDEN, D. J. & HEINTZ, N. 1997. Neurodegeneration in Lurcher mice caused by mutation in delta2 glutamate receptor gene. *Nature,* 388**,** 769-73.